Dissertation
submitted to the
Combined Faculties for the Natural Sciences and for Mathematics
of the Ruperto–Carola University of Heidelberg, Germany,
for the degree of
Doctor of Natural Sciences

presented by
Mochamad Ikbal Arifyanto
born in Jakarta, Indonesia

Oral examination: 2005, December 21st

Kinematics of Nearby Subdwarfs

And the Luminosity Function of
the Galactic Thick Disk

Referees: Prof. Dr. Burkhard Fuchs

Prof. Dr. Joseph Fried

Zusammenfassung

Kinematik von metallarmen Unterzwerg-Sternen : Wir präsentieren eine Untersuchung der Raumgeschwindigkeiten von 895 Unterzwerg-Sternen aus der Stichprobe von Carney et al. (1994; CLLA). Hipparcos Parallaxen und Eigenbewegungen sowie Tycho2 Eigenbewegungen wurden mit Radialgeschwindigkeiten und Metallizitäten von CLLA kombiniert. Das kinematische Verhalten der Sterne wird insbesondere in Hinblick auf ihre Metallizitäten diskutiert. Die meisten der Sterne haben eine Metallizität von -1.0 $\leq$[Fe/H]$\leq$ -0.4 repräsentieren die Geschwindigkeitsverteilung der dicken Scheibe. Wir leiteten die Helligkeitsfunktion der dicken Scheibe mit $1/V_{max}$ Methode ab. Wir fanden, daß die Helligkeitsfunktion in der absoluten Magnitude $M_V = 4 - 5$ mag, gut mit der Helligkeitsfunktion übereinstimmen, die von derstellare Anfangsmassenfunktion abgeleitet wird (Reyle & Robin 2001). Wir analysierten die Kinematik in unserer dicken Scheibe Probe und fanden substrukturen in der dicken Scheibe Population.

Kinematics of Metal Poor Subdwarfs : We present an analysis of the space motions of 740 subdwarf stars based on the sample stars of Carney et al. (1994; CLLA). Hipparcos parallaxes and proper motion and Tycho2 proper motions were combined with radial velocities and metallicities from CLLA. The kinematical behavior is discussed in particular in relation to their metallicities. For stars with metallicity -1.0<[Fe/H]<-0.4, the velocity distribution represent the thick disk population. We derived the luminosity function of thick disk using $1/V_{max}$ method. We found that the luminosity function in absolute magnitude of $M_V = 4 - 5$ mag, agree well with the Luminosity function derived from the stellar initial function (Reyle & Robin 2001). We analayzed the kinematics in our thick disk sample and found substructure in the thick disk population.

Table of Contents

List of Figures

List of Tables

1 Introduction

1.1 Stellar Populations of the Galaxy

A stellar population is a set of stars of the same age and chemical composition. Born together at some point in the Galaxy, stars of the same stellar population will share the same kinematic properties in the Galaxy, whether they be with respect to their circular velocities to the Galactic center or in their random velocities in the Galactic halo.

The study of stellar populations has been widely recognized as one of the main tools to study a variety of astrophysical problems. One of the primary reasons for studying stellar populations in galaxies is to improve our understanding of the formation of galaxies and their evolution in time. The history and implications of such studies in our own Galaxy have been well reviewed by Sandage (1986), Gilmore, Wyse and Kuijken (1989) and Majewski (1993).

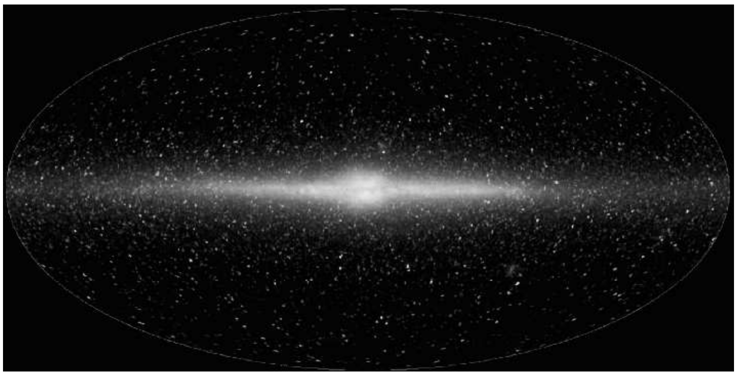

Figure 1: The Galaxy from the COBE satellite

During, the Second World War, Baade (1944), using red photographic plates, discovered that stars in the nucleus of M31 are actually red giants, and therefore very different from the blue stars that could be found in spiral arms. Baade concluded that red giants populate spheroidal components of the galaxy and called them *Population II* in contrast to the stars in the spiral arms which he called *Population I*. He also formulated a prominent correlation between his Population I and II and those of that Oort (1926) found on the basis of kinematical properties: Population II stars seemed to have high velocities, whereas Population I stars did not. This discovery opened a completely new path in galactic physics and sparked a debate that is still very much in progress. After the works of Sandage and Schwarzchild (1952) it became evident that Population II is represented by the old stars, and while both young and old stars constitute Population I. So, at this point age became a player in the "big game". Later, Chamberlain and Aller (1952) introduced one more parameter, the abundance of heavy elements, which were very low for the representatives of the Population II and almost solar for Population I.

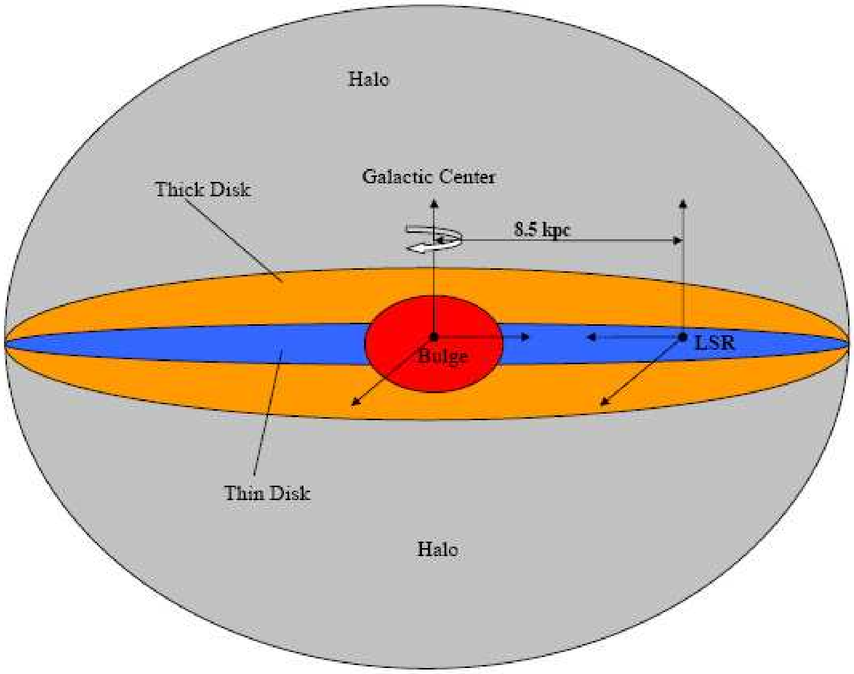

Figure 2: A schematic view of the Galaxy. The four major stellar components, the position of the Sun, and the Galactic center have been marked.

By 1957, the Vatican Conference on Stellar Populations (O'Connel 1958) proposed a compromise scheme of five populations: Extreme Population I, Older Population I, Disk Population, Intermediate Population II, and Halo Population II. More recently, divisions have once again changed from the coarse simplicity of *halo* and *disk*, to the somewhat higher complexity of Young (thin) Disk, Old (thin) Disk, Thick Disk, and Halo. Each group is distributed roughly, normally about the plane along the perpendicular or z-axis direction. The dispersions of the groups are not precisely known and are found to differ from one investigation to another, but are of the order of 100-200 pc for the thin disk and 500-1000 pc for the thick disk. The very old halo population is more nearly spherically distributed with a dispersion in z of several thousand parsecs.

The classical scheme and current usage for both the Milky Way and external galaxies are summarized in the first and second parts of Table 1.1 The top part of Table 1.1 presents the classical view of stellar populations in the Milky Way. Each of the three basic population divisions are further subdivided, with defining examples of observed classes of objects listed. The combinations of spatial distributions, spectral types, kinematics, and chemical abundances are all correlated. It is the set of correlations which provide the evidence for the basic physical validity of the population concept (Cox 2000). The bottom line of the top part illustrates schematically a classical extension of the populations concept to external galaxies. The bottom part illustrates the current appreciation of the stellar populations. Many more details are shown, together with finer subdivisions. The essential features of the population concept however remain unmodified.

Bulge

RR Lyrae in the central bulge of the Galaxy are visible through Baade's window and other regions of low absorptions. Other characteristic stellar tracers of the bulge include K and M giants. These stars span a wide range of metallicity, but over half are in the range $-0.4 < [Fe/H] < 0.3$ (Sadler, Rich & Terndrup 1996). The inner part of the bulge also appears to contain A stars, implying that some star formation has occurred within the past 10^9 year (GWK). The mass of the bulge is about $2 \times 10^{10} M_{\odot}$, or one-third the mass of the disk. The bulge rotates at 60 km s^{-1}.

Thin Disk (Population I)

- **Spiral-arm populations or extreme populations I** are the youngest in the disk. These include HI and molecular clouds, HII regions, protostars, stars of type O & B, supergiants and type I cepheids, which appear to trace spiral pattern of the Milky Way. These tracers are concentrated close to the disk plane with a scale height of 60 pc. They move on nearly circular orbits with net velocities of about 220 kms^{-1}. Their metallicity is somewhat higher than the Sun.

- **The old disk** refers to stars in the disk which are older than a few Gyr. This generally means A type stars or later. They rotate at about 200 km s^{-1}. The total velocity dispersion is about twice that of the young disk, (see Table 2.1). Objects of the old disk include F, G, K and M stars, white dwarfs, planetary nebulae and some types of variable stars. The total mass of the thin disk is

Table 1: Stellar Population. Classical (top) and current (lower) concepts of stellar populations [Cox, 2000]

Population	II	II	Disk	I	I
Characteristic objects and properties	Hallo Pop. II subdwarfs globular clusters RR Lyrae $P > 0.^d4$	Intermediate stars with $V_z \geq 30\ kms$ LPV's, $P < 250^d$	Galactic nucleus RR Lyrae $P < 0.^d4$ weak-line stars	Old Pop. I A stars Me dwarfs strong-line stars	Extreme Pop. I gas, spiral structure supergiants Cepheids
Scale height (pc)	2000	500	300	100	60
central concentration	strong	strong	strong	little	little
τ/τ_u	1.0	1.0–0.8	0.8–0.25	0.25–0.05	0.05–0.00
$\sigma_W (kms^{-1})$	75	25	17	10	8
$Z/Z_\odot$	0.1	0.25	0.5	0.75	1.0
External Galaxies	Elliptical	Elliptical	Bulges	Sp disks, Irr's	Sp disks, Irr's

Population	Extreme Pop. II	Intermediate Pop. II	Bulge/Pop. II	Pop. I	Extreme Pop. I
Characteristic objects and properties	"halo" subdwarfs globular clusters with [Fe/H] < -1 RR Lyrae ΔS > 4	"thick disk" globular clusters with [Fe/H] > -1 RR Lyrae, c-type LPV's, $P\ 250_d$ RHB stars	"bulge" SMR stars ="IR bulge" planetary nebulae ="optical bulge" RR Lyrae ΔS < 4 tri-axial (?)	"old disk" intermediate age disk stars	"young disk" young stars spiral structure Cepheids
$\langle V_{\rm rot} \rangle$	30	170	60	200	220
$\sigma_U : \sigma_V : \sigma_W$	130:100:85	60:45:40	120:120:120	38:25:20	20:10:8
$Z/Z_\odot$	0.03	0.3	0.1-2	0.9	1
τ/τ_u	1.0-0.9	0.9-0.8	1.0-0.5 (?)	0.9-0.1	0.1-0.0
External Galaxies	dE	Sa, SO, gE	Sa, SO, gE	Sbcd, Irr's	Sbcd, Irr's

about $6 \times 10^{10} M_{\odot}$.

Thick Disk (Intermediate Population II)

Star counts suggest that this component is distributed in a disk with scale height of 1 to 1.5 kpc. Less than 1 % of the stars in the vicinity of the sun belong to the thick disk. This component dominates the high-latitude tail of the thin disk at z > 1 kpc. The total mass of the thick disk is only about $10^9 M_{\odot}$.

The true nature of this stellar populations is not fully understood. It was originally classified as part of the halo, but it is much flatter than any other halo population. Kinematics studies imply that the thick disk rotates with a velocity of about 170 km s^{-1} (Gilmore, Wyse, & Kuijken 1989; hereafter GWK), greater than rotation of the halo which is less than 40 km s^{-1}. This shows that the thick disk is closer to the thin disk. Metallicity measurements also support the idea that the thick disk is distinct from the stellar halo. The characteristic metal abundance of the thick disk is $[\mathrm{Fe/H}] = -0.6$, while the halo is poorer in metals (GWK).

It's less obvious that the thick disk is *distinct* from the thin disk since in many respects it represents a continuation of the trends with age in metallicity, velocity dispersion, and scale height as seen in the thin disk. On the other hand, the velocity dispersion and scale height of the thick disk are significantly greater than even the oldest thin disk sub-population, suggesting that some discontinuity might occur between these groups.

Stellar Halo (Extreme Population II)

The stellar halo of the Galaxy includes the system of globular clusters, metal-poor high velocity stars in the solar neighborhood, and metal-poor high latitude stars. The total mass of the stellar halo is only about $10^9 M_{\odot}$. As the oldest visible component of the Galaxy, the stellar halo holds important clues to the formation of the Milky Way.

Metal-poor subdwarfs in the solar neighborhood have large velocities with respect to the Sun and other disk stars. These stars are on highly eccentric orbits about the galactic center; their net rotation is no more than 40 km s^{-1}, while their random motions are quite large. The metallicity of these stars ranges from $-3 < [\mathrm{Fe/H}] < -1$ (Mihalas & Binney 1981). Further explanation on these stars are presented in sections **2.2** and **2.3**.

Globular clusters with $[\mathrm{Fe/H}] < -1$ are the classic tracers of the galactic halo. Their spatial distribution provides the first real clue the true size and shape of the Galaxy. These clusters have a nearly-spherical distribution extending to many times the Sun's distance from the galactic center R_0.

RR Lyrae variables are useful in tracing the large-scale distribution of the halo because they can be identified by their characteristic light variation at large distances.

Table 2: Some population characteristics of disk and halo components in the solar neighborhood (Norris, 2001)

Component	Scale height (pc)	$\langle [Fe/H] \rangle$	$\sigma_{\rm U}, \sigma_{\rm V}, \sigma_{\rm W}$[1] (km s^{-1})	V_{lag}[1] (km s^{-1})	Age (Gyr)	ρ/ρ_{tot}[2]
Old thin disk	300	-0.3	$30, 20, 15$	15	≤ 10	$0.95 - 0.98$
Thick disk	$800 - 1500$	-0.6	$65, 55, 40$	40	$12 - 15$	$0.02 - 0.05$
Metal-weak thick disk	1400	-1.2	Unknown	40	$(12 - 15)$	$(0.0005 - 0.002)$
Flattened halo (also called old, low or collapsed halo)	$1600 - 2000$	-1.6[3]	$130, 100, 90$[3]	160	$12 - 15$	0.0008
Spherical halo (also called younger, high or accreted halo)	Spherical	-1.6[3]	$130, 100, 90$[3]	160	12	0.0002

[1] $\sigma_{\rm U}, \sigma_{\rm V}$ and $\sigma_{\rm W}$ are velocity dispersions in the directions away from the Galactic center, toward Galactic rotation and toward the north Galactic pole, respectively. $V_{\rm lag}$ = ($V_{\rm rot} - V$) measures the asymmetric drift, the velocity by which the component lags the solar neighborhood in its systemic rotation.
[2] Ratio of the density of the component to total density in the solar neighborhood. We assume $\rho_{\rm halo}/\rho_{\rm disk} = 0.001$.
[3] Decomposition of the two halo components has not yet been achieved. The tabulated values are those determined for their admixture in the solar neighborhood. The values of the individual components are thus uncertain.

1.2 Studies of the Thick Disk

The thick disk was defined through star counts 20 years ago (Gilmore & Reid 1983) and is now well-established as a distinct component, not the tail of the stellar halo or of the thin disk. Its origins remain the source of considerable debate.

Since the pioneering work of Gilmore & Reid, several large surveys (most recently Beers et al. 2002, Chen et al. 2001, Ojha 2001, Kerber, Javiel, & Santiago 2001, Chiba & Beers 2000) have been undertaken to constrain the global properties of the thick disk in the larger hopes of unraveling its formation. The Milky

Way thick disk is somewhat metal-poor, with metallicities ranging from $-2.4 <$ [Fe/H]< -0.5 (Beers et al. 2002, Chiba & Beers 2000) but a mean on the higher end (-0.7 to -0.5; Robin et al. 1996, Layden 1995, Gilmore, Wyse, & Jones 1995). While the ages are not as well constrained, the thick disk is thought to be at least as old as the metal-rich globular clusters $47\mathrm{Tuc}$, the globular cluster of the same metallicity ($\propto$ 12 Gyr; Gilmore, Wyse, & Jones 1995). The scale height is now thought to be $600 - 900$ pc, roughly $2 - 4$ times thicker than the old thin disk. The radial scale length is $2.5 - 4.5$ kpc (Reyle & Robin 1996, Ng et al. 1997), giving an overall axial ratio of $3 : 1$ to $7 : 1$.

The kinematics of the thick disk are intermediate between those of the thin disk and those of the stellar halo; in particular, the standard value for the mean azimuthal streaming velocity of the thick disk is $V_{\mathrm{rot}} \sim 170$ km s^{-1} (Norris 1986; Morrison, Flynn & Freeman 1990; Chiba & Beers 2000). Velocity dispersions are generally found to span typical values between 30 and 50 km s^{-1}, sometimes up to 80 km s^{-1} in the radial direction (Ratnatunga & Freeman 1989). The asymmetric drift ranges between $-20\mathrm{to} - 80$ km s^{-1} and the mean metallicity from -0.5 to -0.8 dex. The view of the thick disk has been complicated by the study of Morrison et al. (1990) who brought to the fore low-metallicity stars ($-1.6 < [\mathrm{Fe/H}] < -1.0$) with disk-like kinematics. Chiba & Beers (2000) estimate that 30% of the stars with $-1.6 <$ $[\mathrm{Fe/H}] < -1.0$ belong to the thick disk population. It remains unclear whether this population is separate from the thick disk or its metal-weak tail. However, surveys of faint F/G stars tend to find a lower value, $V_{\mathrm{rot}} \sim 100$ km s^{-1} (e.g. Wyse & Gilmore 1986; Gilmore, Wyse & Norris 2002).

There are two main theories of formation for these stellar components: either they are left-overs from the monolithic dissipative collapse of the protogalaxy (Eggen, Lynden-Bell, & Sandage 1962; ELS) or from the build-up of the Galaxy through hierarchical merging (Searle & Zinn 1978). ELS put forth their model that the stellar halo formed from a rapid collapse of the protocloud, then a rotationally supported disk formed later to explain what they thought was a correlation with metal-poor stars having high orbital eccentricities and low angular momentum. However, their sample was proper-motion selected and modern studies have shown no correlation between metal abundances and eccentricity (e.g. Chiba & Beers 2000). Searle & Zinn put forth their bottom-up model when they found a large (several Gyr) spread in the ages of globular clusters and no abundance gradient with distance from the Galactic center, both predictions of the ELS model. Thus Searle & Zinn argued instead that the stellar halo could have formed from the accretion of independent fragments of masses $10^8 M_{\odot}$.

The thick disk was thought to be dynamically heated (increased velocity dispersion and thus scale height) out of the thin disk, early on when the disk was just forming. One possibility of such heating is simply scattering off of transient spiral density waves (Carlberg & Sellwood 1985) or giant molecular clouds (Lacey 1984). The fairly high values for the velocity dispersions of the thick disk, $\sigma_W \sim 40$ km s^{-1} and $\sigma_{total} \sim 80$ km s^{-1}, argue against normal disk-heating mechanisms (the transient gravitational perturbations in the disk, bits of spiral arms, GMCs) being involved in its formation - those processes generally saturate at the values of the velocity dispersions for the old thin disk, or $\sigma_W \sim 20$ km s^{-1}.

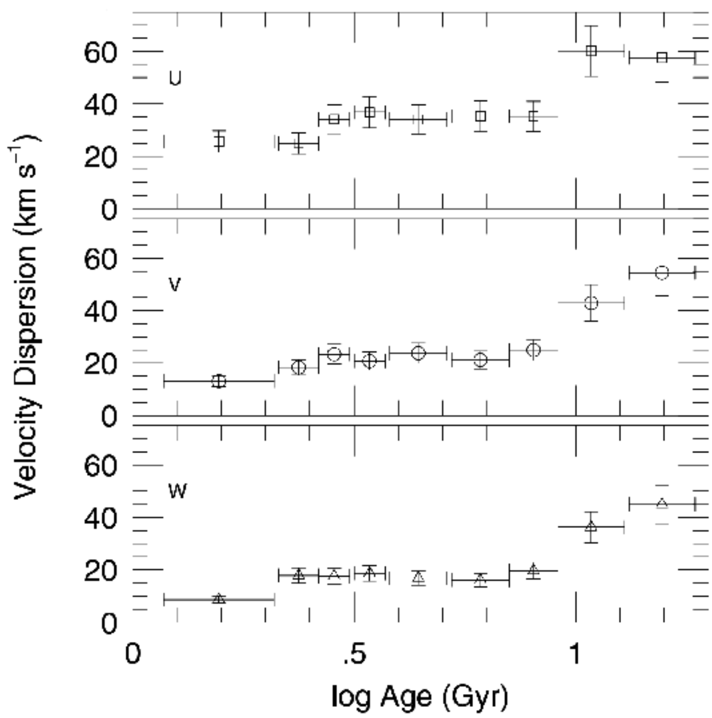

Figure 3: Velocity dispersion in the U (top), V (middle), and W (bottom) directions vs. the logarithm of the age for stars from the Edvardsson et al. (1993) sample. This figure is from Freeman & Bland-Hawthorn (2002).

Figure (3) shows a plot of velocity dispersion vs. age (Edvardsson et al. 1993, Quillen & Garnett 2001). The plot shows three regimes: stars younger than 3 Gyr with a vertical velocity dispersion of 10 km s^{-1} representing stars heated by the process described above, stars of $3 - 10$ Gyr old with $\sigma_W = 20$ km s^{-1} representing the thin disk, and stars older than 10 Gyr with a higher velocity dispersion of 40 km s^{-1} which are the thick disk stars. This sudden doubling of the vertical velocity dispersion at an age of 10 Gyr suggests that the thick disk was formed by a single heating event that occurred 10 Gyr ago and that the disk has not suffered any significant mergers since then.

What signatures of a merger-origin for the thick disk might remain observable today ? Helmi et al. (1999) found by analyzing Hipparcos data the signature of a cold stream in the velocity distribution of the halo stars of the Milky Way. This was confirmed later by Chiba & Beers (2000) using their own data (Beers et al, 2000). Helmi et al. (1999) interpreted this stream as part of the tidal debris of a disrupted satellite galaxy accreted by the Milky Way, which ended up in the halo. Navarro et al. (2004) have argued that Eggens's (1996) Arcturus group is another such a debris stream, but in the thick disk of the Milky Way, dating back to an accretion event $5 \mathrm{to} 8$ Gyrs ago. These observations complement observations of ongoing accretion of satellites such as of the Sagittarius dwarf galaxy (Ibata et al. 1994) or very recent accretion in form of the Monoceros stream discovered in the outer disk of the Milky Way with SDSS data (Newberg et al. 2002, Yanny et al. 2003, Rocha-Pinto et al. 2003, Penarrubia et al. 2005). Extended periods of accretion of satellites onto massive galaxies are also expected theoretically. For instance, recent sophisticated simulations of the formation of a disk galaxy in the framework of cold dark matter cosmology and cosmogony of galaxies by Abadi et al. (2003a, b) suggest that disrupted satellites contribute significantly not only to the stellar halo but also to the disk of a galaxy.

Several models of formation of the thick disk as shown above are proposed which predict peculiar features for the spatial, chemical, kinematical and age distributions of the thick disk, including mean behavior and dispersions, gradients, continuity-discontinuity with other populations. Such predictions are described for instance in Majewski (1993). Therefore, a detailed knowledge of properties of the thick disk is necessary to favor one of the proposed models of formation.

Previous studies of the thick disk properties are numerous but most of them suffer from serious limitations: local samples of selected stars are biased in favor of metal-poor or high velocity stars, samples of tracers (clusters, RR Lyrae...) are small and not necessary representative of the whole thick disk population, while in situ surveys suffer from lower precision due to the lack of astrometric and spectroscopic observations for faint stars. As a consequence, the parameters of the thick disk are not precisely established.

1.3 Outline of the Present Study

Studies of the kinematics of various stellar populations in the Galaxy, in particular the thick disk and the halo, have long been limited by the availability of large samples of stars with measurements of proper motions, radial velocities, distances, and metallicities. Such a database is required in order to constrain plausible scenarios for the formation and evolution of the Milky Way.

Samples of nearby subdwarf stars with high space motions provide an observationally convenient probe of the structure of the Galaxy far from the Galactic plane. The large proper motion selected stellar samples of Carney, Latham, Laird, and Aguilar (1994, hereafter CLLA) have proved particularly valuable for studying the kinematics and chemical abundances within a few kiloparsecs from the Sun.

The Hipparcos catalogue provides a dramatic increase, qualitatively and quantitatively, of the basic available data of distance and proper motion. The cross-identification of CLLA data with Hipparcos improved the accurate space velocities and standardized metallicities of the subdwarfs. Significant works were done by Reid (1998) and Fuchs, Jahreiss and Wielen (1998; hereafter FJW). FJW discussed the kinematical behavior of the 560 subdwarfs, whose parallaxes and proper motions were improved by Hipparcos, in relation to their metallicities.

In this work, we study the kinematical properties and the luminosity function of thick disk population using our sample of subdwarf stars. However, employing proper motion selected sample could introduce the kinematic bias. This bias can be corrected by weighting each star following the examples of Schmidt (1975), and Dawson et al. (1995) using $1/V_{max}$ method. This bias can also be modeled with assumed velocity ellipsoids for the thick disk, although there remains a significant sensitivity towards the kinematic model used. Contamination from the thin disk population could be a problem, since the density ratio of thick to thin disk $1:10$ (Reid et al. 1995). However, imposing a strict lower proper motion can render this negligible. Halo contamination to the thick disk sample can be avoided by imposing a tangential velocity cut-off.

Many studies have employed the method of proper motion selection to determine the spheroid luminosity function, simply because it remains the most efficient method for obtaining samples of local spheroid stars. We will use this method to derive the ’bright end’ thick disk luminosity function. We perform a monte carlo simulation of the sample to allow the biases and effects of sample selection to be taken into account, so the luminosity function could be corrected or at least, correctly interpreted.

We analyzed the fine structure of the phase space distribution function of subdwarfs using a search strategy based on Dekker’s theory of galactic orbits to find overdensely populated regions. The star streams could probably relate to dynamical perturbation by spiral density wave or as part of the tidal debris debris of a disrupted satellite galaxy accreted by the Milky Way.

In the next chapter, we will explain the theoretical backgrounds of the subdwarfs, kinematics of stars in the Galaxy and the method to derive the luminosity function, and the procedure of the monte carlo simulation used in this work. Chapter 3 is focused on the kinematic analysis of the subdwarf data, this chapter is based on paper of Arifyanto et al (2005). In the chapter 4, we will derive the ’bright end’ luminosity function of the thick disk. The fine structure in the phase space distribution of our subdwarf sample will be explained in chapter 5. The last chapter will be the summary and conclusions.

2 Basic Theories

2.1 Subdwarf Stars

Adams and Humanson (1935) called attention to a groups of stars located between the main sequence and white dwarfs, which they called as 'intermediate white dwarfs'. They noted that the hydrogen lines of these stars were narrow and sharp and the metallic lines faint. These stars were later called subdwarfs by Kuiper (1939) since he found them more similar to dwarfs than to white dwarfs. He defined them as stars not over 2-3 magnitudes below the main sequence and described the spectra of objects earlier than about G5 in terms similar to those of Adams et al. (1935).

Subdwarfs are seen to share several interesting properties :

- a spectrum with weak metallic lines
- an ultraviolet (photometric) excess
- a position in the HR diagram below the main sequence
- a large space velocity.

In practice it is found that none of the four characteristics taken individually suffices to define 'subdwarfs'. The spectroscopic criterion is insufficient, because λ Boo stars and Horizontal Branch stars also satisfy this criterion. If we consider the position in the HR diagram, we find that (usually) a trigonometric parallax is either unavailable or not, if it exists, has such a large possible error to make the absolute magnitude poorly determined and the space velocity suffers equally. Therefore, many authors do not use space velocities. Instead they use a very large proper motion or a very large radial velocity (eg. CLLA). If we add the condition that the object must be a permanent member of our Galaxy, its space velocity (V)should be smaller than 400 or 500 kms^{-1} (Jaschek & Jaschek 1987).

Eggen (1979) defined subdwarfs as old, metal poor, high velocity dwarfs. He suggest as a limit $[Fe/H] < -0.6$ and for the space velocity $V > 140kms^{-1}$. This definition seems clear but uses age and composition as parameters which are not easily obtainable. In practice, the 'age' is replaced by space velocity and 'composition' by a photometric weakness-of-line index (Jaschek & Jaschek 1987).

From their large space velocity, the subdwarf stars are belong to the high velocity stars group. This group is defined in a purely kinematic way. A star is called as a 'high velocity object' (HV) if its space velocity is larger than a limiting velocity V.Observation has shown that stars in the solar neighborhood have symmetric velocity distribution up to $V = 62kms^{-1}$, but for higher values the distribution becomes strongly asymmetric. We recall that the space velocity

$$V = (V_r^2 + 4.74\mu^2 d^2)^{1/2} \tag{1}$$

where V_r is the radial velocity corrected by solar motion, μ the total proper motion (in "/year) and d the distance (in pc). V_r and μ can be measured very accurately, but V usually has a large uncertainty from d. Since an error in d propagates into V, a certain number of HV stars appear as such only because of large errors in d. Authors prefer to use a condition on μ alone as a definition of HV stars (eg. CLLA).

In terms of stellar population (see sections 2.1.2 and 2.1.3), the metal-poor subdwarfs are belong to thick disk and halo objects. Eggen (1983) separates these two population stars according to abundance, and defines a halo star as an object with $[Fe/H] \leq -0.6$. GWK argued that the thick disk population has dominated metallicity group $[Fe/H] > -1$ with mean $< [Fe/H] >= -0.6$. While the halo population has $[Fe/H] < -1$.

2.2 Galactic Space Velocities

In order to study the kinematics of nearby stars, one should calculate the galactic space velocity components (*U*, *V*, and *W*) for given proper motion, radial velocity, and parallax. We will use a right-handed coordinate system for *U*, *V*, and *W*, so that they are positive in the directions of the Galactic center, Galactic rotation, and the North Galactic Pole (NGP), respectively. Some authors prefer a left-handed system for *U*, *V*, and *W*, in which *U* is positive toward the Galactic anticenter.

All coordinates used must be for equinox J2000, because that is the system used to define galactic coordinates. In the following, α and δ are equatorial coordinates, while *b* and *l* are galactic latitude and longitude, respectively. The galactic coordinate system is defined by three angles. Some authors use the equatorial position of the North Galactic Pole :

$$\alpha_{NGP} = 12^h 51^m = 192.85948^\circ$$
$$\delta_{NGP} = +27.12825^\circ$$

The third angle, i, is the inclination angle between the galactic equator to the equatorial plane. The point where these two great circles cross is the Node point (α_{Node} and l_{Node}):

$$\begin{aligned} \alpha_N &= 282.86^\circ \\ l_N &= 32.93^\circ \\ i &= 62.87^\circ \end{aligned} \quad (2)$$

Here we will use the last terms to calculate the galactic position and space velocity.

2.3 Transforming Coordinates and Velocities

We will also use the following quantities:

π , the parallax in miliarcsec,
V_r , the radial velocity in kms^{-1},
$\mu''_\alpha = 15\mu^s_\alpha \cos\delta$, the proper motion in right ascension, corrected for declination, in miliarcsec yr^{-1},
μ_δ , the proper motion in declination, in miliarcsec yr^{-1}.

The local velocity components of stars are :

$T_\alpha = \kappa\ \mu_\alpha/\pi$, tangential velocity in right ascension in kms^{-1},
$T_\delta = \kappa\ \mu_\delta/\pi$, tangential velocity in declination in kms^{-1},
V_r , radial velocity

where $\kappa = 4.74045539 \times 10^{-3}$. Transformation matrix to calculate equatorial components from local ones

$$\mathbf{T} = \begin{pmatrix} -\sin\ \alpha & -\cos\ \alpha \sin\ \delta & \cos\ \alpha \cos\ \delta \\ \cos\ \alpha & -\sin\ \alpha \sin\ \delta & \sin\ \alpha \cos\ \delta \\ 0 & \cos\ \delta & \sin\ \delta \end{pmatrix}. \quad (3)$$

Matrix for transforming equatorial components into galactic components is given as

$$\mathbf{A} = \begin{pmatrix} \cos\, l_N \cos\, \alpha_N + \sin\, l_N \sin\, \alpha_N \cos\, i & \cos\, l_N \sin\, \alpha_N - \sin\, l_N \cos\, \alpha_N \cos\, i & -\sin\, l_N \sin\, i \\ \sin\, l_N \cos\, \alpha_N - \cos\, l_N \sin\, \alpha_N \cos\, i & \sin\, l_N \sin\, \alpha_N + \cos\, l_N \cos\, \alpha_N \cos\, i & -\cos\, l_N \sin\, i \\ \sin\, \alpha_N \sin\, i & -\cos\, \alpha_N \sin\, i & \cos\, i \end{pmatrix}. \quad (4)$$

Using the values of α_N,l_N, and i as written in eq. (2.2) the transformation matrix becomes

$$\mathbf{A} = \begin{pmatrix} -0.0548655 & -0.873456 & -0.483802 \\ 0.494138 & 0.20618 & 0.746987 \\ -0.867651 & -0.198081 & 0.456011 \end{pmatrix}. \quad (5)$$

The galactic coordinate components are then,

$$\begin{pmatrix} X \\ Y \\ Z \end{pmatrix} = \mathbf{A} \bullet \begin{pmatrix} \cos\, \alpha \cos\, \delta \\ \sin\, \alpha \cos\, \delta \\ \sin\, \delta \end{pmatrix} \bullet \frac{1}{\pi} \quad (6)$$

and the galactic space velocity components,

$$\begin{pmatrix} U \\ V \\ W \end{pmatrix} = \mathbf{T} \bullet \mathbf{A} \bullet \begin{pmatrix} T_\alpha \\ T_\delta \\ V_r \end{pmatrix} \quad (7)$$

Table 3: Standard, basic, and peculiar solar motion

Solar motion	$U_\odot$	$V_\odot$ (kms^{-1})	$W_\odot$	$v_\odot$	Apex of motion α		δ
Standard	10.0	5.2	7.2	13	270°	(1900)	+30°
Basic	9	11	6	15.4	267°.4	(1950)	+25°
Peculiar	9	12	7	16.6	267°.0	(1950)	+28°

2.4 Correction for the Solar Motion and LSR

The above velocities are heliocentric. The adjustment for the motion of the Sun within a rotating Galactic frame of reference depends on what is chosen as a comparison. The *standard solar motion* is an implicit kinematics definition of the LSR[1] from the mean motion of nearby gas and stars. *The basic solar motion* is an implicit kinematic definition of the LSR from the maximum in the kinematics of nearby stars. *The peculiar solar motion* is a dynamical definition, derived from extrapolation of the asymmetric drift-velocity dispersion relation to zero dispersion (Cox 2000).

We adopt the standard solar motion (Dehnen & Binney, 1998)for correction of solar motion. And the rotation velocity of the LSR about the Galactic center is taken to be $-220\,km\,s^{-1}$.

After correcting the galactic space velocity for the solar motion, we transform them into cylindrical space velocities : *U'*,*V'*, and *W'*:

$$\begin{aligned} U' &= U\cos\phi - V\sin\phi \\ V' &= U\sin\phi + V\cos\phi \\ W' &= W \end{aligned} \tag{8}$$

where,

$$R_\odot = 8500 \text{ pc, Galactocentric distance of the Sun}$$

$$R = \sqrt{Y^2 + (R_\odot - X)^2} \tag{9}$$

$$\cos\phi = (\frac{Y}{R}) \tag{10}$$

$$\cos\phi = (\frac{R_\odot - X}{R}). \tag{11}$$

2.5 Asymmetric Drift

The **asymmetric drift** v_a of a stellar population is defined as the difference between the circular velocity at local standard of rest (LSR) and the mean rotation velocity of this stellar population. The empirical relationship of the asymmetric drift is

$$v_a \equiv v_c - \overline{v_\phi} \simeq \frac{\overline{v_R^2}}{D} \tag{12}$$

[1]The Local Standard of Rest (LSR) is defined as the origin of a velocity system corrected for solar peculiar motion. It is defined empirically, from the mean motion of nearby stars, the kinematic definition, or from the local circular velocity, the dynamical definition

where v_c is the circular speed, v_ϕ rotational velocity, $\overline{v_R^2}$ radial velocity dispersion and $D \simeq 120\, km\, s^{-1}$ (Mihalas & Binney, 1981).

We can now show that this relationship is a consequence with the Jeans equation in cylindrical coordinates

$$\frac{\partial(\nu\overline{v}_R)}{\partial t} + \frac{\partial(\nu\overline{v_R^2})}{\partial R} + \frac{\partial(\nu\overline{v_R v_z})}{\partial z} + \nu(\frac{\overline{v_R^2} - \overline{v_\phi^2}}{R} + \frac{\partial\Phi}{\partial R}) = 0. \tag{13}$$

Since the sun lies close to the galactic equator, we may evaluate equation at $z = 0$, and that $(\partial\nu/\partial z) = 0$ by symmetry (Binney & Tremaine 1987),

$$\frac{R}{\nu}\frac{\partial(\nu\overline{v_R^2})}{\partial R} + R\frac{\partial(\overline{v_R v_z})}{\partial z} + \overline{v_R^2} - \overline{v_\phi^2} + R\frac{\partial\Phi}{\partial R} = 0. \tag{14}$$

Define the **azimuthal velocity dispersion** σ_ϕ^2 by

$$\sigma_\phi^2 = \overline{(v_\phi - \overline{v}_\phi)^2} = \overline{v_\phi^2} - \overline{v}_\phi^2, \tag{15}$$

and substitute $R(\partial\Phi/\partial R) = v_c^2$, we obtain

$$\begin{aligned}\sigma_\phi^2 - \overline{v_R^2} \quad &- \quad \frac{R}{\nu}\frac{\partial(\nu\overline{v_R^2})}{\partial R} + R\frac{\partial(\overline{v_R v_z})}{\partial z} = v_c^2 - \overline{v}_\phi^2 \\ &= \quad (v_c - \overline{v}_\phi)(v_c + \overline{v}_\phi) = v_a(2v_c - v_a).\end{aligned} \tag{16}$$

After some mathematical treatments, we have then

$$\frac{2v_c v_a}{\overline{v_R^2}} \simeq [\frac{\sigma_\phi^2}{\overline{v_R^2}} - \frac{3}{2} - 2\frac{\partial \ln\nu}{\partial \ln R} + \frac{1}{2}\frac{\overline{v_z^2}}{\overline{v_R^2}} \pm (\frac{\overline{v_z^2}}{\overline{v_R^2}} - 1)] \tag{17}$$

where the sign ambiguity covers the range of possible behavior of the velocity ellipsoid near the Sun. If we assume that $\sigma_\phi^2 \simeq \overline{v_z^2} \simeq 0.45\overline{v_R^2}$, that the disk of our Galaxy is exponential,

$$\nu = \nu_0 \exp(-R/R_d), \tag{18}$$

with $R_0/R_d = 2.4$, and that $v_c = 220\, kms^{-1}$, we can use equation (2.17) to find $v_a \simeq \overline{v_R^2}/(110 \pm 7kms^{-1})$, which is in a good agreement with the empirical value $D \simeq 120kms^{-1}$ in equation (12).

2.6 The Luminosity Function

The density of stars varies from point to point within the galaxy. Moreover, within any volume of space there will be both luminous and faint stars. Let the number dN of stars with absolute magnitudes in $(M + dM, M)$ in the volume $d^3\mathbf{x}$ around the point **x** be

$$dN = \Phi(M, x) dM d^3x. \tag{19}$$

To a first approximation it is useful to imagine that the mix of stars of different luminosities is the same everywhere. To express this idea mathematically we approximate the function $\Phi(M, x)$ defined above by the product of two functions $\Phi(M)$ and $\nu(x)$. That is, we write

$$dN = [\Phi(M)dM] \left[\nu(x)d^3x\right] . \tag{20}$$

$\Phi(M)$ is called a luminosity function, which measures the relative fractions of stars of different luminosities, while $\nu(x)$ measures the total number density of stars at the point x. In its simplest form, Φ gives the distribution over luminosity of stars irrespective of their spectral or physical types. In this case we call Φ the general luminosity function.

The Luminosity Function (LF) is basically a histogram, showing the number of stars in consecutive absolute magnitude cells, each cells one or half magnitude wide, and constructed from all stars within a fixed volume space (unit: stars pc^{-3} mag^{-1}).

Malmquist Bias

Most methods for determining a luminosity function involve counting the number dN/dm of objects that have apparent magnitudes in the range $(m + dm, m)$ and that lie within some given area of the sky. The star-count function $A(m) \equiv \frac{dN}{dm}$ clearly depends on both the spatial distribution of the objects and on their luminosity function. Since it is impossible to determine $A(m)$ to arbitrarily faint magnitudes, there will be some limiting magnitude m_l such that $A(m)$ is available only for $m < m_l$. The simplest sample of objects upon which $A(m)$ could be based is magnitude-limited in that it consists of all objects brighter than m_l that lie within a specified area of the sky.

It is not hard to see that the mean absolute magnitude of objects in such a sample will be brighter than the mean absolute magnitude of the population as a whole : the volume within which we can see the most luminous objects is larger than that within which we can also see the faintest objects (a volume-limited sample). Consequently, luminous objects are over-represented in a magnitude-limited sample. Or in term of absolute magnitude, the mean absolute magnitude of stars of a given spectral type in an apparent magnitude limited sample ($\overline{M_m}$) is brighter than the mean absolute magnitude of a volume-limited sample (M_0). This effect is called Malmquist bias after the Swedish astronomer K.G. Malmquist (Malmquist 1922, Malmquist 1936). The systematic bias is expressed by

$$\Delta M = M_m - M_0 = -\sigma \frac{1}{N} \frac{dN}{dm}, \tag{21}$$

where σ is the rms (cosmic) scatter in absolute magnitude and $N(m)$ is the differential number counts for objects of absolute magnitude M.

The correction for these biases is discussed in detail in Stobie et al. (1989), and we follow their technique for estimating corrections for it. They derive (for a uniform space density of stars and an uncertainty in the absolute magnitude σ) a correction $\Delta\Phi$ which must be added to the actual luminosity function Φ to produce the observed LF Φ_{obs},

$$\frac{\Delta\Phi}{\Phi} = \frac{1}{2}\sigma \left[(0.6 \ln 10)^2 - 1.2 \ln 10 \frac{\Phi'}{\Phi} + \frac{\Phi''}{\Phi} \right]. \tag{22}$$

Tinney, Reid & Mould (1993) then used equation 22 to obtain a first-order estimate of the size of this correction. They assumed,

$$\frac{\Delta\Phi}{\Phi} \approx \frac{\delta\Phi_{obs}}{\Phi_{obs}} \tag{23}$$

$$= \frac{1}{2}\sigma \left[(0.6 \ln 10)^2 - 1.2 \ln 10 \frac{\Phi'_{obs}}{\Phi_{obs}} + \frac{\Phi''_{obs}}{\Phi_{obs}} \right], \tag{24}$$

and evaluate an approximation to the true LF by subtracting corrections from the observed LF,

$$\Phi \approx \Phi_{obs} - \frac{\Delta\Phi_{obs}}{\Phi_{obs}}. \tag{25}$$

Lutz-Kelker Bias

A major problem in using trigonometric parallaxes is the systematic error in luminosity calibrations due to the combination of accidental errors of observation with the steeply sloping true parallax distribution. This effect, known as the Lutz-Kelker bias, causes an observed parallax to be on average higher than its true value (Lutz & Kelker, 1973, LK). This overestimate translates into an underestimate of distance, and hence an underestimate of an object's luminosity as derived from its apparent brightness. After the Hipparcos, this bias and its eradication are of some importance.

LK undertook the first quantitative analysis of this effect, which has the same source as Malmquist bias. They determined specific corrections for the case of a uniform stellar distribution, i.e., a parallax distribution, $P(\phi) \propto \pi^{-4}$. Smith (1987) has shown that their calculations can be described by the empirical formula

$$\Delta M_{LK} = 5 \times \log \left\{ [1 + \sqrt{1 - 19(\frac{\sigma_\pi}{\pi})^2}]/2 \right\} \tag{26}$$

Hanson (1979) has demonstrated that the constant-density LK corrections are seldom relevant for analyzing observational samples, where magnitude and proper-motion limits can modify the selection effects. He derived a more general analytic representation of the LK corrections. If the parallax distribution can be characterized as a power law, $P(\pi) \propto \pi^{-n}$, then the LK correction can be approximated as

$$\Delta M_{LK} = -2.17 \times \left[\left(n + \frac{1}{2} \right) \left(\frac{\sigma_\pi}{\pi} \right)^2 + \left(\frac{6n^2 + 10n + 3}{4} \right) \left(\frac{\sigma_\pi}{\pi} \right)^4 \right] \tag{27}$$

Fig.4 (or Fig.1 Reid, 1997) shows, a smaller value of n leads to lower predicted corrections: with fewer stars at smaller parallax, the probability of overestimating an individual parallax measurement is correspondingly reduced. The appropriate exponent to use for a given sample can be estimated empirically using the cumulative proper-motion distribution of the sample of stars for which one has parallax data. If $P(\pi) \propto \pi^{-n}$, and the stellar velocity distribution does not vary significantly within the sampling volume, then $N(\mu) \propto \mu^{-n+1}$.

We adopt the value of the parameter $n = 4$ in calculating the LK absolute magnitude corrections. The resultant LK corrections of our subdwarf sample, which has a mean uncertainty of 11%, amount to only -0.13 mag, but rise to -1.43 mag as the precision drops to 30 %.

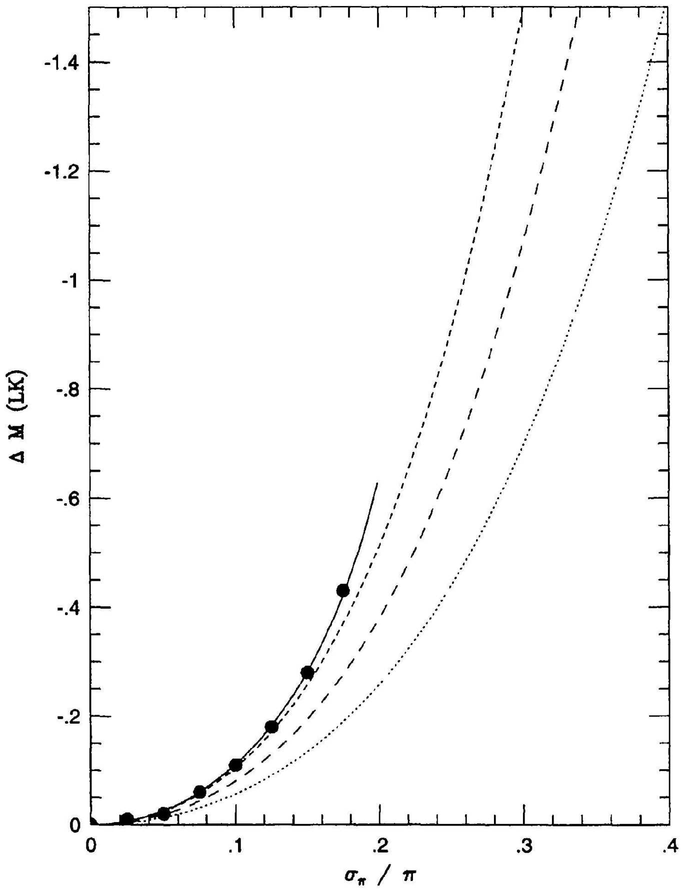

Figure 4: Lutz-Kelker corrections. The solid points mark the systematic offset in M_V as a function of σ_π/π calculated originally by LK and the solid line shows Smith's (1987) analytic representation of these data points. The dotted, long-dashed and short-dashed lines outline the corrections predicted by Hanson's formula for $n = 2, 3,$ and 4, respectively, where n is the exponent of a power-law parallax distribution. The $n = 4$ (uniform density) case is equivalent to the original LK analysis (Fig.1 of Reid (1997))

The Generalized Schmidt's V_{max} Method

Three decades have been passed ever since Schmidt (1975) first intended to determine a LF of halo stars with only 18 high velocity stars using his proposed $1/V_{max}$ method (Schmidt, 1968). This method is to construct a complete magnitude-limited sample and to estimate the maximum distance at which each star in the sample could be seen. This distance, and the solid angle covered by the sample, allow a "maximum volume" (or V_{max}) to be calculated for each star, which is the largest volume of space over which that star could be detected in, given the proper motion and magnitude limits of the survey. This technique implicitly corrects for any bias arising from the proper motion selection.

Felten (1976) shown, that the sum of the inverse of these V_{max} values in a given luminosity bin is an unbiased estimator of $\Phi(M_V)dM_V$. The $1/V_{max}$ technique is essentially a method of allowing the distance limit of a "distance-limited" sample to vary with luminosity. It allows more intrinsically bright objects to be counted in the sample, so that the maximum available information on the LF is extracted (Tinney et al, 1993).

The original $1/V_{max}$ method assumes that the sample is selected from a uniformly distributed population. In reality, stars in the solar neighborhood are concentrated in the plane of the galactic disk. However the effects of a space-density gradient can be allowed for by assuming a density law, as shown by Stobie et al. (1989) and Tinney et al. (1993), by defining a generalized volume V_{gen} enclosed within a distance d,

$$V_{gen} = \Omega \int_0^d \frac{r^2 \rho dr}{\rho_0}, \tag{28}$$

where Ω is the solid angle covered by the sample, ρ_0 is the local space density and r is a distance. We assumed that the local density can be represented by an exponential disk of scale height h,

$$\frac{\rho}{\rho_0} = \exp^{-(z/h)} = \exp^{-(r \sin b)/h}, \tag{29}$$

where z is distance perpendicular to the galactic plane, and b is the galactic latitude. By a straightforward substitution we therefore derive,

$$V_{gen} = \Omega \frac{h^3}{\sin^3 b} \left\{ 2 - (\xi^2 + 2\xi + 2) \right\}, \tag{30}$$

where $\xi = r(\sin b)/h$. We can then construct (by analogy with the $1/V_{max}$ LF) an unbiased estimator for the local LF Φ as the sum of the inverses of the maximum values of V_{gen} available to stars in a luminosity bin of width dM_V centered at M_V. That is, for a star of a given M_V (from which we derive r_{max}), the maximum generalized volume V_{max} is given by

$$V_{max} = \Omega \int_0^{r_{max}} \frac{r^2 \rho dr}{\rho_0}, \tag{31}$$

which can be evaluated using eq. (30) for $\xi = (r_{max} \sin b)/h$, and so that,

$$\Phi = \sum \frac{1}{V_{max}}. \tag{32}$$

If we have a sample with a lower proper-motion limit μ_l and a faint apparent magnitude limit m_f, the maximum distance r_{max} over which any star can contribute to the sample is given by

$$r_{max} = \pi^{-1} \ \max \left[\frac{\mu}{\mu_l}; 10^{0.2(m_f - m)} \right], \tag{33}$$

where π is the parallax, μ is the proper motion, and m is the apparent magnitude. Similarly, if the sample is complete only to an upper proper-motion limit μ_u and a bright apparent magnitude m_b, the minimum distance for inclusion would be

$$r_{min} = \pi^{-1} \ \min \left[\frac{\mu}{\mu_u}; 10^{0.2(m_b - m)} \right]. \tag{34}$$

Finally, if the sample covers only a fraction β of the sky, then the maximum volume in which a star can contribute to the sample is

$$V_{max} = \frac{4}{3}\pi\beta \int_{r_{min}}^{r_{max}} \frac{r^2 \rho dr}{\rho_0}, \tag{35}$$

with $\Omega = \frac{4}{3}\pi\beta$.

In estimating the errors in the LF we adopt the assumption of Poissonian errors (Felten, 1976),

$$\sigma_\Phi = \sum \frac{1}{V_{max}^2}. \tag{36}$$

The $\langle V/V_{max} \rangle$ Test

The overall completeness of the stellar sample can be estimated by using the $\langle V/V_{max} \rangle$ test. For each star the ratio of the volume V (corresponding to its distance

r) to V_{max} is calculated, and the mean of this quantity should be 0.5 for a complete survey evenly sampling the survey volume. The error in this mean is $1/(12N)^{\frac{1}{2}}$, where N is the number of stars in the sample.

$$\left\langle \frac{V}{V_{max}} \right\rangle = \left\langle \left(\frac{r}{r_{max}} \right)^3 \right\rangle \tag{37}$$

2.7 Correction for Kinematic Bias

Consider a stellar population with local galactic kinematics characterized by their known average velocity components in galactic coordinates $\langle U \rangle, \langle V \rangle$, and $\langle W \rangle$, with corresponding velocity dispersions σ_U, σ_V, and σ_W. Denote by $\tau(t)$ the resulting distribution of tangential speeds relative to the local standard of rest, such that $\tau(t)dt$ is the fraction of stars having tangential speeds between t and $t + dt$. From this population a complete sample is selected such that every star in the sample has an annual proper motion $\mu \geq \mu_0$. If μ_0 is sufficiently large to ensure that the sample stars are nearby, then it is safe to assume that they have a constant space density ρ. A complete shell of thickness dr at distance r has a volume of $4\pi r^2 dr$, and contains $4\pi r^2 \rho dr$ stars. Of those, only the fraction with tangential speeds $t \geq k\mu_0 r$, where $k = 4.74$, will be included in a catalogue whose entries have $t \geq \mu_0$, and only they can contribute to the sample's distribution of tangential speeds, which is denoted by $C(t \mid \mu)$ (the conditional distribution of t, given μ). It follows that

$$C(t \mid \mu) \propto 4\pi\rho \int_0^\infty r^2 \tau(t) H(t - k\mu_0 r) dr, \tag{38}$$

where

$$H(t - k\mu_0 r) = \begin{cases} 1, & \text{if } t \geq k\mu_0 r \\ 0, & \text{otherwise} \end{cases} \tag{39}$$

is the unit step function. The proportionality constant depends on the form of $\tau(t)$. The equation is readily evaluated to demonstrate that

$$C(t \mid \mu) \propto \tau(t) \int_0^\infty r^2 H(t - k\mu_0 r) dr, \tag{40}$$

$$\propto t^3 \tau(t) \tag{41}$$

in the general case. To cite a specific example, if

$$\tau(t) = \frac{t}{\sigma^2} \exp\left(-\frac{t^2}{2\sigma^2}\right), \tag{42}$$

(a convenient, and not unrealistic, description) then, properly normalized,

$$C(t \mid \mu) = \frac{1}{3}\sqrt{\frac{2}{\pi}}\frac{t^4}{\sigma^5} \exp\left(-\frac{t^2}{2\sigma^2}\right). \tag{43}$$

The significance of expression (40) in the present context is its implicit suggestion that it may be worthwhile to explore the possibility of weighting a star's velocity components by some factor proportional to t^{-3} in order to reduce or eliminate kinematic bias in a proper motion-selected sample of which it is a member. An obvious choice for that weight factor is the quantity V_{max}^{-1} (Eq. 31 and 35).

In the simplest case, all of the sample stars have $r_{max} = \mu r/\mu_0$. Since $\mu r = t/k$, then

$$V_{max}^{-1} = \frac{3(k\mu_0)^3}{4\pi\beta\, t^3} \tag{44}$$

which has the sought-for t-dependence.

Dawson et al. (1995) used the $1/V_{max}$ as weight to the stellar kinematic data of high proper motion stars of old disk population, yields the velocity ellipsoid in very good agreement with one based on a kinematically unbiased sample.

2.8 Monte Carlo Simulation

Sandage & Fouts (1987) have suggested that the halo was formed during a very rapid collapse, on a time scale of a few $\times 10^8$ years, in which there was continuous chemical enrichment and increasing spin-up with time. Their argument based on an analysis of UBV data for kinematically selected stars, which had a linear dependence of rotational velocity about the Galactic center on abundance (in the range $-2.3 < [\mathrm{Fe/H}] < 0.2$). However, Norris (1986) found a nonlinear dependance suggestive of a decoupling of the halo and disk components of the Galaxy, based on non-kinematically selected samples. Norris & Ryan (1989) presented Monte Carlo Simulation of Sandage & Fouts (1987) selection criteria and examine the role of errors of observation and calibration in their analysis and found that the decoupling of disk and halo is still evident in kinematically selected object.

Monte Carlo sampling of a model of the population being studied allows the biases and effects of the analysis procedure to be taken into account, and the results corrected for these effects. The technique permits numerous different effects operating simultaneously to be followed through the stages of sources selection, observation, and analysis, to determine the net effect of numerous (and possibly inter-connected) influences (Ryan & Norris, 1993). Richstone & Graham (1981) used a combination of analytic and Monte Carlo procedures in their efforts to compensate halo density estimates made from high proper motion star data for exclusion of low velocity stars. Bahcall & Casertano (1986) seek not only to determine the incompleteness in measurements of the halo density, but also tried to estimate the degree to which the observed kinematics were biased. Dawson et al (1995) used a simple technique for obtaining an unbiased estimate of the parameters of a population's velocity ellipsoid from a complete, proper motion-limited and apparent magnitude-limited sample of member stars by utilizing the Schmidt's $1/V_{max}$ method, and checked by means of a series of Monte Carlo simulations.

The luminosity function derived from the kinematically selected sample (i.e, halo, thick disk or white dwarf population) are expected to have some kinematical biases and distortions. A monte carlo simulations of a model population is expected to allow the biases and effects of sample selection to be – or, at least, correctly interpreted – provided that a detailed simulation from the stage of source selection is performed accurately (García-Berro, et al., 1999). García-Berror & Torres (1997), Wood (1997) and Wood & Oswalt (1998) investigated systematically the statistical uncertainties associated with the derived age of the disk of the white dwarf LF. These authors use the theoretical white dwarf LF obtained from the standard methods to assign probabilities and to assign luminosities to the white dwarf in the simulated sample.

User Inputs

The user inputs to the MC simulations include the initial number of "stars" for each calculation (N_{samp}), number of "stars" in the final sample N_{obs}, region covers by the sample in equatorial system, the maximum distance (in parsecs)for the sample objects D_{max}, velocity ellipsoid ($\sigma_U, \sigma_V, \sigma_W, and V_{asym}$)of certain galactic population (thin disk, thick disk or halo), the lower proper motion limit μ_{min} (in mas per year), the apparent magnitude limit $m_{V,lim}$, and integrated theoretical LF (Bergbusch & Vandenberg, 1992), and the number of simulations (N_{sim}).

We use the following notation : $P(0,1)$ indicates a uniform deviate between the limits 0.0 and 1.0, and $G(\sigma)$ indicates a normal (Gaussian) deviate with variance σ and zero mean. The normal deviate is calculated using the Box-Muller method (cf. Press et al.,1986).

Theoretical Selection

The algorithm at the heart of this MC simulation is quite simple. We populate a volume V_{samp} with N_{samp} objects, drawing our "observationally selected" subsample from this population.

1. We randomly choose two numbers for the equatorial coordinates (α, δ) of each star in the sample within approximately $r < 120$ pc from the Sun, assuming a constant space density.

2. The decision was made as to wether the "star" belongs to the thin disk, thick disk or halo. We then determined its components of space velocity and asymmetric drift by drawing 3 numbers from the normal distribution,

$$U = G(\sigma_U) \quad (45)$$

$$V = V_{asym} + G(\sigma_V) \quad (46)$$

$$W = G(\sigma_W) \quad (47)$$

3. Next is the discrimination based on the LF. For this we use the isochrone from Bergbusch & Vandenberg (1992) as the discriminator; this curve is normalized to a peak of unity on input, and spline interpolation coefficients are computed. For each trial, two uniform deviate random number are drawn. The first of these is scaled to provide a value for absolute magnitude M_V between the maximum and minimum values for the samples,

$$M_{V,test} = P(2,7)\mathrm{mag}. \quad (48)$$

The spline-interpolated value of the normalized LF at this random trial luminosity, $\Phi_{LFINT}(M_V)$ is compared with the value of the second random number Φ_{test}. If $\Phi_{test} < \Phi_{LFINT}(M_V)$, i.e., if the test point is below the appropriate curve, then the object "exists" in V_{samp} at the location $(\alpha, \delta, r, U, V, W, M_V)$.

4. Given $(\alpha, \delta, r, U, V, W, M_V)$, we compute radial velocity, proper motion, and apparent magnitude.

5. The next step is to determine whether the object makes it into the observationally selected subsample– i.e., whether the proper motion and m_V magnitude are within the the specified observational limits.

2.9 The Wavelet Transform

The concept of the wavelet transform was introduce by Morlet in 1983 for the analyzing of seismic data (Goupillaud et al., 1984). Since his pioneering work and taking benefit of developments especially carried out in France, other kind of signals, in one or two-dimensional form, have been analyzed (Daubechies et al., 1986), sound, speech recognition, images, fractal structures etc. In astronomy, the wavelet transform was used to study the galaxy distribution (Slezak et al., 1990), analyzing satellite data, finding substructure in the distribution of stars (Skuljan et al., 1999), etc.

The basic ide is elementary. The wavelet transform of a signal $s(x)$ with respect to the analyzing wavelet $g(x)$, which has always a zero mean and can be complex-valued, is the 2D function

$$h(x, a) = s(x) \otimes \frac{1}{a^{1/2}} g(\frac{x}{a}), \tag{49}$$

where $\otimes$ is the correlation symbol and a a scale variable.

Each of its values is the product of the signal with an elementary bounded function, a wavelet, which is constructed from $g(x)$ by means of dilatations and translations; the signal is decomposed on a wavelet basis. Owing to the localization, smoothness and oscillating properties of $g(x)$, the half-plane defined by these values, the so-called wavelet coefficients, describes the data both in space and scale. It results a time-frequency analysis (if x is interpreted as "time"), which differs from the Wigner-Ville's transform one (Slezak et al., 1990).

The Wavelet Analysis

To perform a wavelet transform of a function $f(x, y)$ we define a so-called analyzing wavelet $\psi(x/a, y/a)$, which is another function (or another family of function), where a is the *scale* parameter. By fixing the scale parameter we can select a wavelet of a given particular size out of a family characterized by the same shape ψ. The wavelet transform $w(x, y)$ is then defined as a correlation function, so that at any given point (ξ, η) in the XY plane we have one real value for the transform :

$$w(\xi, \eta) = \int_{-\infty}^{\infty} \int_{-\infty}^{\infty} f(x, y)\psi\left(\frac{x - \xi}{a}, \frac{y - \eta}{a}\right) \mathrm{d}x\mathrm{d}y, \tag{50}$$

which is called the wavelet coefficient at (ξ, η). Since we usually work in a discrete case, having a certain finite number of bins in our XY plane, this means that we shall have a finite number of wavelet coefficients, one value per bin.

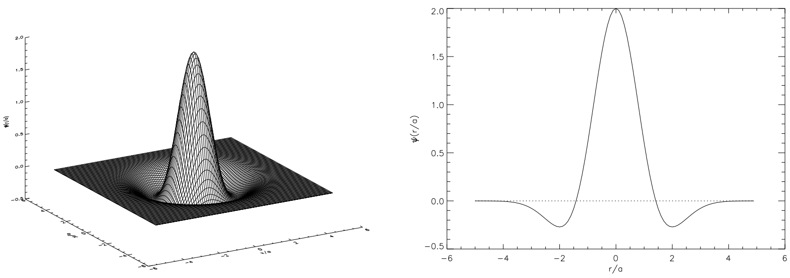

Figure 5: The Mexican hat in two and three dimensions

The actual choice to analyze the wavelet ψ depends on the particular application. When a given data distribution is searched for certain groupings (overdensities) then a so called Mexican hat is most commonly used (Skuljan et al., 1999). A two dimensional Mexican hat (Fig. 5) is given by:

$$\psi(r/a) = \left(2 - \frac{r^2}{a^2}\right) e^{-r^2/2a^2}, \tag{51}$$

where $r^2 = x^2 + y^2$. The main property of the function ψ is that the total volume is equal to zero, which is what enables us to detect any over-densities in our data distribution (Skuljan, et al, 1999). The wavelet coefficients will be all zero if the analyzed distribution is uniform; but if there is any significant 'bump' in the distribution, the wavelet transform will be give a positive value at that point.

If we normalize the Mexican hat using a factor a^{-2}, then we will be able to estimate the half-width of the 'bump', by simply varying the scale parameter a: the wavelet coefficient in the center of the bump will reach its maximum value if the scale a is exactly equal to σ, assuming that the 'bump' is a Gaussian of the form: $\exp(-\rho^2/2\sigma^2)$, ρ being the distance from the center.

3 Kinematics of Subdwarf Stars

Studies of the kinematics of various stellar populations in the Galaxy, in particular the thick disk and the halo, have long been limited by the availability of large samples of stars with measurements of proper motions, radial velocities, distances, and metallicities. Such data are required in order to constrain plausible scenarios for the formation and evolution of the Milky Way. Samples of nearby subdwarf stars with high space motions provide an observationally convenient probe of the structure of the Galaxy. The large, proper-motion-selected, stellar samples of Carney, Latham, Laird, and Aguilar (1994, hereafter CLLA) have proved particularly valuable for studying the kinematics and chemical abundances within a few kiloparsecs of the Sun.

The correlation between kinematics and metallicity gives useful information for formulating theories of galactic structure. Differences in chemistry and space velocities are crucial in defining the different populations within the Galaxy and inferring their origins. Relevant studies of the kinematical behavior of stars ,in particular in relation to their metallicities ,were presented by e.g. Morrison, Flynn, & Freeman (1990, hereafter MFF) using a sample of K giants whose metallicities are measured using the DDO photometric system, Nissen & Schuster (1991) using late F and G dwarfs and subgiants, Chiba & Yoshii (1998) using red giants and RR Lyrae stars, Martin & Morrison (1998) with a sample of nearby RR Lyrae stars and Chiba & Beers (2000) using 1203 metal-poor solar-neighborhood stars.

The Galactic halo is characterized by a roughly spherical space distribution with close to zero net rotation. Its stars are metal poor, with a peak metallicity at [Fe/H] $= -1.6$ (Laird et al. 1988). The halo population in the solar neighborhood is not purely a relic of a monolithic, “rapid” collapse (Carney et al. 1996). There have been several suggestions of a two-component halo, with a flattened component in the inner halo and a more spherical outer halo (Sommer-Larsen & Zhen 1990; Carney et al. 1996).

The Galactic thick disk is the kinematically hottest portion of the disk of the Galaxy, with a scale height of 1.0 to 1.5 kpc and rotates with a velocity of about 170 km s^{-1} (Gilmore, Wyse, & Kuijken 1989). The thick disk is usually considered to be dominated by stars in the range [Fe/H] > -1 (Freeman 1987), peaking at about [Fe/H] $= -0.5$ (Carney et al. 1989). Many workers have claimed the existence of a metal weak tail of the thick disk component in the range $-1.6 \leq$ [Fe/H] ≤ -1 (MFF; Beers & Sommer-Larsen 1995; Chiba & Beers 2000). MFF found a fraction of 72% of the stars in this metallicity range in a "metal-weak thick disk" (MWTD), rotating rapidly at $V_{\rm rot} \approx 170$ km s$^-1$. Another large fraction of MWTD was found also by Beers & Sommer-Larsen 1995). Their MWTD, rotating at $V_{\rm rot} \approx 195$ km s$^-1$, accounts for about 60 % of the stars in the range $-1.6 \leq$ [Fe/H] ≤ -1 in the solar neighborhood, and it possesses an extremely metal-weak tail down to [Fe/H] ≤ -2. Chiba & Beers (2000) estimated the fraction of MWTD at about 30 % of the metal-poor stars in the abundance range $-1.7 \leq$ [Fe/H] ≤ -1, which is smaller than the fraction derived by MFF and Beers & Sommer-Larsen (1995), but larger by $\sim 10\%$ than the result of Chiba & Yoshii (1998) using solar neighborhood red giants and RR Lyrae stars.

The investigation of thick-disk and halo kinematics may only be applicable to a specific place in the Galaxy and may have fine structure of the velocity distribution smoothed out by the velocity resolution of the study (Martin & Morrison 1998). Here, we study the kinematics of solar neighborhood subdwarf stars based on the sample of high proper motion stars by CLLA. CLLA have measured photometric parallaxes, radial velocities, and metallicities of mainly A to early G stars, many late G and some early K stars in the *Lowell Proper Motion Catalogue*. In total the CLLA sample contains 1464 stars. In their paper there are listed 1269 stars with kinematical parameters and 1261 stars with metallicity parameters, and there are 1447 stars with radial velocities in their catalog. The radial velocity precision of their sample lies in the range of 0.4 to 1.3 km s^{-1}. About 15% of their sample are binaries or multiple systems. The typical accuracy of the metallicities was estimated to be ± 0.13 dex.

The photometric parallax of CLLA was replaced in our study by using the high precision parallax of Hipparcos catalogue. We used the *Astrometric Catalog TYC2+HIP* (Wielen et al. 2001) for the proper motions of stars with Hipparcos parallaxes. This catalogue is derived from a combination of the Hipparcos Catalogue with proper motions given in the Tycho-2 catalogue with direct solutions (Wielen et al. 2001) and previous earthbound measurements. We still use the high precision radial velocities and metallicities of the CLLA catalogue for our study. Previous work using Hipparcos subdwarfs was done by Reid (1998) and Fuchs, Jahreiß and Wielen (1998; hereafter FJW). In this previous work we discussed the kinematical behaviour of the 560 subdwarfs for which improved parallaxes and proper motions were obtained by Hipparcos, in relation to their metallicities. In the present paper we increase the size of the sample considerably by applying a correction to the photometric CLLA distances determined using stars with Hipparcos parallaxes.

3.1 The Data

In studying the kinematics of the nearby metal-poor subdwarfs we need the sample of subdwarf stars which include proper motion, radial velocities, distance and metallicities data. Many authors presented catalogues of metal poor halo stars including the subdwarfs, eg. Carney et al. (1990), Ryan & Noris (1991), Nissen & Schuster (1991), Carney et al. (1994).

The data, which we have analyzed for this work, is based on the sample of high proper-motion stars by Carney et al. (1994). They have measured the photometric parallaxes, radial velocities, and metallicities of most of the A, F, and early G, many of the late G, and some of the early K stars in the *Lowell Proper-Motion Catalog*. In their paper, there are 1269 stars with kinematical parameters and 1261 stars with metallicity parameters of the 1464 stars in the complete survey, and there are 1447 stars with radial velocities in their catalogs. The radial velocity precision of their sample lies in the range of 0.4 to 1.3 kms^{-1}. About 15 % of their sample are binaries or multiple systems.

Hipparcos and Tycho astrometric satellite (ESA 1997) are providing accurately parallax and proper motion data of nearby stars. The new parallax data by Hipparcos have led to accurate distance estimates for more extensive sample of nearby halo subdwarfs. The median standard error of Hipparcos parallax and proper motions are 0.97 mas and 0.8 mas/year, respectively (Turon 1999).

The CLLA data set of 1447 stars has been cross-identified with Astrometric Catalogue TYC2+HIP (Wielen et al. 2001) and we found 545 stars in common. But for some stars there were not all data available or some Hipparcos parallax were not accurate enough ($\pi/\sigma_\pi < 3$) for stars with large distances ($\pi < 5\,mas$).

About 700 CLLA stars which are not appeared in the TYC2+HIP Catalogue were cross identified with the Tycho-2 Catalogue (Høg et al. 2000), and we found about 259 stars with Tycho-2 proper motions. The proper motion accuracy of Tycho-2 is about 2.5 mas/yr derived from a comparison with the Astrographic Catalogue and 143 other ground-based astrometric catalogues. CLLA used Luyten's NLTT proper motions for the calculation of the space velocity components. These proper motions have typical errors of 20 to 25 mas/year. Therefore, Hipparcos and Tycho-2 proper motions provide an enormous improvement in the accuracy of the tangential velocities.

We omit the binaries and common proper motion stars because the double weighted stars could influence the distribution. Table 3.1 summarized our samples information.

It should be emphasize here that our present identification was carried out with a limited Hipparcos and Tycho samples. Reid et al. (2001) have searched for unrecognized metal poor subdwarfs in the Hipparcos catalogue and identified 317 stars with precision of better than 15 percent.

Table 4: Sample of Subdwarfs

Sample	N	Parallax	Proper motion	R_V
A	545	Hipparcos	TYC2+HIP	CLLA
B	72	Calibrated Hipparcos	TYC2+HIP	CLLA
C	259	Calibrated Hipparcos	Tycho-2	CLLA

3.2 Selection Criteria

Color Magnitude Diagram

Figure 6 shows the color magnitude diagram for all 545 identified CLLA stars with photometric distance. The absolute magnitudes and their standard errors are based on Hipparcos parallaxes and errors. The B-V colors were taken from Hipparcos catalogue.

Some stars which no distance was given, already recognize by CLLA as subgiant. However, we can see obviously from CM-diagram Fig. 6 that contamination by previously undetected subgiants and giants still present. To avoid these, we should remove all stars lying above a line in the CM-diagram defined by the zero age main sequence of stars with solar metallicity shifted upwards by $\Delta M_V = 0.8\, mag$. About 8% contaminations were found in present investigation.

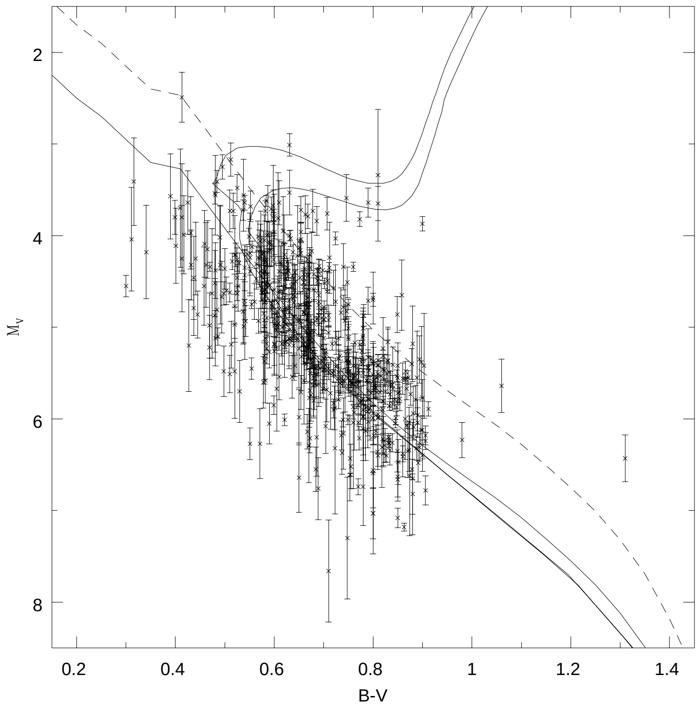

Figure 6: Color-Magnitude-diagram for all identified CLLA stars. Hipparcos parralaxes were used to determined M_V and its standard error. The full lines indicate the mean main sequence and old open clusters M 67 and NGC 188. The dashed line is the ZAMS shifted upward by $\Delta M_V = 0.8$ mag, used to remove the contamination by subgiants and giants

Test of Photometric Parallaxes

We determined the overall correction of the photometric distance scale of CLLA by analyzing the parallax difference. There are 539 CLLA stars which have both photometric and trigonometric parallaxes in our sample (CLLA-TYC2+HIP). We compared the Hipparcos parallaxes with the photometric parallaxes of CLLA (see Fig. 7). The error bars represent both Hipparcos and CLLA parallax errors. A typical error in absolute magnitude of CLLA stars $\Delta M_{\rm V} = 0.3$ mag is assumed. This errors could be corrected to the parallax error using relation

$$\Delta M_{\rm V} = 2.1715 \, \frac{\sigma_{\pi_{\rm phot}}}{\pi_{\rm phot}} \tag{52}$$

where $\pi_{\rm phot}, \sigma_{\pi_{\rm phot}}$ and $\Delta M_{\rm V}$ denote the photometric parallax, the error in photometric parallax and the error in absolute magnitude, respectively.

We used the least χ^2 method applicable when the data have errors in both coordinates to fit our data. The χ^2-function is chosen according to Press et al. (1992)

$$\chi^2 = \Sigma_{i=1}^{N} \frac{(y_i - bx_i)^2}{\sigma^2_{y_i} + b^2\sigma^2_{y_i}} \tag{53}$$

The slope of the regression b derived from our 539 subdwarfs, is $b = 1.116 \pm 0.008$. For comparison, a sample with $\pi_{\rm Hipp} \leq 25$ mas leads to a larger correction of $b = 1.169 \pm 0.028$. We also tried to cut in the metallicities, with the result that for more metal-poor stars a larger correction was needed. For stars with $[Fe/H] > -1.0$, which dominated by thick disk stars, $-1.6 < [Fe/H] < -1.0$, and extreme metal-poor stars with $[Fe/H] < -1.6$ we find slopes of the regression line $b = 1.093 \pm 0.010$, $b = 1.324 \pm 0.042$ and $b = 1.394 \pm 0.043$, respectively.

Since the halo stars in the CLLA sample have an average smaller parallaxes than the disk stars, the latter correction should be applied to halo stars. FJW and Jahreiss et al. (1997) have found similar correction on the basis of a smaller sample of subdwarfs. The data points at the upper right corner of the first plot of Fig. 7 (All Data) and the fourth plot ($-1.6 < [Fe/H] < -1.0$) represent the star HIP 57939, which is the nearest star in our sample with $\pi_{\rm Hip} = 109$ mas. No significant

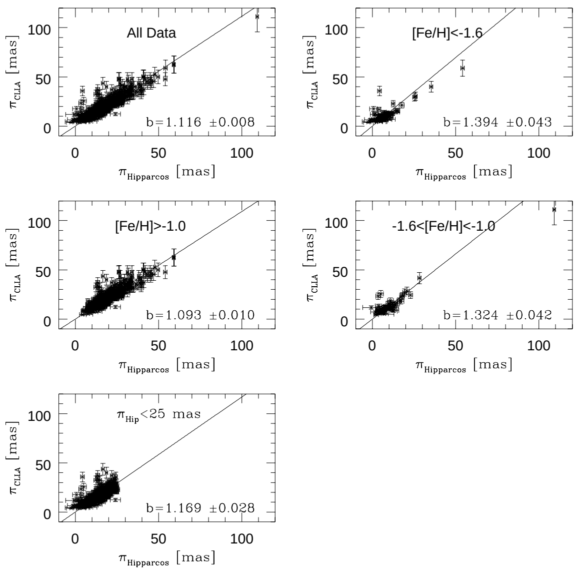

Figure 7: Hipparcos trigonometric parallaxes versus the photometric parallaxes of CLLA, for 539 stars (top-left) and for different metallicity cuts : [Fe/H] < -1.6 (top-right), [Fe/H] > -1 (center-left), $-1.6 \leq$ [Fe/H] ≤ -1 (center-right), and for stars at large distances, $\pi_{\rm Hip} < 25$ mas (bottom-left). The full line is a linear fit to the data.

changes in the slopes of both plots (less than 1σ) are found, if we omit HIP 57939 when calculating the slopes.

All these corrections are used to calibrate CLLA photometric parallaxes in our sample which undetected by Hipparcos and about 35 stars with low accuracy Hipparcos parallaxes ($\pi_{\rm Hip} < 5$ mas and $\sigma_{\pi_{\rm Hip}}/\pi_{\rm Hip} < 3$). There are 740 stars which are survived the selection criteria, 481 subdwarfs have Hipparcos parallaxes and TYC2+HIP proper-motions and 259 with calibrated parallaxes and Tycho-2 proper-motions. We use then these astrometric information to calculate the galactic space velocity of our sample.

3.3 Kinematical Properties

Using the parallaxes supplied by the Hipparcos catalogue, proper motions by the TYC2+HIP and Tycho-2 catalogue, and radial velocities given in CLLA, the space velocity components $U, V,$ and W, which are directed to the Galactic center, direction of galactic rotation, and north galactic pole, respectively, have been calculated

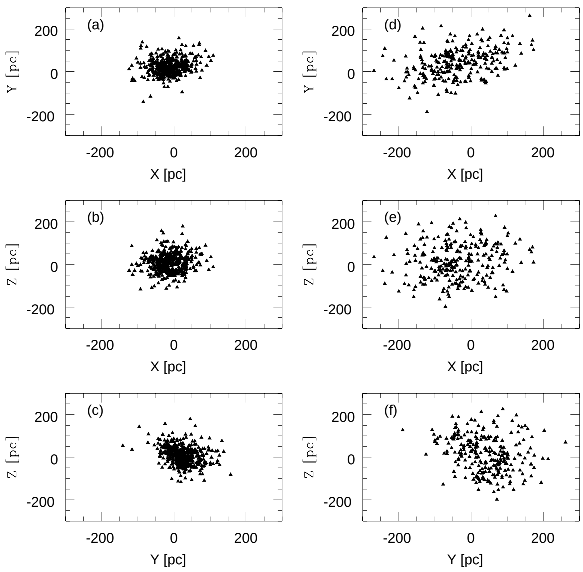

Figure 8: Spatial distribution of the samples CLLA-TYC2+HIP (a) to (c) and CLLA-Tycho-2 (d) to (f) , respectively. X points towards the Galactic center, Y in the direction of galactic rotation and Z towards the Galactic north pole.

with respect to the Sun and then reduced to the LSR (local standard of rest). For the latter Dehnen & Binney's (1998) values $+10.0, +5.2, +7.2$ km s^{-1} were adopted for $U_{\odot}, V_{\odot}, W_{\odot}$, respectively. Finally, the velocity components were transformed onto a frame rotating with circular velocity $V_{\rm circ} = -220$ km s^{-1} relative to the LSR, i.e. the expected rest frame of our Galaxy (e.g. Wielen 1986). The rotational velocity is defined as $V_{\rm rot} = V - V_{\rm circ}$.

Figure 9 shows the U, $V_{\rm rot}$, and W velocities of the samples CLLA-TYC2+HIP and CLLA-Tycho2 as scatter plots. The U-distribution indicates that the present sample was kinematically selected. The CLLA Catalog is based on a proper motion catalog so that stars with small tangential velocities are missing. We can see clearly that for small U-values the diagrams are sparsely populated. This is also seen in the V-velocities. The stars with metallicities [Fe/H] > -1 lag on the average by about 40 km s^{-1}, i.e. are thick disk stars. The old thin disk stars are missing (cf. also Fig.10). In the W-velocities no kinematical bias is visible; it is apparently lost in projection. However, since we are mainly interested in the kinematics of the halo stars, this bias is of no consequence in the present context. It is evident from this figure that metal-poor stars with [Fe/H] < -1 have larger random motions compared with metal-rich ones [Fe/H] > -1. This shows that the kinematic properties change rather abruptly at [Fe/H] ≈ -1 to -2, which is probable the transition region from halo to disk component (Ryan & Norris 1991 and Chiba & Yoshii 1998).

The mean motion with respect to the LSR and velocity dispersions were calculated for different groups in [Fe/H]. The results are presented in Table 5. The most metal-deficient stars in the samples, more metal poor than [Fe/H] $= -1.6$, are dominated by members of the halo population. These stars exhibit a radially elongated velocity ellipsoid $(\sigma_{\rm U}, \sigma_{\rm V}, \sigma_{\rm W}) = (189 \pm 13, 97 \pm 7, 98 \pm 7)$ and $(157 \pm 12, 87 \pm 7, 77 \pm 6)$ km s^{-1} and show no net rotation, $\langle V_{\rm rot} \rangle = 1 \pm 13$ and 15 ± 14 km s^{-1} for the CLLA-TYC2+HIP and CLLA-Tycho2 samples, respectively, which are in good agreement with RR Lyrae kinematics of Martin & Morrison (1998) and Layden et al. (1996). Chiba & Beers (2000) found a lower velocity dispersion in the U-direction, $(\sigma_{\rm U}, \sigma_{\rm V}, \sigma_{\rm W}) = (141 \pm 11, 106 \pm 9, 94 \pm 8)$ km s^{-1} from their 1203 non-kinematically selected stars.

The velocity dispersion components of the sample in the more metal-rich abundance ranges decrease as the contribution of the thick disk component progressively increases. In particular, for [Fe/H] > -1.0 the contribution of the halo component is expected to be negligible. Our CLLA+TYC2+HIP sample in this metallicity range has velocity dispersions $(\sigma_{\rm U}, \sigma_{\rm V}, \sigma_{\rm W}) = (74 \pm 2, 50 \pm 1, 37 \pm 1)$ with $V_{\rm rot} = 176$ km s^{-1}, which is in agreement with thick disk samples of Martin & Morrison (1998) of RR Lyrae stars and Chiba & Beers (2000) of solar-neighborhood stars.

Table 5: Mean Velocities and Velocity Dispersion of the Sample Stars

	N	$\langle U \rangle$	$\langle V \rangle$	$\langle W \rangle$	$\sigma_{\rm U}$	$\sigma_{\rm V}$	$\sigma_{\rm W}$
dex				km s^{-1}			
CLLA-TYC2+HIP							
$[\rm Fe/H] > -1.0$	381	-10 ± 4	-50 ± 3	-3 ± 2	74 ± 2	50 ± 1	37 ± 1
$-1.6 \leq$ [Fe/H] ≤ -1.0	47	-38 ± 23	-171 ± 12	-1 ± 11	152 ± 11	86 ± 6	72 ± 5
$[\rm Fe/H] < -1.6$	53	-4 ± 26	-226 ± 13	-1 ± 13	189 ± 13	97 ± 7	98 ± 7
CLLA-Tycho2							
$[\rm Fe/H] > -1.0$	169	-8 ± 8	-97 ± 6	-6 ± 4	110 ± 4	81 ± 3	57 ± 2
$-1.6 \leq$ [Fe/H] ≤ -1.0	50	52 ± 17	-187 ± 10	5 ± 9	121 ± 9	68 ± 5	61 ± 4
$[\rm Fe/H] < -1.6$	40	38 ± 25	-212 ± 14	-19 ± 12	157 ± 12	87 ± 7	77 ± 6

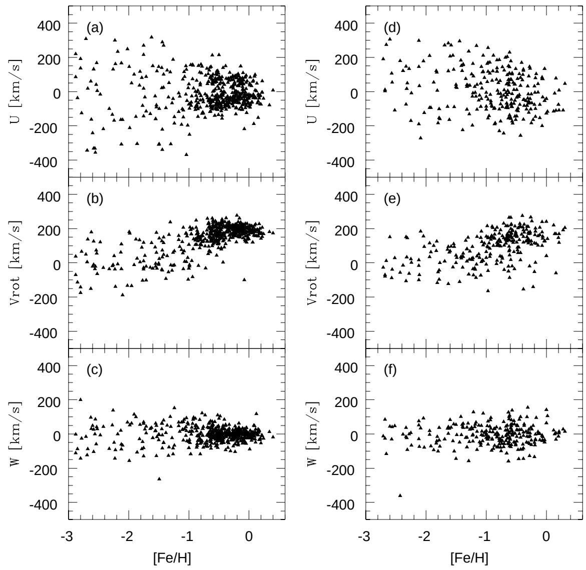

Figure 9: Space velocity components (U, V_{rot}, W) versus metallicity [Fe/H] of the samples CLLA-TYC2 (a) to (c) and CLLA-Tycho2 (d) to (f), respectively.

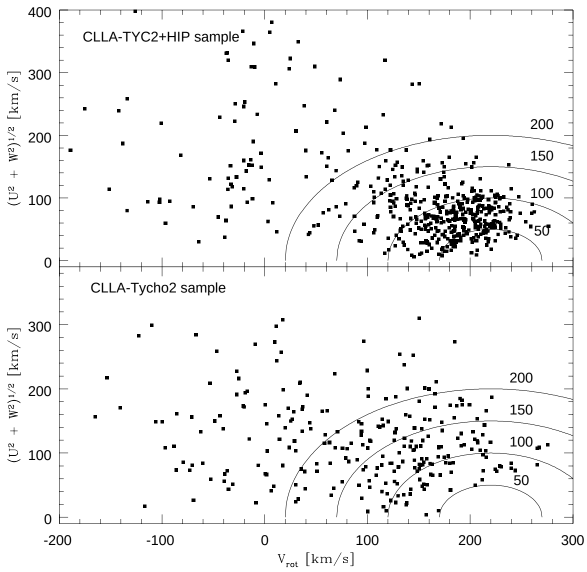

Figure 10: Toomre diagram: $(U^2 + W^2)^{1/2}$ versus $V_{\rm rot}$ distributions of CLLA-TYC2+HIP and CLLA-Tycho2 samples. The solid lines represent total velocities of $50, 100, 150$ and 200 km s^{-1}, respectively.

Our CLLA-Tycho2 sample is more sparsely distributed than the CLLA- TYC2+HIP sample in the metallicity range [Fe/H] > -1. To understand this, we note that the CLLA-Tycho2 sample was drawn from the CLLA stars that are not in the Hipparcos catalogue. This might imply that mainly CLLA stars with magnitudes brighter than 10.5 mag fall in our CLLA-TYC2+HIP sample and stars with magnitudes fainter than 10.5 mag are in the CLLA-Tycho2 sample. Stars with fainter apparent magnitudes are at larger distances and velocities compared to the Hipparcos stars. The minimum distances for each sample are 17 and 40 pc for CLLA-TYC2+HIP and CLLA-Tycho2, respectively. Figure 8, where we plot the spatial distributions in X, Y and Z shows this clearly. We can find the minimum tangential velocity using the minimum distances and mean proper motions for both samples, using

$$V_{\mathrm{T\,min}} = 4.74\frac{\langle\mu\rangle}{1000}d_{\min} \quad (54)$$

where $\langle\mu\rangle$, $d_{\min}$, and $V_{\mathrm{T\,min}}$ denote mean proper motions in mas yr^{-1}, minimum distances in parsecs and minimum tangential velocities in km s^{-1} for each subdwarf sample. We found for the CLLA-Tycho2 sample $V_{\mathrm{T\,min}} > 50$ km s^{-1}, which might explain why there are comparatively few thick disk stars in this sample (cf. Fig.10).

3.4 V_{rot} Distributions of Subdwarfs

The corresponding V_{rot}-velocity distributions for the samples CLLA-TYC2+HIP and CLLA-Tycho2 are shown in Figs.11 and 12, respectively. The first group, [Fe/H] > -1 dex, represents what are obviously the thick disk stars. The third group, [Fe/H] < -1.6 dex, consists of extreme metal-poor stars, dominated by members of the halo population. The histograms of the samples CLLA-TYC2+HIP and CLLA-Tycho2 can be fitted by Gaussian distributions.

The second group, $-1.6 \leq$ [Fe/H] ≤ -1 dex, shows a peculiar kinematics. A Kolmogorov-Smirnov test, which avoids binning of the data, shows that the velocity distribution of the very metal-poor stars, [Fe/H] ≤ -1.6, in the combined sample is statistically different from the velocity distribution of the intermediate population, $-1.6 \leq$ [Fe/H] ≤ -1.0. The maximum deviation of the normalized cumulative distribution between the two groups is $D = 0.241$ and thus significantly larger

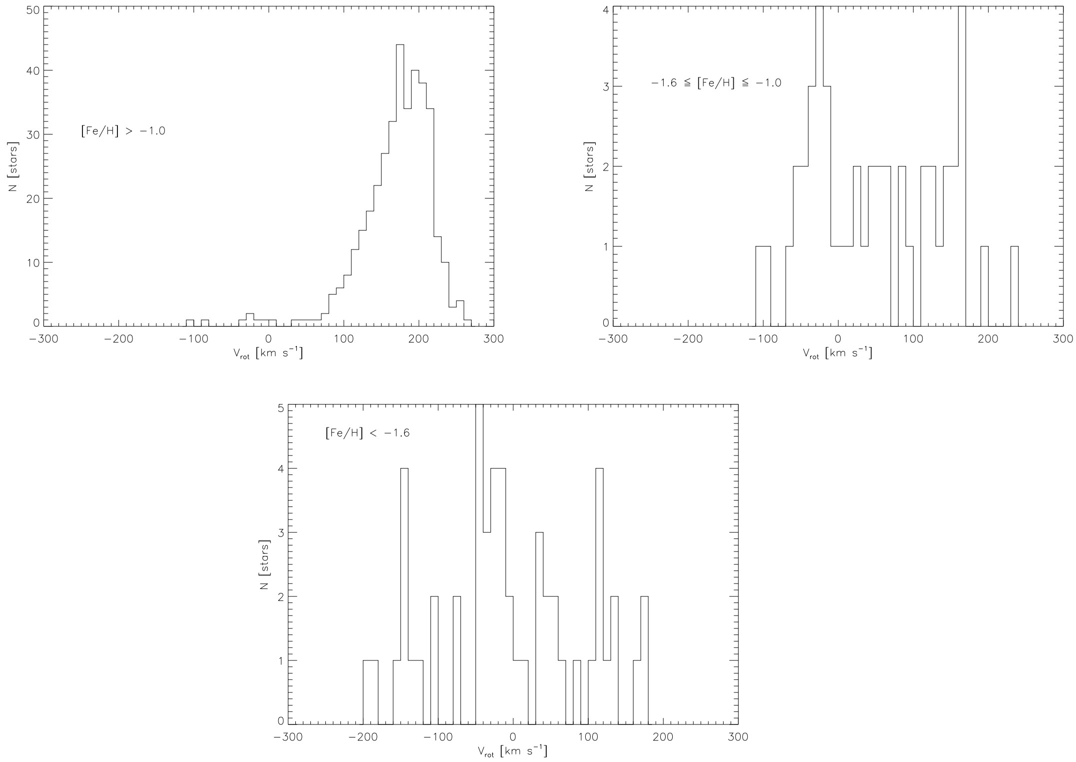

Figure 11: Rotational velocity (V_{rot}) distributions of sample CLLA-TYC2+HIP grouped according to their metallicities. The velocities are reduced to the local standard of rest.

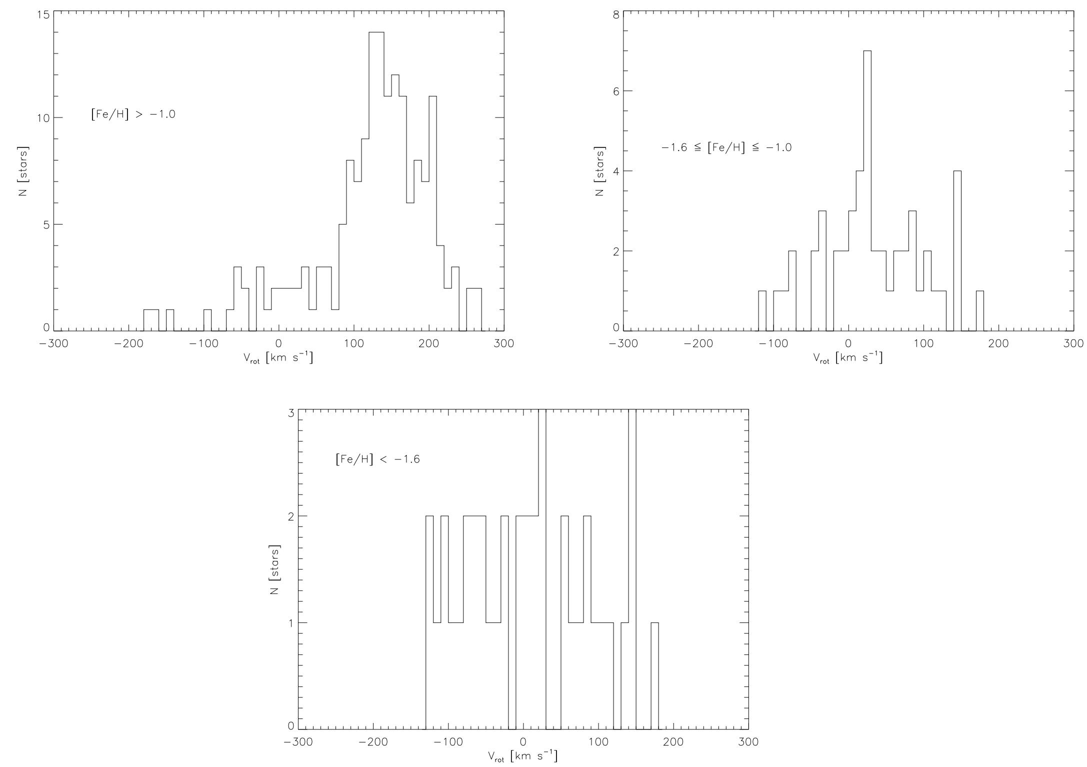

Figure 12: The same as Fig. 11, but for sample CLLA-Tycho2.

than the critical value $D_{0.05} = 0.196$ (Sachs 1988), which leads to a rejection of the hypothesis of the statistical similarity of the velocity distributions of the two groups. Similarly we have shown that the velocity distribution of the metal-poor stars is symmetric with respect to $V_{\rm rot} = 0$ km s^{-1} ($D = 0.149$, $D_{0.05} = 0.282$), whereas the velocity distribution of the intermediate group is asymmetric ($D = 0.375$, $D_{0.05} = 0.300$). Thus the intermediate group seems to represent a different population of halo stars.

On the other hand, the asymmetric drift ratio $\langle V\rangle/\sigma_{\rm U}^2 = -0.007$ (CLLA-TYC2+HIP) is very similar to that of the thick disk stars, $\langle V\rangle/\sigma_{\rm U}^2 = -0.008$. We conclude tentatively that the stars in the $-1.6 \leq$ [Fe/H] ≤ -1.0 metallicity range represent a population of the dynamically hot metal-weak thick disk (MWTD).

3.5 Summary and Discussion

We have analyzed the kinematics of 740 nearby metal-poor subdwarf stars from the CLLA catalogue. The subdwarfs were cross-identified with the TYC2+HIP and Tycho 2 Catalogues to find accurate trigonometric parallaxes and proper motions. The accurate Hipparcos parallaxes lead to an upward correction factor of 11% of the photometric distance scale of CLLA, and it was used to correct the photometric distances of CLLA-Tycho2 stars.

The present analysis indicates that the solar neighborhood subdwarf stars with [Fe/H] $<$-1.6 show halo kinematics characterized by a radially elongated velocity ellipsoid and no significant rotation. At a metallicity range of [Fe/H] > -1, our samples show *disklike* kinematics. In the metallicity range $-1.6 \leq$ [Fe/H] ≤ -1.0 we found a significant number of stars with kinematics not of halo stars but that of a dynamically not-metal-weak tail of the thick disk.

Chiba & Beers (2000) obtained a fraction of 30 % of low-metallicity stars in their nonkinematically selected solar neighborhood sample with $-1.7 <$ [Fe/H] $\leq$ -1.0, which is consistent with our result of 18%. Chiba & Yoshii (1998) analyzed the kinematics of red giants and RR Lyrae stars in the solar neighborhood based on Hipparcos data. They found in both red giant and RR Lyrae samples in the range $-1.6 <$ [Fe/H] $\leq$ -1.0, a fraction of $\sim$ 10 % of stars in a population with a mean velocity $\langle V_\phi \rangle_{\rm disk} = 195$ km s^{-1}.

We must try to understand the implications of a significant population of MWTD stars for theories of the formation and evolution of the Galaxy. It should be kept in mind that, although the MWTD population may contribute a large fraction of the *local* metal-poor stars, the (inner) halo population is probably still dominated by the stars with [Fe/H] ≤ -1.6 within a few kiloparsecs of the Sun. Furthermore, although we have emphasized the possible importance of the MWTD population, it certainly still appears to be a minor constituent of the entire thick disk population (Beers et al. 2002).

If there is indeed a significant fraction of thick disk stars with metal abundance $-1.6 \leq$ [Fe/H] ≤ -1, as we have argued, this finding may have significance for formation scenarios of the Galaxy. An interesting scenario for the origin of an MWTD component may be the merging of satellite galaxies (Searle & Zinn 1978), which are then accreted by a thin, fast rotating, possibly metal-poor, Galactic disk

(Quinn et al. 1993; Wyse 2001). The dynamical heating of the stellar component of this disk in connection with the accretion process produces the thick disk. The kinematics of the halo depends on the dynamics of the merging satellites, whereas the kinematics of the thick disk are determined by the heating of the rotating thin disk. Based on this merging picture of galaxy formation, one might argue that the "shredded satellite" stars retain a kinematic signature distinct from the thick disk part that results from the heated thin disk. The kinematic trace of the destroyed satellite, which is probably the origin of the MWTD stars, would be visible in the mean orbital rotational velocity of stars. Based on a spectroscopic survey of ~ 2000 F/G stars $0.5 - 5$ kpc above the Galactic plane Gilmore et al. (2002) determined a mean rotational velocity lag of the shredded galaxies of ~ 100 km s^{-1}. The actual lag expected from the shredded satellite depends predominantly on the initial orbit and the amount of angular momentum transport in the merger process and is not initially predictable in a specific case (Gilmore et al. 2002).

4 The Thick Disk Luminosity Function

The stellar thick disk was first detected in the Milky Way by Gilmore & Reid (1983) although thick disks were seen in other early-type galaxies before then (van der Kruit & Searle, 1981). They undertook a survey of $12,500$ stars over 18 square degrees towards the South Galactic Pole, deriving absolute magnitudes from photometric parallaxes for the entire sample. They were particularly interested in older, red stars so they used I and V plates. Their sample was magnitude-limited to $I < 18$ mag and $V < 19$ mag. The goal of the observations was to derive the luminosity function in the solar neighborhood and look for variations with distance from the Galactic plane. They performed their analysis both for a constant metallicity with height and a metallicity gradient of -0.3 kpc^{-1} for $0 < z < 5$ kpc and then no gradient for $z > 5$ kpc. They then computed star counts in bins of z and M_V. Note that they do assume that all the detected stars are on the main sequence and that the in plane density of the faint ($9 < M_V < 19$) stars is the same as the brighter stars ($3 < M_V < 11$). The luminosity function is plotted in Figure 13 for the metallicity gradients of 0 (left) and -0.3 kpc^{-1}(right). At about $z = 1$ kpc, the luminosity function steepens rapidly for $M_V < +4$. This strongly suggests that the young stars are confined to the plane while at heights above 1 kpc, an older population of stars dominates.

Gilmore (1984) has discussed a model of galactic population in which the thick disk population has a spheroid luminosity function, having about 10% of the mass of the thin disk and an order of magnitude more Population II stars than in the spheroid (Fig.14).

The thick disk population has a mean metallicty $[Fe/H] \sim -0.4 - -0.7$ (eg. Gilmore et al. 1995; Robin et al. 1996; Buser et al. 1999) which is similar to the disk globular cluster 47 Tuc (Carney et al. 1989). The thick disk LF considered to have the same shape of metal rich globular cluster 47 Tuc (Buser et al. 1999). Until now no direct measurement of the thick disk LF has been done. Reyl$\acute{e}$ and Robin (2001) derived the LF from their thick disk Initial Mass Function (IMF) based on the star counts at high and intermediate galactic latitudes.

In this study, we will derive the LF of thick disk using the subdwarf sample of CLLA. The old metal arm subdwarfs with both accurate metallicities and with accurate Hipparcos/Tycho-2 parallax and Proper motion measurement are reliable

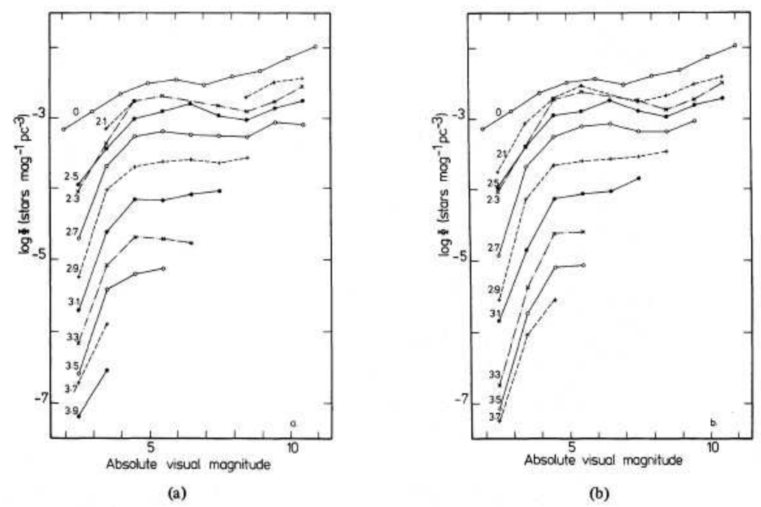

Figure 13: Gilmore & Reid's (1983) stellar luminosity function for metallicity gradients ($d[\mathrm{Fe/H}]/dz$) of (a) 0 and (b) -0.3 kpc^{-1}. The logarithmic distances from the plane are labeled.

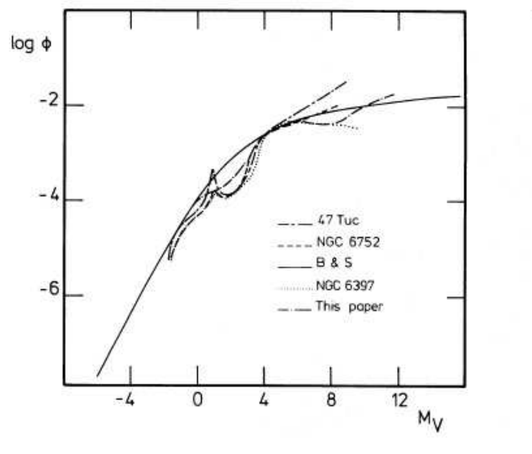

Figure 14: Figure 6 of Gilmore (1984). The luminosity function of thick disk, which has a spheroid luminosity function, together with that adopted from Bahcal & Soneira (1981) and several LFs of globular cluster from da Costa (1982).

samples to determine the thick disk LF. The CLLA subdwarfs covers only F,G and early K populations.

4.1 The Sample

The data set constructed by Arifyanto et al. (2005; herafter AFJW) (chapter 3) is based on the sample of F and G subdwarfs of Carney et al. (1994, CLLA). While keeping the precise radial velocity and metallicity data of CLLA, AFJW have significantly improved the accuracy of the distances and proper motions of a subset of the CLLA sample. The original CLLA sample contains 1464 stars, but kinematical and metallicity data are not available for every star. Many of the CLLA stars were observed with Hipparcos and AFJW identified 481 stars in the astrometric TYC2+HIP catalogue (Wielen et al. 2001) and replaced the parallaxes and proper motions of CLLA by Hipparcos parallaxes and proper motions, respectively. The Hipparcos parallaxes were then used to recalibrate the photometric distance scale of the rest of the CLLA stars. AFJW could identify 259 CLLA stars in the Tycho-2 catalogue (Hog et al. 2000) and adopted the proper motions given there. Thus the sample of AFJW, which forms the basis of our analysis, contains 740 subdwarfs with greatly improved parallax and proper motion data. While the photometric distances were corrected by a factor of about 10%, the old NLTT proper motions were improved from an accuracy of 20 to 30 mas yr^{-1} to 2.5 mas yr^{-1}.

4.2 Selection of Thick Disk Stars

Measurement of the thick disk LF is considerably more difficult than measurement of the Population I LF, because the thick disk population represents a small fraction of stars locally and is a population which is not easily separated and studied apart from other stellar populations. It overlaps probably both the old thin disk and the halo in terms of kinematics and metallicities. There is no obvious predetermined way to define a sample of purely thick disk stars in the solar neighborhood. There are essentially three ways of finding local thick or thin disk stars: pure kinematical approach (Grenon 1987; Bensby et al. 2003), by pure metallicity selection sample (Carney et al. 1989), or by looking at a combination of kinematics, metallicities (Schuster et al. 1993) and ages (Fuhrman 1998). It should be kept in mind that one has to be careful concerning biases in one's stellar samples and in one's methods when studying the thick disk.

Nissen & Schuster (1991) used the $[\mathrm{Fe/H}]-V_{rot}$ diagram for separating the halo stars from the "high-velocity disk" stars. Then in the paper of Schuster et al. (1993) they defined the stellar population parameter "X" and used it to make a diagonal cut connecting $([\mathrm{Fe/H}], V_{rot}) = (-0.3, 0\ \mathrm{kms}^{-1})$ and $(-1.5, 175\ \mathrm{kms}^{-1})$ to isolate more cleanly the thick disk stars. In their most recent work, Schuster et al. (2005) indicates that the range $-21 \leq X \leq -6$ gives a fairly clean thick-disk sample, with only small contamination by the halo and old thin disk. In Schuster et al. (1993) the cut $-21 \leq X \leq -18$ was used to define an even cleaner thick-disk sample, but here too few stars are found in this reduced X interval. Recently, Karataş et al. (2005) used the X criteria, provides 22 thick-disk stars. They found $\sigma_W = 32 \pm 5$ km s^{-1}, $< V_{rot} >= 154 \pm 6$ km s^{-1} and $< [M/H] >= 0.55 \pm 0.03$ dex for these thick-disk stars, which is in agreement within the range of $30 - 37$ km s^{-1} given by Norris (1987), Croswell et al. (1991), and Carney et al. (1989).

Bensby et al. (2004) use only kinematic criteria to separate the thin disk, thick disk, and halo. They do not use the metallicity. Assuming that the space velocities have Gaussian distributions for each stellar population component it is possible to calculate a "probability" for each star that it belongs to either the thin disk, the thick disk, or the halo :

$$f(U,V,W) = k.\exp\left(-\frac{U'^2}{2\sigma_U^2} - \frac{(V' - V_{asym})^2}{2\sigma_V^2} - \frac{W'^2}{2\sigma_W^2}\right) \tag{55}$$

where

$$k = \frac{1}{(2\pi)^{3/2}\sigma_U \sigma_V \sigma_W} \tag{56}$$

normalizes the expression.

To get the probability that a given star belongs to a specific population, we have to multiply the probabilities from Eq.(55) by the observed fractions (X) of each population in the solar neighborhood. Finally, by dividing the probability for thick disk membership (D) with the probabilities for thin disk membership (TD) and the halo membership (H), respectively, two dimensionless ratios that express how much more likely it is that a star belongs to the thick disk than the thin disk and the halo, respectively, can be constructed:

$$TD/D = \frac{X_{TD}}{X_D}.\frac{f_{TD}}{f_D}, \quad TD/H = \frac{X_{TD}}{X_H}.\frac{f_{TD}}{f_H}. \tag{57}$$

In order to select the thick disk sample one have used $TD/D > 2$ and $TD/H > 1$ (assuming the 10% normalization). This will ensure that the probability of belonging to the thick disk always will be greater than the probability of belonging to the thin disk (i.e. $TD/D > 1$), even if the true value for normalization of the thick disk actually is as low as 2% or as high as 14% (Bensby 2004).

Carney et al. (1989) used only the metallicity to isolate the thick disk stars from sample of stars selected from the Lowell Proper Motion Catalog with metallicities published by Laird, Carney, and Latham (1988). They select the thick disk stars with metallicities $-0.65 \leq [Fe/H] \leq -0.35$ and calculated the thick disk asymmetric drift of 35 ± 5 km s^{-1} suggest a net Galactic rotational velocity V_{rot} of 185 ± 5 km s^{-1}. Their data based on the proper motion selected sample, so there had biases to the higher proper motion.

We select for the thick disk all stars with $-1.0 \leq$ [Fe/H] ≤ -0.4. There are 289 stars among 740 stars in our subdwarf sample. These are all brighter than $m_V = 12.5$ mag. and with proper motion larger than $\mu = 155$ mas yr^{-1}. However the sample is not completed to that magnitude and proper motion. In Fig.15 and 16 we explore the completeness of our sample.

For this purpose, the Log-cumulative star counts of subdwarfs with apparent magnitude brighter than $m_V = 12.5$ is shown in the left panel of Fig.15. For a complete sample distributed according to a homogenous spatial density, the logarithm of the cumulative star counts of subdwarfs with apparent magnitude brighter $m_{V,faint}$ are proportional to m_V with a slope of 0.6 (Mihalas & Binney 1981). We also show in the left panel of Fig. 15 a straight line with such slope. It is evident that our sample is not distributed homogenously at apparent magnitude fainter than

Table 6: Characteristic velocity dispersions (σ_U, σ_V, and σ_W) in the thin disk, thick disk, and stellar halo. X is the observed fraction of stars for the populations in the solar neighborhood and V_{asym} is the asymmetric drift (Bensby et al. 2003).

	X	σ_U	σ_V	σ_W	V_{asym}
			[km s^{-1}]		
Thin Disk (D)	0.90	35	20	16	-15
Thick Disk (TD)	0.10	67	38	35	-46
Halo (H)	0.0015	160	90	90	-220

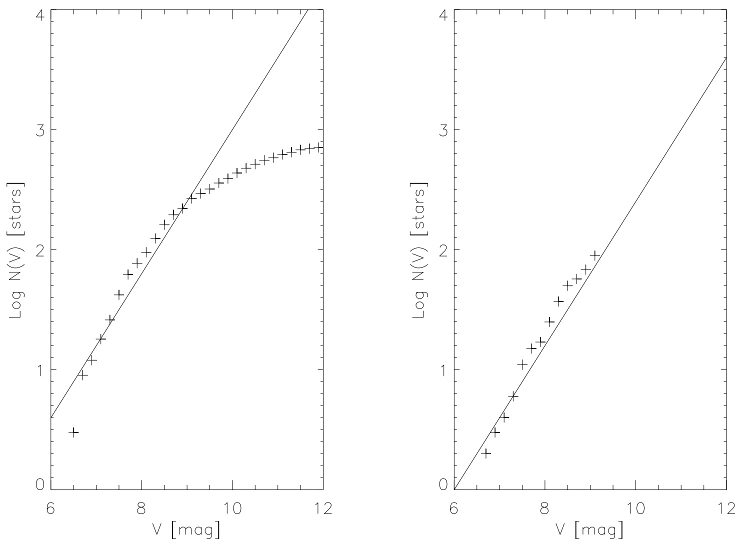

Figure 15: The cumulative histogram of apparent magnitude for all subdwarfs with metallicity $-1.0 < [\mathrm{Fe/H}] < -0.4$ (left) and the restricted sample (right). The straight lines with a slope of 0.6 represent the homogenous and complete distribution in apparent magnitude (see e.g. Mihalas & Binney 1981).

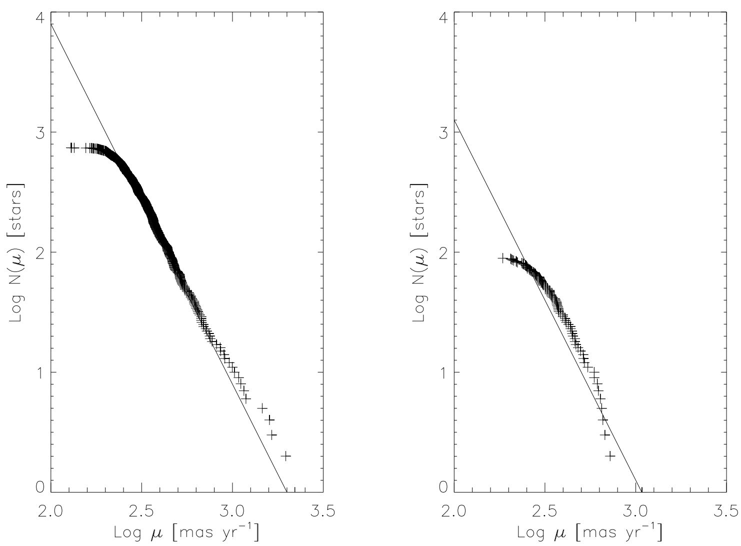

Figure 16: The cumulative histogram of proper motion for all subdwarfs with metallicity $-1.0 < [\mathrm{Fe/H}] < -0.4$ (left) and the restricted sample (right).The straight lines with a slope of -3 represent the homogenous and complete distribution in proper motion (see e.g. Mihalas & Binney 1981).

$m_V \sim 9.2$ mag. Therefore we can now asses the completeness in apparent magnitude of the restricted sample, since the turn-off for this sample occurs at $m_V \sim 9.2$ mag.

The completeness of the restricted sample in proper motion can be assessed in a similar way. Again, the assumption of an homogenous and complete sample in proper motion leads to the conclusion that the logarithm of the cumulative star counts of our sample with proper motion larger than μ_l should be proportional to μ with a slope of -3. We also show in the left panel of Fig. 16 with such a slope. The exact value of the turn-off is $\mu_l \sim 180$ mas yr^{-1}. This is in good agreement with the lower proper motion of NLTT catalog.

We defined the general restriction of the sample, in which our sample is complete, $m_V \leq 9.2$ mag. and $\mu_l \geq 180$ mas yr^{-1}. We can see the right panels of Figs. 15 and 16 the restricted sample in apparent magnitude and proper motions, respectively, with mean metallicity $< [Fe/H] >= -0.61$ and $\sigma_{[Fe/H]} = 0.13$. There are only 89 thick disk stars within the complete sample. The contamination of thin disk stars in our proper motion selected sample could be minimize by setting up the minimum proper motion cut ($\mu_l > 180$ mas yr^{-1}). The proper motion selection magnifies the contribution from the higher-velocity old populations, since they are effectively sampled over larger volumes than the lower-velocity disc stars (Reid 1997; Cooke & Reid, 2000). The number of stars of each population in a proper motion selected sample is proportional to the mean population tangential velocity :

$$N(\mu > \mu_{min}) \propto \rho_0 \langle V_T \rangle^3, \tag{58}$$

with ρ_0 the local space density of the population (Hanson, 1983; Reid 1984; Digby et al.,2003). This therefore amplifies the contribution of the higher velocity population above the ratio of the local space densities by the amount :

$$A_\mu = \left(\frac{\langle V_T^1 \rangle}{\langle V_T^2 \rangle} \right)^3 . \tag{59}$$

This amplification has an effect on the likelihood of high velocity stars entering the proper motion sample, and demonstrates the efficiency of proper motion selection in selecting thick disk and spheroid stars. For example, a spheroid to disc number ratio of $N_{disk} : N_{spheroid} = 400 : 1$ for a volume limited sample can be increased to $N_{disk} : N_{spheroid} = 5 : 1$ for a proper motion sample. However, this richness has a price – any sample of stars selected on the basis of proper motion is inevitably tainted by kinematic bias. The bias may manifest itself in a number of ways, but is most obvious in the velocity ellipsoid of the sample stars, where the dispersions, particularly along the "long" axis, are distorted and the magnitude of the asymmetric drift is significantly increased. The effect is evident in a number of early attempts to establish the velocity parameters for stars of extreme Population II, and has been discussed by a number of investigators, e.g. Bahcall & Casertano (1986), Ryan & Norris (1993), Dawson et al. (1995) and Digby et al. (2003).

There is still contamination by the halo stars, however the halo to thick disk density ratio is about 1.5%. We tried to minimize contamination by the halo stars by setting the maximum tangential velocity cut-off $V_T < 200$ km s^{-1}. This cut-off will also cause the high velocity tail of the thick disk population to be excluded from the sample, but our results allow us correspondingly correct the derived LF.

4.3 The Parameter of the Thick Disk

To determine the kinematic and spatial parameters that describe thick disk accurately, we must correct our sample for the kinematic biases it contains. We use the Schmidt's $1/V_{max}$ to weight the velocity components of each stars in our sample. The weight is proportional to V_T^{-3} for a proper motion limited sample. The star which has a low tangential velocity (proper motion) or close to the lower limit for the sample, can have higher weight than the star which has larger proper motion. However, the contaminated thin disk star which has low V_t can cause a large error in the calculation.

The Monte Carlo simulations (explained in chapter 2.8) of a model of the populations allows the biases and effects of the analysis procedure to be taken into account, and the results corrected for these effects. We generate a fake catalog of about 3×10^5 stars with model input for thick disk, and do selection criteria of $m_V \leq 9.2$ and $\mu_l \geq 180$ mas yr^{-1}. We repeat the simulations 200 times in order to test the sensitivity of our results to the adopted scheme and have found no significant differences in the derived mean kinematics parameters.

Kinematics Parameter

The mean kinematics parameter of 89 thick disk subdwarfs in our complete sample are shown in Table 7. Taken at face value, the 'biased' thick disk asymmetric drift (or velocity lag) 51 ± 5 km s^{-1} suggest a net Galactic rotational velocity $V_{rot} = 169 \pm 5$ km s^{-1}. After we corrected for the kinematics bias, the asymmetric of our thick disk sample is $V_{asym} = 41 \pm 5$, or $V_{rot} = 179 \pm 5$ km s^{-1}. The velocity dispersion components of our thick disk stars has $(\sigma_U, \sigma_V, \sigma_W)$ = $(66 \pm 5, 46 \pm 3, 39 \pm 3)$ without kinematics correction. Weighting by the $1/V_{max}$ for each velocity components, the thick disk velocity dispersion would be $(\sigma_U, \sigma_V, \sigma_W)$ = $(60 \pm 4, 45 \pm 3, 38 \pm 3)$. Our corrected result is in good agreement with the non-kinematics sample of Martin & Morrison (1998) of RR Lyrae stars and Soubiran et al. (2003) of stars in NGP (see Table 7 for comparison).

Fig.17 shows the U, V and W distribution of the sample. We fitted the histogram of the biased kinematics distribution (full lines), and the dashed lines represent unbiased (corrected) velocity distributions.

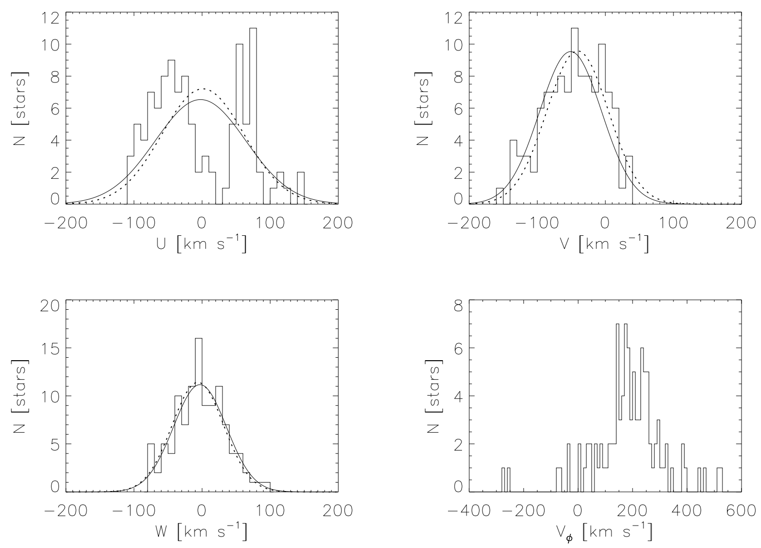

Figure 17: The histogram of the galactic velocity distributions of thick disk stars in U, V, W, and V_ϕ (from the radial velocities) directions. The full line represent the gaussian fit of the biased data and the dashed line show the unbiased (corrected) distributions.

The use of high proper motion as a selection criterion will preferentially select the higher velocity stars in any given population. The velocity dispersions σ_U and σ_W are expected to be overestimated by the uncorrected samples since we preferentially selected stars with extreme velocities. While this expectation is borne out for

σ_U, it is less obvious for σ_W, which differs generally by less than 10% between the non-kinematic and kinematic samples. This come about because the dispersion in U is larger than in W, so as the sky is searched in a proper motion survey, stars with extreme U velocities will be found more readily than will stars with extreme W velocities. In the biased sample, σ_V is underestimated because the sun is located in one wing of the thick disk V distribution, and the proper motion selection procedure preferentially accepts stars in the retrograde wing rather than in the prograde wing. The resulting distribution is thus reduced in width and shifted to a lower V than the parent distribution. The largest bias of all is in mean V, since the V velocity difference between the thick disk and the sun is greater than the velocities which are readily encountered in the U and W distributions (Ryan & Norris 1991).

Table 7: Comparison of various thick disk sample

Sample	V_{rot}	σ_U	σ_V	σ_W	<[Fe/H]>
			Kinematically unbiased sample		
Soubiran (1993)	179 ± 16	56 ± 11	43 ± 6	-	-
Edvardsson et al. (1993)	183 ± 6	59 ± 6	48 ± 4	38 ± 4	-
Martin & Morrison (1998)	185 ± 11	54 ± 8	52 ± 8	31 ± 4	-
Chiba & Beers (2000)	200	46 ± 4	50 ± 4	35 ± 3	-
Soubiran et al. (2003)	169 ± 5	63 ± 6	39 ± 4	39 ± 4	-0.48 ± 0.05
			Kinematic selected sample		
This work	179 ± 6	60 ± 4	45 ± 3	38 ± 3	-0.61 ± 0.01
Carney et al. (1989)	185 ± 5	99 ± 10	51 ± 8	47 ± 5	~ -0.5
Bartašiūtė (1994)	181 ± 5	64 ± 5	49 ± 3	42 ± 3	-

There is an alternative method for computing the lag velocity for solar neighborhood proper motion stars which overcomes both the proper motion bias and the dependence on the distance scale. Applied to a nearby sample, the $\hat{V}_{rot}$[2] quantity defined by Frenk & White (1980) is independent of distance. Furthermore, since it

[2]We used the term $\hat{V}_{rot}$ (with *hat*)for the rotational velocity derived from the Frenk & White (1980) formalism using the radial velocity data only, and V_{rot} for rotational velocities derived from proper motion & radial velocities data

uses measurements only of radial velocities which lie orthogonal to the proper motion component used in the selection procedure, *it contains no knowledge of proper motion bias*, and is an unbiased estimator of the kinematics of the sample. The geometrical weighting terms in Frenk & White (1980) formalism, based on the Galactic coordinates of the stars, ensure that only radial velocity components in the direction of galactic rotation contribute to the computed $\hat{V}_{rot}$. As a consequence of $< V >$ being biased towards more negative values, and $\hat{V}_{rot}$ being unbiased (Ryan & Norris, 1993). We emphasize the important result that the $\hat{V}_{rot}$ quantity correctly recovers the rotational characteristics of the parent distribution even after the proper motion selection criteria have been applied, because the radial velocity data are unbiased.

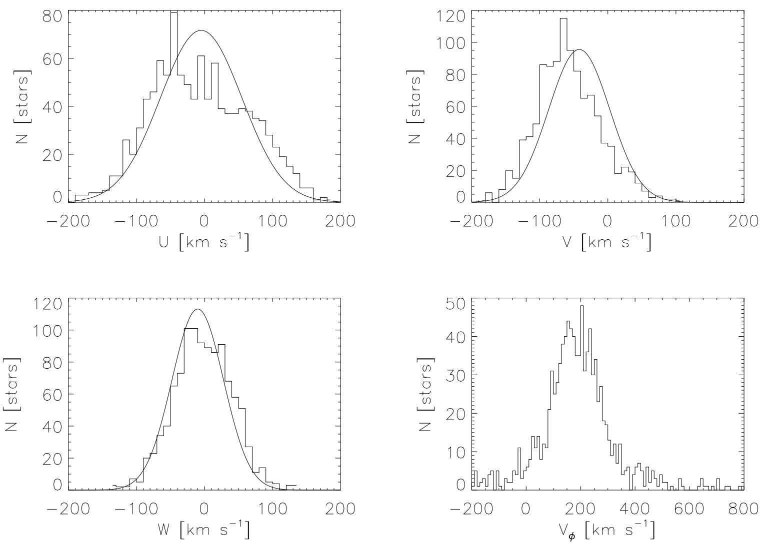

Figure 18: The histograms of the galactic velocity distributions of simulated thick disk stars in U, V, W, and V_ϕ directions. The smooth curves represent the gaussian fit of the input model. Sample=1000 stars

The unbiased $\hat{V}_{rot}$ for our subdwarf sample is 185 ± 9 km s^{-1}, which is in good agreement with the corrected kinematics $V_{rot} = 179 \pm 6$ and other results from the non-kinematic samples shown in Table 7.On the bottom left panel of Fig.17, we plot the V_ϕ distribution, calculated via Frenk & White formalism using the radial velocity data. The V_ϕ velocity has a wide spread distribution due to the geometric factor, however the median gives the value of 185 km s^{-1}.

We performed the monte carlo simulation, following the selection criteria from our sample, giving the input kinematic parameter of ($\sigma_U, \sigma_V, \sigma_W, V_{asym}$) = $(60, 45, 38, -41)$ km s^{-1}. We generate a simulated catalog of 3×10^5 stars, with $\delta > -20^o$, within $d < 100$ pc, assuming a uniform density in the galactic disk. Figure 18 shows the comparison of input model and the restricted sample obtained Monte Carlo simulation of high proper motion study. The smooth gaussian curves are model velocity distribution (input parameters) and the histograms are the velocity distribution of the restricted sample.

From the top left panel of Fig.18, the effect of the proper motion selection criteria on the measured U dispersion may be seen. As a result of the sun being located near the center of the U velocity distribution, the failure of some stars to survive the proper motion selection criteria results in a preferential depopulation of the peak of the distribution whilst the wings are maintained (Ryan & Norris 1993). The restricted sample yields $\sigma_U = 72$ km s^{-1}, whereas the parent distribution had $\sigma_U = 60$ km s^{-1}. The σ_U and V_{asym} overestimated in proper motion selected samples, in this example by a factor of 1.2. The result simulation for the W velocity component are less extreme than those for the U velocity. The W velocities, having a much smaller range than the U component, are rarely sufficiently large to contribute significantly to the total space velocity, with consequence that they are linked much more weakly to the selection criteria.

We performed a statistical test to know whether our simulated samples are drawn from the same parent distribution as our thick disk stars. We used the Kolmogorov-Smirnov tests, which avoids binning of the data, give the probabilities that samples were drawn from the same parent distributions, are probability (U) = 0.46, probability (V) = 0.51 and probability (W) = 0.56. It is clear that our simulated sample agree very well with the observed U, V, and W distributions.

4.4 The Luminosity Function

The luminosity function is derived by V/V_{max} method for the 89 thick disk subdwarf stars. For each star a maximum distance is adopted from from which a maximum volume is derived. The adopted maximum distance is the smaller of the maximum distance defined by the proper motion limit and the magnitude limit. Each star represents a single sampling over the maximum volume. Therefore each will contribute to the LF $1/V_{max}$ and sum of all the sample stars (ref. chapter 2.6).

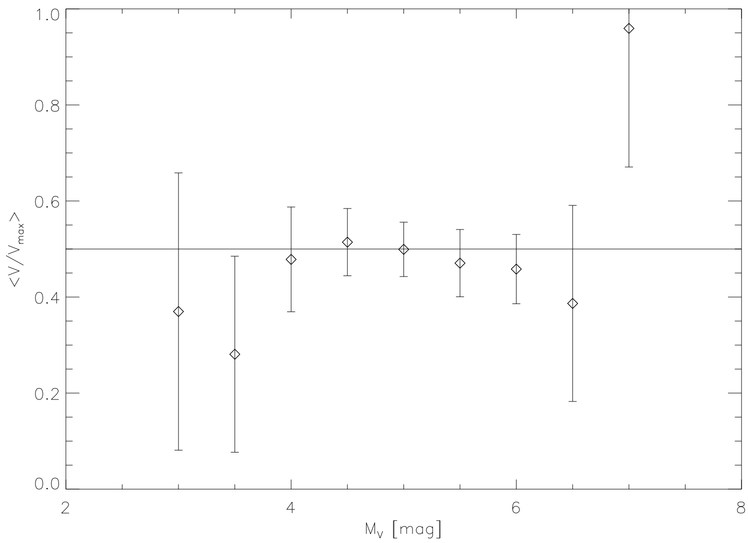

Figure 19: Completeness fraction, measured in terms of $< V/V_{max} >$ as a function of absolute magnitude M_V. The horizontal line indicates the values for the complete sample $< V/V_{max} >= 0.5$

The sample stars in our sample cover $\sim 2/3$ or $\beta = 0.6378$ of the whole sky since their $\delta > -20^o$. The number and luminosity function at each absolute magnitude in Table8 is observed number of stars in each unit magnitude interval and logarithm of number of stars per unit magnitude and unit volume. The completeness of the sample is tested by the average $< V/V_{max} >$ shown in Fig.19.

Table 8: Thick Disk Luminosity Function from Subdwarf sample

M_V	$\Phi(M_V)$	σ_Φ	N
3.00	0.8146E-06	0.8088E-06	1
3.50	0.3810E-05	0.1823E-05	2
4.00	0.2450E-04	0.5152E-05	10
4.50	0.7607E-04	0.1285E-04	19
5.00	0.2294E-03	0.2150E-04	30
5.50	0.2543E-03	0.3036E-04	19
6.00	0.2136E-03	0.3278E-04	7
6.50	0.1182E-04	0.1996E-04	1

The correction factor for stars omitted by the selection criteria of tangential velocity (or proper motion) can be estimated numerically (Richstone & Graham 1981) and by Monte Carlo simulation (Bahcall & Casertano 1986), with input of V_{asym} and the velocity dispersions. We performed again our Monte Carlo simulations and derive the correction factor (χ_{TD}) and simulated LF. We run 200 simulations, each simulation, we generate 3^5 stars, and took 89 surviving stars from the selection criteria, which is the same number of observed thick disk stars in our sample. The discovery fraction χ_{TD} of 0.53 is adopted from our simulation. We scale the thick disk LF following the method use by Digby et al. (2003),

$$\Phi_{TD}^{true} = \frac{1}{\chi_{TD}} \Phi_{TD}^{sample}. \quad (60)$$

We will consider any possible contamination by the thin disk stars. Assuming they are also included in the sample with $\mu_l \geq 180$ mas yr^{-1}, then the derived LF will comprise a total for thin disk and thick disk members. The thick disk LF can then be calculated from the total (Disk and Thick Disk) by

$$\Phi_{TD}^{sample} = \lambda_{TD} \Phi_{D+TD}^{sample}, \quad (61)$$

where λ_{TD} is the fraction of thick disk stars in the sample. This is given by

$$\lambda_{TD} = \frac{1}{(\chi_{TD}/\chi_D)(n_{TD}/n_D) + 1}, \quad (62)$$

where χ_D, χ_{TD} are the fraction of thin disk and thick disk stars with $\mu_l \geq 180$ mas yr^{-1} and n_D, n_{TD} are the local number densities of thin disk and thick disk stars (from Table 6). The discovery fraction of thin disk χ_D is known from Monte Carlo simulation with input parameter from Table 6.

4.5 Result and Discussion

Our measurement of the thick disk luminosity function is aimed at only the limited range in luminosity corresponding the nearby F,G and early K subdwarf stars. Nonetheless, this result offer a means to understand the thick disk population. We plotted the luminosity function in Figure 20, is based on sample of nearby subdwarfs. Therefore the result is for the bright part of the thick disk luminosity function. This LF has been obtained from 89 subdwarfs for $M_V = 3.0 - 6.5$ mag. The LF has a steep slope in the absolute magnitude of $M_V = 3 - 5$ mag. And constant density of $M_V = 5 - 6$ mag. At absolute magnitude of $M_V = 6.5$ the luminosity function decrease. The reason of this decreasing could be the Wielen Dip in $M_V \sim 7$ and incompleteness in our sample. We performed Monte Carlo simulations to understand the selection bias in our sample. We use the LFs of Bergbusch & Vandenberg (1992) for metallicity [Fe/H]=-0.65 with ages of 12 Gyrs. Bergbusch & Vandenberg (1992) use their LF to fit with the observed luminosity function of 47 Tuc. The simulated LFs for metallicity [Fe/H]=-0.65 with ages of 12 Gyrs agree well with the luminosity function derived by Reyle & Robin (2001) for $M_V = 3.0 - 6.0$.

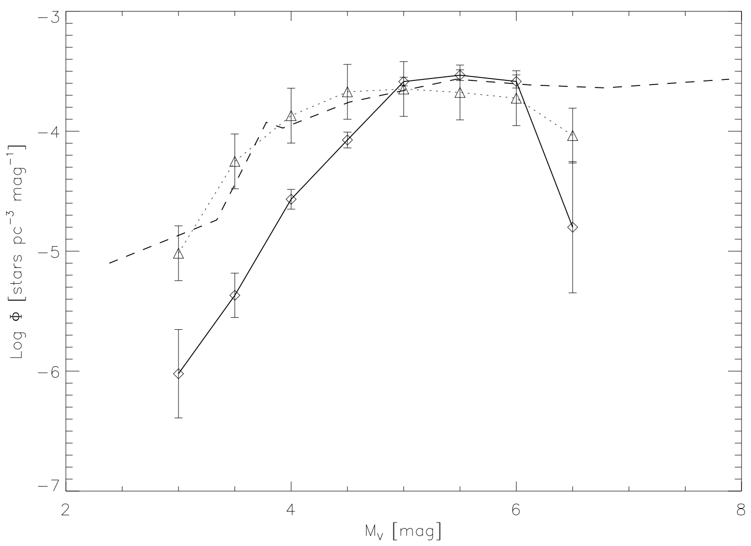

Figure 20: Simulated luminosity function taken from Bergbusch & Vandenberg (1992) for metallicity [Fe/H]=-0.65 with ages 12 Gyrs (dotted line) and 14 Gyrs (dashed line). We plot also the luminosity function of thick disk (full line) derived from the initial mass function (Reyle & Robin 2001).

The differences in the slope in absolute magnitude of $M_V = 3-5$ mag. between the simulations and the observed one could be due to lack of bright stars in the subdwarfs sample. However, the V/V_{max} plot in Figure 19 shows that our sample is completed within the absolute magnitude $4.0 \leq M_V \leq 6.0$. Gilmore & Reid (1983) (see Figure 13)found that the LF at $z > 1$ kpc, steepens rapidly for $M_V < 4.0$ mag.

5 Fine Structure In The Phase Space Distribution of Nearby Subdwarfs

Fine structure in the velocity distribution of stars in the Milky Way was discovered and studied during almost all O.J. Eggen (Eggen 1996 and references therein). Some of Eggens's star streams are associated with young open clusters and can be naturally interpreted as clouds of former, now unbound, members drifting away from the clusters. Other streams contain only very old stars with ages older than 10 Gyrs. Especially, since for many members distances were not known, but had to be assumed in order to construct space velocities, the real existence of such old streams was often doubted. However, modern data seem to confirm the concept of old star streams. Helmi et al. (1999) found analyzing Hipparcos data the signature of a cold stream in the velocity distribution of the halo stars of the Milky Way. This was confirmed later by Chiba & Beers (2000) using their own data (Beers et al. 2000). Helmi et al. (1999) interpreted this stream as part of the tidal debris of a disrupted satellite galaxy accreted by the Milky Way, which ended up in the halo. Indeed numerical simulations have shown that relic stars from disrupted satellites can stay on orbits close together for many Gyrs (Helmi et al. 2003, Helmi 2004). These show then up as over-densities in phase space. In the same vein Navarro et al. (2004) have argued that Eggens's (1996) Arcturus group is another such a debris stream, but in the thick disk of the Milky Way, dating back to an accretion event 5 to 8 Gyrs ago. These observations complement observations of ongoing accretion of satellites such as of the Sagittarius dwarf galaxy (Ibata et al. 1994) or very recent accretion in form of the Monoceros stream discovered in the outer disk of the Milky Way with SDSS data (Newberg et al. 2002, Yanny et al. 2003, Rocha-Pinto et al. 2003, Penarrubia et al. 2005). Extended periods of accretion of satellites onto massive galaxies are also expected theoretically. For instance, recent sophisticated simulations of the formation of a disk galaxy in the framework of cold dark matter cosmology and cosmogony of galaxies by Abadi et al. (2003a, b) suggest that disrupted satellites contribute significantly not only to the stellar halo but also to the disk of a galaxy.

Old moving groups are also observed in the velocity distribution of thin disk stars in the solar neighborhood. Using Hipparcos parallaxes and proper motions Dehnen (1998) found by statistical methods a new evidence of the Pleiades - Hyades and Hercules star streams. Even more convincingly these streams show up in the extensive data sample of three-dimensional kinematical data of F and G stars in the solar neighborhood by Nordstrom et al. (2004). The crowding of these stars on orbits in certain parts of velocity space is attributed to dynamical effects. Dehnen (2000) and Fux (2001) have demonstrated that the Hercules stream may be well due to an outer Lindblad resonance of the stars with the central bar of the Milky Way. The Pleiades - Hyades Stream, on the other hand, is probably due to orbital resonances of stars in the solar neighborhood with spiral density waves in the Milky Way disk (De Simone et al. 2004, Quillen & Minchev 2005). However, there are also hints that further over-densities in velocity space might be relics of accreted satellites (Helmi et al. 2005).

In this chapter we use our own data (chapter 2 or Arifyanto et al. 2005; hereafter AFJW) of the kinematics of nearby subdwarfs and develop a new strategy to search for signature of old star streams in the phase space distribution of the stars.

5.1 Data and Search Strategy for Streams

Data

The data set constructed by AFJW is based on the sample of F and G subdwarfs of Carney et al. (1994, hereafter CLLA). While keeping the precise radial velocity and metallicity data of CLLA, AFJW have significantly improved the accuracy of the distances and proper motions of a subset of the CLLA sample. The original CLLA sample contains 1464 stars, but kinematical and metallicity data are not available for every star. Many of the CLLA stars were observed with Hipparcos and AFJW identified 483 stars in the astrometric TYC2+HIP catalogue (Wielen et al. 2001) and replaced the parallaxes and proper motions of CLLA by Hipparcos parallaxes and proper motions, respectively. The Hipparcos parallaxes were then used to re-calibrate the photometric distance scale of the rest of the CLLA stars. AFJW could identify 259 CLLA stars in the Tycho-2 catalogue (Hog et al. 2000) and adopted the proper motions given there. Thus the sample of AFJW, which forms the basis of our analysis, contains 742 subdwarfs with greatly improved parallax and proper motion data. While the photometric distances were corrected by a factor of about 10%, the old NLTT proper motions were improved from an accuracy of 20 to 30 mas yr^{-1} to 2.5 mas yr^{-1}.

Search Strategy

The aim of our search is to find in phase space over-densities of stars on orbits which stay close together. For that purpose we use Dekker's (1976) theory of galactic orbits. Since the latter is despite its usefulness not well known, we repeat here the basic steps to estimate the parameters of stellar orbits. The first step is to separate the planar from the vertical motion of a star. This assumption is justified, because we are treating orbits of stars with disk-like kinematics. Concentrating now on the planar motion in the galactic plane the equation of motion of a star moving in the meridional plane is given by

$$\ddot{R} = -\frac{\partial \Phi_{eff}}{\partial R} = -\frac{\partial}{\partial R}\left(\Phi(R) + \frac{1}{2}\frac{L^2}{R^2}\right), \tag{63}$$

where R denotes the galactocentric radius. The effective potential $\Phi_{\rm eff}$ is constructed in the usual way with the gravitational potential $\Phi(R)$, which is assumed to by axisymmetric, and the vertical z-component of the angular momentum of the star L,

$$\Phi_{\rm eff}(R) = \Phi(R) + \frac{1}{2}\frac{L^2}{R^2}. \tag{64}$$

Dekker's theory proceeds then like standard epicycle theory by choosing a mean guiding center radius for the orbit of a star R_0 by setting

$$L = R_0^2\Omega(R_0)\; with\; \Omega(R) = \sqrt{\frac{1}{R}\frac{\partial \Phi}{\partial R}} \tag{65}$$

the mean angular frequency of a stellar orbit. The energy of a star on the circular mean guiding center orbit is obviously given by

$$E_0 = \Phi(R_0) + \frac{1}{2}R_0^2\Omega^2(R_0) \tag{66}$$

and κ us the epicyclic frequency defined by

$$\kappa^2(R_0) = 4\Omega^2(R_0)\left[1 + \frac{1}{2}\frac{d\ln\Omega}{d\ln R}\bigg|_{R_0}\right] \tag{67}$$

The key point of Dekker's (1976) formalism is to expand the potential with respect to $\frac{1}{R}$ around $\frac{1}{R_0}$ as

$$\begin{aligned} \Phi(R) &= \Phi(R_0) + \left.\frac{d\Phi}{d(\frac{1}{R})}\right|_{R_0} \left(\frac{1}{R} - \frac{1}{R_0}\right) \\ &+ \frac{1}{2}\left.\frac{d^2\Phi}{d(\frac{1}{R})^2}\right|_{R_0} \left(\frac{1}{R} - \frac{1}{R_0}\right)^2 \end{aligned} \tag{68}$$

which is asymmetric with respect to R_0 and thus more realistic than the Taylor expansion of $\Phi(R)$ in the standard epicyclic theory. With the definition of $\Omega(R)$ in eq. (65) we have

$$\begin{aligned} \left.\frac{d\Phi}{d(\frac{1}{R})}\right|_{R_0} &= -R^3\Omega_0^2, \\ \left.\frac{d\Phi}{d^2(\frac{1}{R})^2}\right|_{R_0} &= R^4(3\Omega^2 + 2\Omega R\left.\frac{d\Omega}{dR}\right|_{R_0}) \\ &= R^4(\kappa_0^2 - \Omega_0^2) \end{aligned} \tag{69}$$

We thus find

$$\Phi(R) = a_0 - \frac{b_0}{R} + \frac{c}{R^2} \tag{70}$$

with the coefficients

$$\begin{aligned} a_0 &= E_0 + \frac{1}{2}R_0^2\kappa_0^2, \\ b_0 &= R_0^3\kappa_0^2 \\ c_0 &= \frac{1}{2}R_0^4(\kappa_0^2 - \Omega_0^2). \end{aligned} \tag{71}$$

The turning points of the radial motion of a star R_t are defined by the condition $E = \Phi_{\text{eff}}(R_t)$. If the potential (70) is inserted, this leads to

$$\frac{R_t}{R_0} = \frac{1}{1 \pm e}\text{with}e = \sqrt{\frac{2(E - E_0)}{R_0^2\kappa_0^2}}. \tag{72}$$

The orbits are thus characterized by the two isolating integrals of motion angular momentum L and energy E. Dekker (1976) has shown by her approximation (68) with various forms of the exact potential that it gives reliable results up to eccentricities of $e \approx 0.5$. L and e can be estimated directly for each star in our sample. We assume that every star is essentially at the position of the Sun and find

$$L = R_\odot(V + V_{LSR}) = R_0 V_{LSR} \tag{73}$$

Here $R_\odot$ denotes the galactocentric distance of the Sun, for which we adopt 8 kpc, V is the velocity component of the star pointing into the direction of galactic rotation, and V_{LSR} is the circular velocity of the local standard of rest, for which we adopt 220 km s^{-1}. The eccentricity e is given by

$$e_{R_0} = \sqrt{\frac{U^2 + \frac{\kappa_0^2}{\Omega_0^2}V^2}{R_0^2\kappa_0^2}}, \tag{74}$$

with $U = -\dot{R}$ the radial velocity component of the star. In the following we assume a flat rotation curve implying $\kappa_0^2/\Omega_0^2 = 2$ and $R_0^2\kappa_0^2 = 2V_{LSR}^2$. The search for overdensities in phase space of stars on essentially the same orbits is carried out in practice in a space spanned up by $\sqrt{U^2 + 2V^2}$ and V. In addition we study also the distribution of stars in our sample in ($|W|, V$) velocity space. Since the Sun is located very close to the galactic midplane, $|W|$ is a measure of energy associate with the vertical motion of a star.

5.2 Result and Discussion

Thin Disk

The stars in our sample with metallicities $[\mathrm{Fe/H}] > -0.6$ dex have kinematics of the old thin disk of the Milky Way. In Fig. (21) we show the distribution of 309 stars, which have $|W|$ velocities $< 50\,\mathrm{km\,s^{-1}}$, over $\sqrt{U^2 + 2V^2}$ versus V and $|W|$ versus V, respectively. The space velocities have been reduced to the local standard of rest by adding the solar motion $(U, V, W)_\odot = (10.0, 5.2, 7.2)\,\mathrm{kms^{-1}}$ (Dehnen & Binney 1998) to the observed space velocities. Instead of scatter plots we show in Fig. (21) color coded wavelet transforms of our data. For this purpose we have used the two-dimensional Mexican hat wavelet transform described by Skuljan et al. (1999). After some experimentation we found that a wavelet scale of 10 km s^{-1} showed the overdensities in the data samples in the clearest way. The Hercules stream ranging from $V \approx 30$ km s^{-1} to $V \approx 70$ km s^{-1} is clearly visible and to a lesser degree the Hyades-Pleiades stream at $V \approx 15$ km s^{-1}, in both cases exactly where expected (Dehnen 2000, Nordström et al. 2004). Since these streams have been discussed widely in the literature we do not go into any further details in this letter. We present them mainly here to demonstrate that by recovering previously known streams our method is well suited to search for cold star streams.

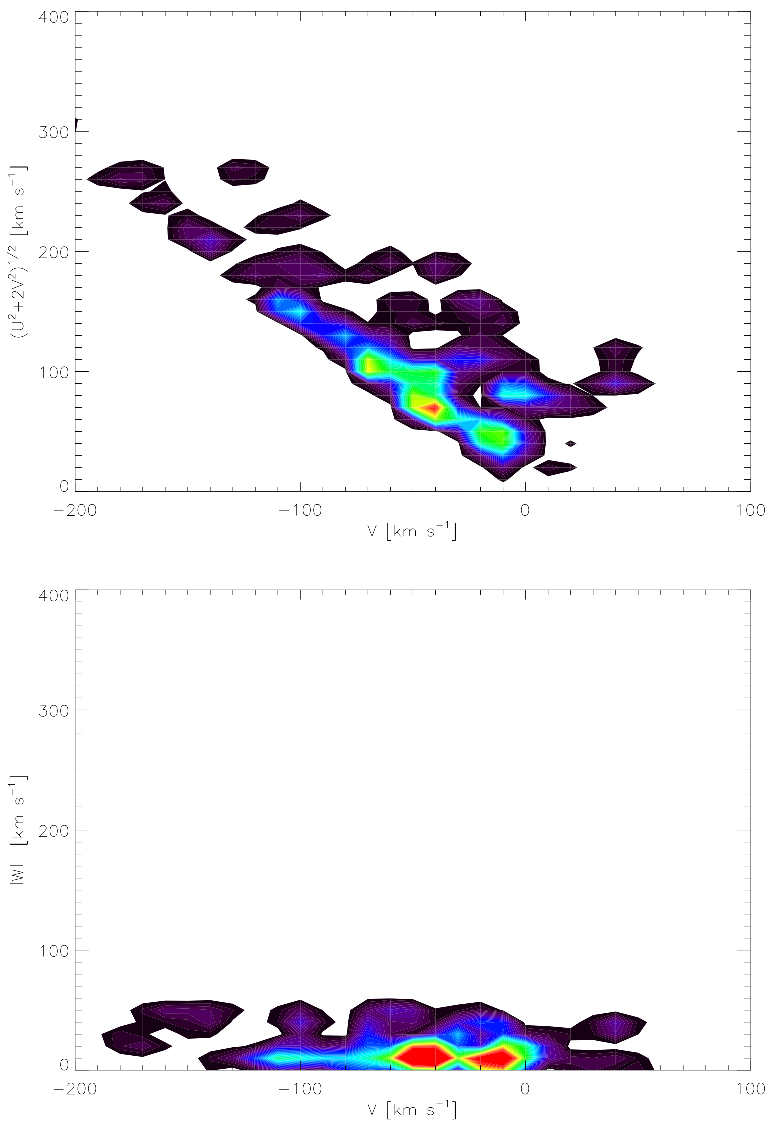

Figure 21: Wavelet analysis of the distribution of thin disk stars over $\sqrt{U^2 + 2V^2}$ versus V (top panel) and over $|W|$ versus V (bottom panel). The wavelet scale of the Mexican hat kernel is 10 km s^{-1} and a linear color table from black over lilac, green, yellow to red is adopted.

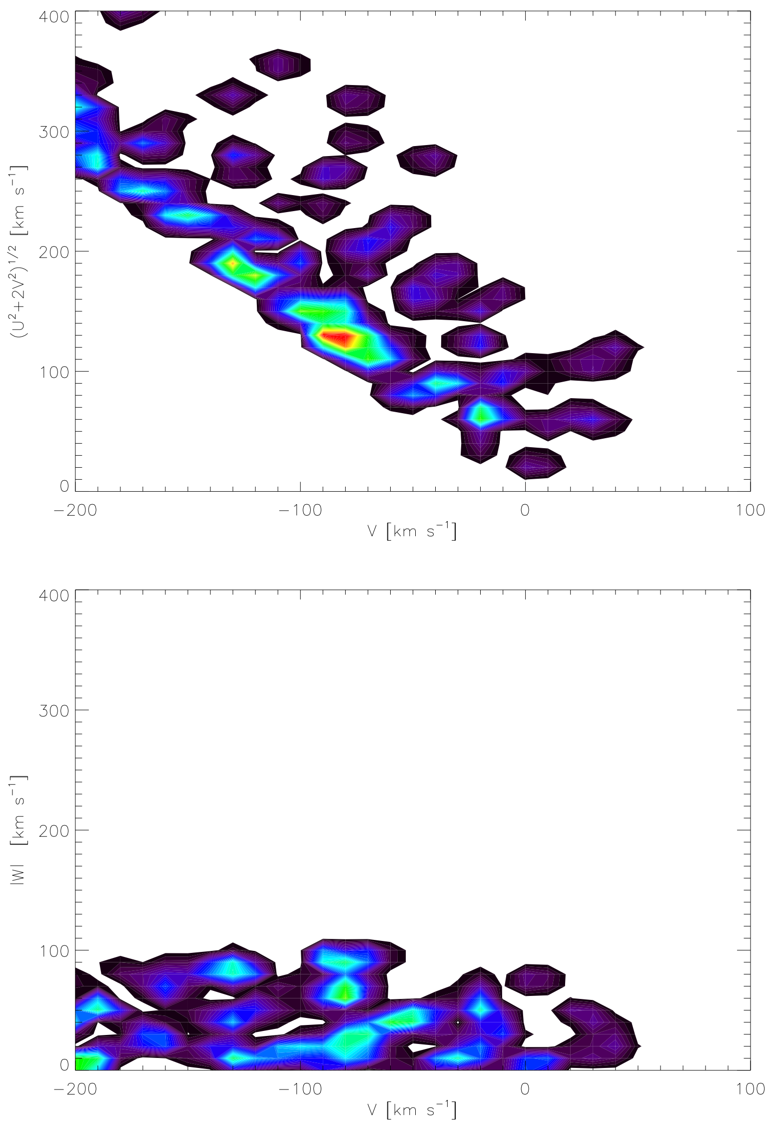

Figure 22: Same as Fig.21, but for thick disk stars

Thick Disk

The remaining stars of our sample with metallicities $[\mathrm{Fe/H}] < -0.6$ dex belong to the thick disk and halo of the Milky Way. The distribution of 382 stars is shown in Fig.(22) in the same way as above, but now restricted to $|W| < 100$ km s^{-1}. There are two distinct features in the phase space distribution function. The lesser feature at $V \approx 125$ km s^{-1} corresponds to the familiar Arcturus stream (Eggen 1996, Navarro et al. 2004). Actually there is one common star, G2-34. The kinematics and metallicities agree so well with each other that, even though the reality of overdensities is difficult to assess, we are confident that both investigations have identified the same stream. Arcturus itself, although not a CLLA star, lies in Fig.(22) at $V = -114$ km s^{-1}, $\sqrt{U^2 + 2V^2} = 165$ km s^{-1}, and $|W| = 4$ km s^{-1}, respectively. With a metallicity of $[\mathrm{Fe/H}] = -0.55$ (Luck & Heiter 2005) it fits well to the rest of the presumed stream members. We place the center of the stream at $V = -125$ km s^{-1} and $\sqrt{U^2 + 2V^2} = 185$ km s^{-1} implying $|U| = 55$ km s^{-1}. According to equation (73) the guiding center radius of the stars passing now close to the Sun is $R_0 = 0.43 R_\odot = 3.5$ kpc. The eccentricity is $e_{R_0} = 0.59$ implying an outer turning radius of $R_t = 2.5 R_\odot = 8.5$ kpc. The stars are apparently close to apogalacticon, when they are at their slowest on their orbits and the detection probability is highest. In Fig.(23) we show a color-magnitude diagram of the presumed members of the Arcturus stream listed in Table 1. Overlaid are theoretical isochrones of subdwarfs with an age of 12 Gyrs calculated for metallicities $[\mathrm{Fe/H}] = -0.5, -1$, and -1.5, respectively (Yi et al. 2001). The good fit of the isochrones indicates that the selected stars must be very old. Judging from the ages and metallicities of the stars and the similarity of their kinematics with that of a disrupted satellite in the vicinity of the Sun we follow Navarro et al. (2004) in the conclusion that the members of the Arcturus stream are of extragalactic origin. As can be seen in Fig.(22) there is a second strong feature in the phase space distribution of the thick disk stars. This seems to be even more significant than the overdensity in the Arcturus region. The stars in this overdense region are listed in Table 2. To our knowledge the existence of a cold star stream in this part of phase space has not been suggested before. As can be seen from Tables 1 and 2 the velocity and metallicity distributions of the members of the proposed new stream and the Arcturus steam are practically identical. Also the color-magnitude diagram shown in Fig.(23) seems to indicate that the stars stem from the same population. We place the center of the proposed new stream at $V = -80$ km s^{-1} and ,$\sqrt{U^2 + 2V^2} = 130$ km s^{-1} implying $|U| = 64$ km s^{-1}. The mean guiding center radius of these stars passing now close to the sun is $R_0 = 0.64 R_\odot = 5.1$ kpc. The eccentricity is $e_{R_0} = 0.42$ and the outer turning radius is at $R_t = 1.7 R_\odot = 8.7$ kpc. Thus also the stars of the proposed new stream are on their orbits close to apogalacticon. We can at present only speculate about the possible origin of the stream. However, the similarity of the characteristics of the new stream with the Arcturus stream, seems to point also to an extragalactic origin.

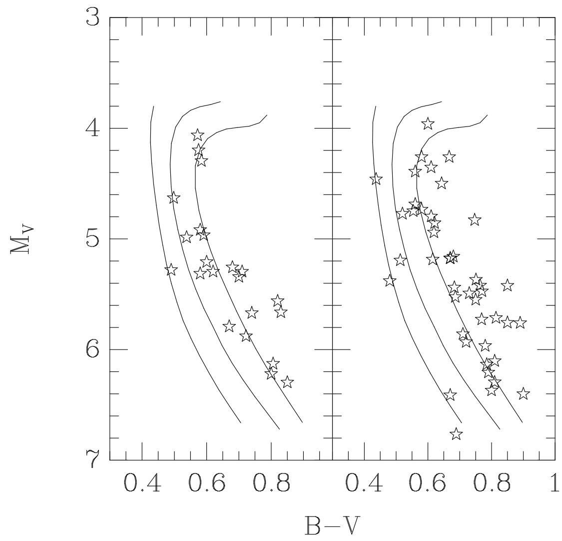

Figure 23: Color-magnitude diagrams of the presumed members of the Arcturus stream (left panel) and proposed new stream (right panel). Overlaid are theoretical isochrones for subdwarfs with an age of 12 Gyrs and metallicities of $[Fe/H] = -0.5, -1$ and -1.5 (from right to left)

6 Summary and Conclusion

Our samples based on the CLLA surveys are kinematically biased, and it is possible that some of the results discussed above could have been produced by some combination of biases. Comparing to the non-kinematically sample of Chiba and Beers (2000), our kinematics properties are somewhat higher, because the lack of stars in low velocity regions. The next steps of this work could be to try to model the kinematics biases and remove them and obtain kinematically unbiased samples. Another important bias related to the analysis of trigonometric parallax is the Lutz-Kelker bias (Lutz & Kelker, 1973). This effect causes a systematic bias such that measured parallaxes will on average yield too small distances ($René$ et al. 1998). Reid (1998) used Monte Carlo simulations to determined the expected extent of this bias in the Hipparcos subdwarf sample. He found that for a sample of stars with parallaxes measured to a formal precision of 30 % ($\sigma_\pi/\pi < 0.3$) at $M_V = 3$ mag. would have predicted bias $\Delta M_V = 1$ mag. Hence, for the $\sigma_\pi/\pi > 0.3$, the absolute magnitudes for the intrinsically brightest stars, which remain in the sample at distances of more than 500 pc, are biased to a greater extent than the $M_V = 6$ stars (Reid 1998).

Hipparcos parallaxes and proper motions improve the accuracy of kinematic properties of CLLA subdwarfs sample. Our sample A and A+B are local samples, since the distance of 90% of the samples are below than 150 pc, and distance perpendicular to the galactic plane is $|Z|$< 100 pc. However, the kinematical properties of sample C (CLLA-Tycho2) stars are somewhat 'colder' than the other samples. The completeness of the Tycho2 catalogue is at $m_V < 11.5$ mag., while about 30% of our CLLA-Tycho2 sample have visual magnitudes fainter than the completeness limit. We tried to make some distance cut at $d \leq 150$ pc in the sample and found that the rotation velocity of the metal poor subdwarfs becomes higher, $V_{rot} \sim 60$ kms^{-1}. However, this bias will not change our result that there is a considerable overlap between the halo and thick disk.

Our finding of the 'metal weak thick disk' (MWTD), from 740 kinematically selected sample of nearby subdwarfs, for metal poor stars in the range $-1.6 < [Fe/H] < -1$ confirms the previous results by e.g. Morrison et al. (1990), Chiba & Yoshi (1998), Chiba & Beers (2000) and recently Beers et al. (2002). The local fraction (i.e. within 300 pc from the Sun) of metal poor stars that might be associate with the MWTD is on the order of 20%-40% and rotate at velocity of $V_{rot} \approx 120\, kms^{-1}$.

For stars with metallicity [Fe/H]>-1.0 shows the disklike kinematics. We concentrate for stars with $-1.0 \leq$ [Fe/H] ≤ -0.4 to locate the thick disk population. We derived the luminosity function of thick disk using the magnitude and proper motion. We found the kinematics parameter of the thick disk ($\sigma_U, \sigma_V, \sigma_W, V_{asym}$) = $(60, 45, 39, -41)$ km s^{-1}, which is in good agreement with other values from the non-kinematically selected sample (Martin & Morrison, 1993).

Over the past decade, a number of claims for a significant population of metal poor stars with disklike kinematics have been made, but their presence has been cast into doubt because of incorrectly assigned metallicities (Beers et al. 2002). Based on metallicities from the expanded sample of proper motion survey by CLLA and the accuracy of Hipparcos trigonometric parallaxes and proper motions, we confirm the existence of the MWTD.

We must try to understand the implications of a significant population of MWTD stars for theories of the formation and evolution of the Galaxy. It should be keep in mind that, although the MWTD population may contribute a large fraction of the *local* metal poor stars, the (inner) halo populations is probably still the dominant reservoir of stars with $[Fe/H] \leq -1.6$ within a few kiloparsecs of the Sun. Furthermore, although we have emphasized the possible importance of the MWTD population, it certainly still appears to be a minor constituent of the entire thick disk population (Beers et al. 2002).

If there is indeed a significant fraction of thick disk stars with metal abundance $-1.6 < [Fe/H] < -1$, as we have argued, this finding may have significance to formation scenarios of the Galaxy. An interesting scenario for the origin of a MWTD component may be the merging of satellite galaxies (Searle & Zinn, 1978), which are then accreted by a thin, fast rotating, possibly metal poor, Galactic disk (Quinn et al. 1993; Wyse 2001). The dynamical heating of the stellar component of this disk in connection with the accretion process produces the thick disk. The kinematics of the halo depends on the dynamics of the merging satellites, whereas the kinematics of the thick disk are determined by the heating of the rotating disk. This scenario offers a natural explanation for the striking kinematical discontinuity between halo and thick disk stars(see Fig. **??**)(see Gilmore & Wyse 1985, Gilmore, Wyse & Kuijken 1989, Nissen & Schuster 1991). An overlap in abundance at

$-1.6 < [Fe/H] < -1$ (MWTD population) may occur, because the satellite galaxies and the Galactic disk have separate chemical evolutions (Nissen & Schuster, 1991). In the recent paper of Gilmore et al. (2002), they find evidence for two probable cccomponents within the thick disk by studying stars $0.5 - 5.0$ kpc from the galactic plane. Suprisingly they find a V_{rot} a few kpc above the plane of only 100 km s^{-1} compared to the expected 180 km s^{-1}, and conclude that this is probably evidence for a merger event with the disk of the Milky Way some 10-12 Gyr ago, that their sample is dominated by the remnants of a disrupted satellite galaxy.

Bibliography

[1] Abadi, M.G., Navarro, J.F., Steinmetz, M., Eke, V.R., 2003a, ApJ 591, 499

[2] Abadi, M.G., Navarro, J.F., Steinmetz, M., Eke, V.R., 2003b, ApJ 597, 21

[3] Adams, Humanson (1935) PASP, 47, 52

[4] Arifyanto, M.I., Fuchs, B., Jahreiß, H., Wielen, R., 2005, A&A 433, 911

[5] Baade, W. (1944) ApJ, 100, 137

[6] Beers, T.C., Chiba, M., Yoshii, Y., Platais, I., Hanson, R.B., Fuchs, B., Rossi, S. (2000) AJ, 119, 2866

[7] Beers, T.C., Drilling, J.S., Rossi, S., Chiba, M., Rhee, J., Fü hrmeister, B., Norris, J.E., von Hippel, T. (2002) AJ, 931

[8] Beers, T.C., Sommer-Larsen, J. (1995) ApJS, 96, 175

[9] Bensby, T., Feltzing, S., & Lundstrom, 2003, A&A, 527

[10] Bergbusch, P.A., & Vandenberg, D.A., 1992, ApJS, 81, 163

[11] Binney, J., Tremaine, S. (1987) "Galactic Dynamics", Princeton Univ. Press.

[12] Binney, J., Merrifield, M. (1998)"Galactic Astronomy", Princeton Univ. Press.

[13] Buser, R., Rong, Jinxiang, & Karaali, S., 1999, A&A, 348, 98

[14] Carney, B.W. (1993) in "Galaxy Evolution: The Milky Way Perspective" ASP Conf. Series 49, S.R. Majewski (ed.), p.83

[15] Carney, B. W., Aguilar, L., Latham, D. W., and Laird, J. B. (1990), AJ, 99, 201

[16] Carney, B.W., Laird, J.B., Latham, D.W., Aguilar, L.A. (1996) AJ, 112, 668

[17] Carney, B.W., Latham, D.W., Laird, J.B., Aguilar, L.A. (1994) AJ, 107, 2240 (**CLLA**)

[18] Carney, B. W., Latham, D. W., Laird, J. B., & John, B. 1989, AJ, 97, 423

[19] Chiba, M., Beers, T.C. (2000) AJ, 119, 2843

[20] Chiba, M., Yoshii, Y. (1998) AJ, 115, 168

[21] Cox, A.N. (2000) Allen's Astrophysical Quantities 4th edition, Springer Verlag

[22] Dawson, P.C., 1990, J.R.A.S.Canada, 84, 175

[23] Dehnen, W., 2000, AJ 119, 800

[24] Dehnen, W., Binney, J., 1998, MNRAS 298, 387

[25] Dekker, E., 1976, Phys. Reports 24, 315

[26] Delhaye, J. 1965, in Galactic Structure, Stars and Stellar Systems 5, 61

[27] Digby, Hambly et al., 2003, MNRAS, 344, 583

[28] ESA (1997) The Hipparcos and Tycho Catalogues (ESA SP-1200) (Noordwijk: ESA)

[29] Eggen, O. J., (1983)

[1996] Eggen, O.J., 1996, AJ 112, 1595

[30] Eggen, O. J., Lynden-Bell, D., and Sandage, A.R., (1962) ApJ, 136, 748

[31] Freeman, K. C. 1987, ARA&A, 25, 603

[32] Frenk, C.S., White, S.D.M., 1982, MNRAS,198,173

[33] Fuchs, B., Jahreiss, H., Wielen, R. (1998) Ap&SS, 265, 175 (**FJW**)

[34] Fux, R., 2001, A&A 373, 511

[35] Garcia-Berro, E., Torres, Santiago, Isern, Jordi, & Burkert, A., 1999 MNRAS, 302, 173

[36] Gilmore, G., Wyse, R.F.G. (1985) AJ, 90, 2015

[37] Gilmore, G., Wyse, R.F.G., Kuijken, K. (1989) ARA&A, 27, 555(**GWK**)

[38] Gilmore, G., Wyse, R. F. G., & Norris, J. N. 2002, AJ, 574, L39

[39] Gizis, J.E. & Reid, I.N., 1999, AJ, 117, 508

[40] Helmi, A., White, S.D.M., de Zeeuw, P.T., Zhao, H., 1999, Nature 402, 53

[41] Helmi, A., Navarro, J.F., Meza, A., et al., 2003, ApJ 592, L25

[42] Helmi, A., 2004, MNRAS 351, 643

[43] Helmi, A., Navarro, J.F., Nordström, B., et al., 2005, MNRAS, in press (astro-ph/05055401)

[44] Høg, E., Fabricius, C., Makarov, V. V., Urban, S., Corbin, T., Wycoff, G., Bastian, U., Schwekendiek, P., Wicenec, A. (2000) A&A, 355, 367

[45] Ibata, R., Gilmore, G., Irwin, M.J., 1994, Nature 370, 194

[46] Jahreiss, H., Fuchs, B., Wielen, R. (1997) in ”Hipparcos-Venice ’97”, M.A.C. Perryman, P.L. Bernacca (eds.), ESA SP-402, p. 587

[47] Jaschek, Jaschek (1987) ”The Classification of Stars”, Cambridge

[48] Karatas, Y., Bilir, S., Schuster., W.J., 2005, MNRAS, 360, 1345

[49] Kuiper (1939) ApJ, 89, 548

[1988] Laird, J. B., Rupen, M. P., Carney, B. W., & Latham, D. W. 1988, AJ, 96, 1908

[1996] Layden, A. C., Hanson, R. B., Hawley, S. L., Klemola, A. R., & Hanley, C. J. 1996, AJ, 112, 2110

[50] Linblad, B. (1927) MNRAS, 87, 553

[1994] Luck, R.E., Heiter, U., 2005, AJ 129, 1063

[51] Lutz, T.E., Kelker, D.H. (1973) PASP, 87, 617

[52] Majewski, S. R. (1993) ARA&A, 31, 575

[1998] Martin, J. C., & Morrison, H. L. 1998, AJ, 116, 172

[53] Mihalas, D., Binney, J. (1981) “Galactic Astronomy”, W.H. Freeman & Co.

[54] Morrison, H.L., Flynn, C., Freeman, K.C. (1990), AJ, 100, 1191

[55] Mould, J.R. (1982) ARA&A, 20, 91

[56] Navarro, J.F., Helmi, A., Freeman, K.C., 2004, ApJ 601, L43

[57] Newberg, H.J., et al., 2002, ApJ 569, 245

[58] Nissen, P. E., Schuster, W. J. (1991) A&A, 251, 457

[59] Nordström, B., et al., 2004, A&A 418, 989

[60] Norris, J.E.,2001, in “Encyclopedia of Astronomy and Astrophysics”, Nature Publishing Group, UK

[61] O’Connel, D.J.K. (1958) “Stellar Populations”, North Holland

[62] Peñarrubia, J., Martínez-Delgado, D., Rix, H.W., et al., 2005, ApJ 626, 128

[63] Press, W.H., Flannery, B.P., Teukolsky, T.A., Vetterling, W.T (1992) Numerical Recipes in Fortran, Cambridge Univ. Press.

[64] Quillen, A.C., Minchev, I., 2005, AJ 130, 576

[65] Quinn, P.J., Hernquist, L., Fullagar, D.P. (1993) ApJ, 403, 74

[66] Reid, I.N. (1998) AJ, 115, 204

[67] Reid, I. N., van Wyk, F., Marang, F., Roberts, G., Kilkenny, D., Mahoney, S. (2001) MNRAS, 325, 931

[68] Rocha-Pinto,, H.J., Majewski, S.R., Skrutskie, M.F., Crane, J.D., 2003, ApJ 594, L115

[69] Reyle, C. & Robin, A.C., 2001, A&A, 373, 886

[70] Ryan, S.G., Norris, J.E. (1991) AJ, 101, 1835

[71] Ryan, S.G., Norris, J.E. (1993) in "Galaxy Evolution: The MIlky Way Perspective" ASP Conf. Series 49, S. Majewski (ed),103

[72] Sachs, L. 1988, Statistische Methoden, Springer Verlag, Berlin.

[73] Sandage, A. R. (1986) ARA&A, 24, 421

[74] Sandler, Rich, Terndrup (1996) AJ, 112, 171

[75] Schuster, W>J., Parrao, L. Contreas-Martinez, M.E., 1993, A&AS, 97,951

[76] Searle, L., Zinn, R. (1978) ApJ, 225, 357

[77] De Simone, R.S., Wu, X., Tremaine, S., 2004, MNRAS 350, 627

[78] Skuljan, J., Hearnshaw, J.B., Cottrell, P.L., 1999, MNRAS 308, 731

[79] Sommer-Larsen, J., & Zhen, C. 1990, MNRAS, 242, 10

[80] Turon, C. (1999) in "Post-Hipparcos Cosmic Candles", A. Heck and F. Caputo (eds.), Kluwer Academic Publishers, Nederland

[81] Wielen, R. 1986, Transactions Intern. Astron. Union 19B, 93

[82] Wielen, R., Schwan, H., Dettbarn, C., et al. 2001, *Astrometric Catalogue TYC2+HIP Derived from a Combination of the HIPPARCOS Catalogue with the Proper Motions Given in the TYCHO-2 Catalogue*, Veröff. Astron. Rechen-Inst. Heidelberg No. 39

[83] Wood, Matt A. & Oswalt, Terry D. 1998, ApJ, 497,870

[84] Wyse, R.F.G. (2001) in "Galaxy Disks and Disk Galaxies" ASP Conf. Series 230, J.G. Funes & E.M. Corsini (eds.), 71

[85] Yanny, B., et al., 2003, ApJ 588, 824

[86] Yi, S., Demarque, P., Lejeune, T., Barnes S., 2001, ApJS 136, 417

7 Appendix: Data tables

The following tables contain the sample of subdwarf stars from CLLA catalog which the trigonometric parallaxes and the proper motions from are coming from the TYC2-HIP and Tyco2 catalogs.

Column 1: Hipparcos or Giclas Name

Column 2: Right Ascencions α epoch 2000 [deg]

Column 3: Apparent magnitude V [mag]

Column 4: Declination δ epoch 2000 [deg]

Column 5: Trigonometric Parallax (π) [mas]

Column 6: Proper Motion $\mu_{\alpha}*$ [mas/yr]

Column 7: Proper Motion μ_{δ} [mas/yr]

Column 8: Error in Parallax σ_{π} [mas]

Column 9: Error in Proper Motion $\sigma_{\mu_{\alpha}*}$ [mas/yr]

Column 10: Error in Proper Motion $\sigma_{\mu_{\delta}}$ [mas/yr]

Column 11: Color (B-V) in magnitude

Column 12: Radial Velocity [km/s]

Column 13: Error in Radial Velocity [km/s]

Column 14: Metallicity [Fe/H] dex

Column 15: Remarks : 11 : Parallax and Proper Motion from TYC2-HIP catalog

22 : Hipparcos stars with Corrected Parallax

33 : Stars with corrected parallax and with Proper Motion from Tycho2 catalog

Star	α_{2000}	δ_{2000}	V	π	$\mu_{\alpha*}$	μ_δ	σ_π	$\sigma_{\mu_{\alpha*}}$	σ_{μ_δ}	B-V	V_{rad}	$\sigma_{V_{rad}}$	[Fe/H]	*remarks*
(HIP/Gic)	(deg)	(deg)	(mag)	(mas)	$(mas\ yr^{-1})$	$(mas\ yr^{-1})$	(mas)	$(mas\ yr^{-1})$	$(mas\ yr^{-1})$	(mag)	$(km\ s^{-1})$	$(km\ s^{-1})$	(dex)	-
(1)	(2)	(3)	(4)	(5)	(6)	(7)	(8)	(9)	(10)	(11)	(12)	(13)	(14)	(15)
81	0.24341455	-4.93253374	8.57	23.43	-184.41	-172.42	1.26	0.75	0.49	0.642	0.0	0.7	-0.60	11
348	1.08959222	12.95729160	8.60	16.79	317.51	97.36	1.13	0.83	0.65	0.640	18.2	0.6	-0.26	11
352	1.11211336	58.06869125	10.42	12.99	437.69	-37.99	1.76	1.24	1.26	0.800	-90.0	0.7	-0.46	11
569	1.72450304	-3.62626290	8.23	18.71	-123.46	-222.27	1.04	0.91	0.62	0.580	-28.0	0.5	-0.33	11
1437	4.47774220	0.37782174	8.88	16.24	330.16	98.38	1.24	0.95	0.66	0.542	48.6	0.7	-0.48	11
1813	5.75087070	22.37500000	7.57	24.68	202.55	-221.23	0.89	0.78	0.51	0.639	-30.7	0.7	-0.21	11
2350	7.49946499	-5.76400185	9.44	18.62	-107.69	-224.14	1.35	1.10	0.84	0.886	9.7	0.4	-0.18	11
2563	8.14190960	28.19763184	8.66	17.80	194.07	64.99	1.29	1.02	0.81	0.650	-1.2	6.9	-0.65	11
2600	8.25589275	44.73008347	10.27	9.52	223.44	-44.98	1.57	0.91	0.92	0.780	50.0	0.5	-0.11	11
2712	8.62380123	47.91554260	7.38	21.20	397.39	60.05	0.87	0.53	0.61	0.549	-12.2	0.3	-0.18	11
3026	9.63311195	-8.30927658	9.25	9.57	20.13	-546.84	1.36	1.02	0.77	0.465	-48.6	0.8	-1.50	11
3054	9.69775009	31.01914978	9.04	16.48	-245.88	-58.44	1.19	1.01	0.73	0.630	-81.7	0.6	-0.51	11
3430	10.93479156	72.17864227	10.20	6.04	324.42	92.29	1.14	0.90	0.92	0.401	-122.1	0.8	-2.27	11
3956	12.69722080	51.38268661	9.65	11.70	248.33	-47.05	1.57	0.91	0.78	0.620	45.7	0.4	-0.55	11
3960	12.71424770	10.36427307	10.51	12.09	277.88	60.66	2.16	1.55	0.95	0.789	35.6	0.5	-0.38	11
3979	12.79520035	-5.03927946	6.98	45.27	262.34	-119.63	0.95	0.75	0.61	0.663	-3.7	0.3	-0.28	11
4039	12.95339680	74.47397614	9.77	7.08	237.72	61.50	1.15	0.92	0.86	0.490	-2.4	0.8	-1.17	11
4754	15.27709579	16.37264824	10.65	6.62	342.32	-150.17	1.80	1.09	0.94	0.540	-86.6	0.9	-1.71	11
4907	15.73842621	69.22705841	7.67	38.73	223.83	-148.19	0.78	0.56	0.73	0.756	-19.9	0.6	-0.18	11
5031	16.11029625	-2.36659646	9.15	25.48	-207.61	-136.98	1.14	0.79	0.63	0.801	-14.0	1.0	-0.67	11
5106	16.36037064	63.72129440	8.29	18.19	227.80	-164.22	0.98	0.68	0.78	0.600	-28.8	0.4	0.17	11
5163	16.52147293	1.70641172	9.50	12.72	160.02	-147.42	1.34	0.91	0.66	0.603	28.3	0.8	-0.70	11
5301	16.95275879	-8.23370552	8.45	18.18	191.43	18.68	0.95	0.88	0.58	0.662	34.6	0.5	-0.26	11
5335	17.05201912	21.97700691	7.61	30.84	400.93	-47.58	0.86	0.73	0.52	0.710	-24.0	0.5	-0.36	11
5527	17.68610573	10.99983215	9.08	20.00	220.75	46.60	1.33	0.98	0.96	0.771	2.8	0.6	-0.26	11
5775	18.53016853	-16.42639160	10.10	8.64	198.69	-111.32	2.20	1.28	1.16	0.670	85.1	0.5	-0.76	11
5806	18.62217331	-5.04738712	7.50	25.96	-161.59	-138.89	0.77	0.64	0.48	0.575	-19.8	0.5	-0.12	11
6159	19.74993896	-8.93949413	8.90	14.91	-230.44	-458.83	1.21	0.86	0.72	0.596	-5.4	0.5	-0.78	11
6306	20.26459122	51.98366928	7.62	16.64	288.40	-103.79	0.85	0.58	0.62	0.582	13.9	0.5	0.04	11
6309	20.26657295	38.03420639	7.83	20.25	277.59	17.35	1.14	0.83	0.82	0.661	13.9	0.5	-0.05	11
6613	21.22476196	18.49992943	8.49	30.24	544.96	-191.12	1.08	0.80	0.56	0.912	7.0	0.8	-0.31	11

Star (HIP/Gic) (1)	α_{2000} (deg) (2)	δ_{2000} (deg) (3)	V (mag) (4)	π (mas) (5)	$\mu_{\alpha*}$ $(mas\ yr^{-1})$ (6)	μ_{δ} $(mas\ yr^{-1})$ (7)	σ_{π} (mas) (8)	$\sigma_{\mu_{\alpha*}}$ $(mas\ yr^{-1})$ (9)	$\sigma_{\mu_{\delta}}$ $(mas\ yr^{-1})$ (10)	B-V (mag) (11)	V_{rad} $(km\ s^{-1})$ (12)	$\sigma_{V_{rad}}$ $(km\ s^{-1})$ (13)	[Fe/H] (dex) (14)	*remarks* - (15)
6833	21.98151398	-1.99149251	8.60	19.92	-167.14	-143.89	1.03	0.71	0.59	0.656	-42.1	0.9	-0.56	11
7217	23.24000168	23.69567871	9.04	15.33	-204.88	-162.06	1.23	0.82	0.67	0.623	-53.4	0.9	-0.55	11
7221	23.25903511	53.03375626	8.41	19.58	220.66	13.36	1.01	0.74	0.56	0.710	-20.0	0.4	0.17	11
7339	23.63859940	68.94813538	6.52	47.65	-378.92	114.69	0.60	0.41	0.46	0.686	-33.2	0.6	-0.15	11
7452	24.00544930	49.71186447	10.14	6.85	133.44	-153.16	1.45	1.03	1.00	0.462	-133.0	0.9	-1.42	11
7626	24.55910301	17.82942963	9.40	20.45	263.21	-157.17	1.37	1.10	0.96	0.810	25.5	0.7	-0.24	11
7902	25.40720749	66.90994263	7.70	27.28	692.15	-264.90	0.95	0.60	0.58	0.691	17.3	0.6	-0.16	11
8130	26.12433243	44.46387100	10.21	11.33	309.04	1.29	1.43	0.94	0.73	0.498	38.8	0.7	-0.64	11
8221	26.46512604	20.30818939	9.17	14.72	218.56	-112.55	1.23	0.90	0.81	0.780	-12.6	0.3	-0.26	11
8314	26.80161476	73.47422028	9.94	6.46	-206.34	162.86	1.26	1.07	0.93	0.417	-269.0	1.1	-1.62	11
8349	26.91716194	-3.23746896	8.22	12.64	180.98	123.96	1.12	0.92	0.76	0.517	22.1	0.6	-0.50	11
8720	28.04364777	-2.80501771	10.91	10.10	-66.99	-236.29	1.91	1.46	1.16	0.762	-0.3	0.6	-0.64	11
8798	28.27582741	-1.32694447	7.43	26.56	-187.03	-349.83	1.05	0.77	0.58	0.635	-16.8	0.4	-0.48	11
9080	29.23373795	11.66352558	10.52	13.26	378.47	2.28	1.97	1.38	1.38	0.785	-10.7	0.9	-0.39	11
9238	29.69472885	69.02400970	9.29	9.53	353.75	-34.26	1.04	0.76	0.86	0.578	0.9	0.6	-0.04	11
9269	29.77763748	33.20968246	7.14	40.74	243.44	-352.68	0.88	0.74	0.67	0.773	-35.1	0.4	-0.05	11
9714	31.24457550	22.80226517	9.51	19.49	360.77	-344.90	1.45	1.06	0.90	0.890	-9.9	0.6	0.06	11
10031	32.28442764	71.55200958	6.57	36.57	307.75	-239.33	0.65	0.45	0.46	0.551	0.5	0.5	-0.19	11
10140	32.60219955	29.80657387	8.76	17.66	289.44	-266.23	1.27	0.99	0.84	0.580	27.1	0.5	-1.03	11
10245	32.94532776	45.92424774	9.67	18.81	277.83	-8.32	1.35	0.99	0.89	0.890	-6.6	0.6	0.11	11
10449	33.66791153	-1.20142400	9.08	16.17	994.57	-80.53	1.32	0.82	0.73	0.582	27.8	0.8	-1.02	11
10510	33.86390686	27.35726166	8.12	26.89	286.63	-138.53	1.04	0.71	0.75	0.705	1.2	0.3	0.03	11
10599	34.11555099	12.37976360	7.99	29.35	225.75	-220.25	1.06	0.81	0.74	0.790	-20.7	0.4	-0.09	11
10629	34.20505142	64.95260620	8.30	25.82	-342.89	-318.59	1.06	0.66	0.75	0.674	-32.3	0.4	-0.55	11
10652	34.27974319	21.56681061	9.06	14.43	473.77	83.43	1.29	0.77	0.69	0.621	-21.1	0.9	-0.89	11
10921	35.16384888	13.67014027	9.12	18.40	260.64	-37.41	1.31	1.05	0.87	0.790	42.1	0.3	-0.54	11
11083	35.67352676	18.41065216	8.83	29.51	261.20	87.10	1.30	0.74	0.74	0.906	42.3	0.6	-0.03	11
11111	35.75283051	71.17691040	8.94	26.92	533.81	-172.65	1.06	0.78	0.81	0.882	-15.8	0.6	0.15	11
11270	36.28577423	46.49966812	9.55	12.00	152.13	-140.49	1.23	0.83	0.89	0.671	49.7	0.3	0.18	11
11309	36.39140701	11.97122860	7.36	15.05	-122.34	-281.97	0.91	0.70	0.60	0.495	-8.9	0.4	-0.46	11
11532	37.17171478	17.80597687	10.22	10.65	-120.65	-176.62	1.73	1.18	0.95	0.830	-18.7	0.6	-0.11	11

Star	α_{2000}	δ_{2000}	V	π	$\mu_{\alpha*}$	μ_{δ}	σ_{π}	$\sigma_{\mu_{\alpha*}}$	$\sigma_{\mu_{\delta}}$	B-V	V_{rad}	$\sigma_{V_{rad}}$	[Fe/H]	*remarks*
(HIP/Gic)	(deg)	(deg)	(mag)	(mas)	$(mas\ yr^{-1})$	$(mas\ yr^{-1})$	(mas)	$(mas\ yr^{-1})$	$(mas\ yr^{-1})$	(mag)	$(km\ s^{-1})$	$(km\ s^{-1})$	(dex)	-
(1)	(2)	(3)	(4)	(5)	(6)	(7)	(8)	(9)	(10)	(11)	(12)	(13)	(14)	(15)
11949	38.54442215	42.78525543	7.59	32.63	406.02	-193.25	1.00	0.68	0.77	0.677	16.5	0.6	-0.12	11
11952	38.54603577	-12.38429260	9.77	8.67	60.47	-185.07	1.78	1.21	1.24	0.437	24.0	0.7	-1.82	11
11983	38.64398193	5.44630623	9.81	24.80	-290.60	-575.88	1.64	1.08	1.13	0.906	-76.6	0.6	-0.43	11
12294	39.58959961	2.44565916	10.51	6.67	358.38	9.40	2.02	1.25	1.16	0.474	57.4	0.6	-1.12	11
12306	39.61609268	30.81662560	7.36	27.89	-487.68	-387.71	1.09	0.75	0.68	0.583	-99.9	0.8	-0.63	11
12456	40.10822296	42.26283264	9.59	14.33	247.52	-220.89	1.41	1.06	1.12	0.830	24.9	0.4	-0.19	11
12579	40.44058609	47.35035706	9.16	14.51	49.66	-289.67	1.25	0.80	0.80	0.520	-12.6	20.6	-0.86	11
12926	41.56336212	25.64990044	7.89	38.95	238.76	-149.41	1.11	0.79	0.66	0.840	14.4	0.6	-0.14	11
13111	42.15594864	22.59843445	10.10	11.03	55.03	-359.47	1.55	1.07	0.97	0.580	-22.3	0.7	-1.00	11
13366	42.99314499	11.36997795	8.38	15.38	36.50	-444.89	1.31	1.07	0.85	0.564	6.3	0.6	-0.69	11
14241	45.91232681	-5.66629934	8.08	28.33	333.25	-264.62	1.20	0.95	0.93	0.677	-20.2	0.6	-0.56	11
14401	46.44294739	45.08970642	9.71	18.42	235.63	-156.77	1.39	0.91	0.85	0.873	-37.0	0.8	-0.60	11
14594	47.10662079	26.33094215	8.04	25.85	-209.50	-830.27	1.11	0.85	0.75	0.486	-140.5	0.8	-2.12	11
14705	47.49863052	15.37323570	9.06	21.30	-95.88	-281.49	1.34	0.90	0.72	0.825	-26.4	0.6	0.06	11
15126	48.76982498	1.03755450	10.23	12.64	361.97	116.56	1.64	1.20	1.01	0.674	88.2	1.0	-0.85	11
15495	49.91604996	33.59864807	9.67	21.57	404.54	-560.56	1.54	0.98	1.03	0.834	-108.1	0.8	-0.68	11
15904	51.20984650	12.25657749	10.76	12.65	569.24	-494.46	2.19	1.32	1.16	0.571	86.2	0.6	-1.09	11
15934	51.30442810	42.12312698	9.43	13.56	183.80	-154.92	1.21	0.91	0.84	0.780	0.4	0.4	-0.15	11
16169	52.08785248	-6.53092098	8.23	21.98	358.02	-195.35	1.13	1.00	0.76	0.619	63.5	0.5	-0.58	11
16240	52.32770157	1.97539926	10.42	14.58	249.58	-207.37	1.75	1.15	1.15	0.821	32.4	0.6	-0.43	11
16404	52.82249832	66.73028564	9.91	17.58	1191.05	-1066.61	1.53	0.72	1.00	0.667	-162.4	0.8	-2.10	11
16405	52.81426239	20.76807404	8.08	20.04	-112.71	-195.80	1.16	0.95	0.77	0.680	-3.1	0.2	0.04	11
16494	53.09944153	-8.60372162	8.05	15.48	-21.42	-236.30	1.08	0.91	0.95	0.585	-16.0	0.2	0.07	11
16581	53.36176300	59.41676331	8.08	31.12	161.68	-306.81	1.09	0.77	0.83	0.871	-36.5	0.3	0.40	11
16770	53.95347977	-9.06075382	8.64	14.46	-92.69	-209.05	1.00	0.89	0.86	0.669	-37.0	0.7	-0.23	11
16788	54.01323318	16.46739388	7.65	22.25	-287.01	-282.28	1.04	0.84	0.79	0.580	-27.5	0.8	-0.34	11
17015	54.72690582	42.39300156	8.98	20.24	189.94	-299.06	1.26	0.97	0.85	0.810	-3.9	0.4	-0.03	11
17147	55.09193802	-3.21697974	6.68	41.07	690.50	-213.58	0.85	0.86	0.79	0.554	120.3	0.6	-0.85	11
17266	55.47230530	-5.93939734	10.02	14.46	273.49	210.42	1.58	1.31	1.23	0.774	124.0	0.5	-0.45	11
18064	57.91341782	79.70836639	10.80	9.85	84.46	-163.26	1.45	1.04	1.26	0.671	66.2	0.6	-0.45	11
18324	58.76601028	61.16680908	7.84	46.95	437.67	-245.40	0.94	0.67	0.69	0.831	38.4	0.5	-0.21	11

Star (HIP/Gic) (1)	α_{2000} (deg) (2)	δ_{2000} (deg) (3)	V (mag) (4)	π (mas) (5)	$\mu_{\alpha*}$ $(mas\,yr^{-1})$ (6)	μ_{δ} $(mas\,yr^{-1})$ (7)	σ_{π} (mas) (8)	$\sigma_{\mu_{\alpha*}}$ $(mas\,yr^{-1})$ (9)	$\sigma_{\mu_{\delta}}$ $(mas\,yr^{-1})$ (10)	B-V (mag) (11)	V_{rad} $(km\,s^{-1})$ (12)	$\sigma_{V_{rad}}$ $(km\,s^{-1})$ (13)	[Fe/H] (dex) (14)	*remarks* - (15)
18433	59.11970139	22.67439651	7.84	21.41	175.16	-232.35	1.22	0.75	0.71	0.688	39.5	0.5	-0.27	11
18608	59.73028946	65.10186005	9.53	16.25	133.73	-261.75	1.48	1.03	1.22	0.802	-5.6	1.2	0.24	11
18915	60.81249619	35.27327728	8.51	54.14	1732.55	-1365.30	1.08	0.76	0.65	0.863	-25.6	0.7	-1.73	11
19208	61.76432800	54.18371964	9.61	8.26	139.15	-298.09	1.59	1.13	1.00	0.551	-41.0	0.8	-0.64	11
20094	64.62312317	35.99168777	8.36	22.53	-141.68	-343.97	1.21	0.91	0.90	0.670	-42.9	0.4	-0.57	11
20298	65.24282837	45.81993866	9.91	9.15	340.15	-123.00	1.67	1.15	0.97	0.724	33.0	0.9	-0.41	11
20834	66.97055054	24.44477654	9.40	24.05	374.03	109.33	1.54	0.98	0.84	0.894	68.1	0.9	-0.39	11
21227	68.30910492	46.69824982	9.26	9.93	176.07	-152.84	1.82	0.92	0.92	0.551	67.1	0.4	-0.06	11
21306	68.60818481	12.73421001	9.68	12.62	21.58	-332.10	1.91	1.19	1.02	0.600	-82.2	0.5	-0.54	11
21921	70.70925140	66.73581696	8.29	27.55	355.03	91.24	1.04	0.64	0.75	0.710	-59.8	0.5	-0.43	11
22020	71.01499176	52.98161697	9.10	10.76	64.35	-294.97	1.38	1.04	1.00	0.667	30.2	0.3	0.20	11
22060	71.17525482	25.93599892	10.13	7.82	200.43	-27.30	1.92	1.45	1.19	0.610	174.4	0.3	0.08	11
22246	71.82657623	45.98626328	10.12	24.07	237.56	-87.52	2.93	1.62	1.41	0.800	95.8	0.5	-0.22	11
22528	72.71925354	67.16678619	9.51	11.28	-164.58	-197.07	1.06	0.67	0.76	0.630	-34.2	0.4	-0.23	11
22596	72.93148804	45.83416367	6.94	33.44	375.61	-562.41	1.11	0.84	0.62	0.586	28.7	0.4	-0.51	11
22777	73.48664093	69.23905945	9.78	13.44	219.93	-124.84	1.54	0.92	1.11	0.850	-45.6	0.5	-0.42	11
22879	73.82263947	70.63336182	8.89	12.27	133.10	-264.27	1.15	0.56	0.83	0.570	49.8	0.5	-0.54	11
22973	74.15148926	72.95162964	9.89	15.17	-142.86	189.72	1.39	0.78	1.05	0.790	-45.0	0.5	-0.61	11
23016	74.25051117	73.83947754	9.45	10.97	79.45	-196.19	1.04	0.74	0.85	0.690	-16.1	0.5	-0.53	11
23080	74.49739075	34.26802063	8.15	30.22	581.50	-202.37	1.13	0.92	0.76	0.750	38.8	0.3	-0.33	11
23344	75.31925964	4.11028814	9.79	7.80	155.82	-144.59	2.00	0.99	0.82	0.413	173.8	0.9	-2.78	11
23431	75.54096222	14.08156395	8.19	34.88	86.07	-405.37	1.38	0.79	0.64	0.720	-27.0	0.5	-0.61	11
23688	76.36962128	40.25732422	9.65	8.32	310.04	-71.14	1.50	1.07	0.78	0.441	105.8	0.6	-0.78	11
24030	77.48732758	5.55742788	9.71	10.29	269.99	-71.18	1.64	1.26	0.97	0.520	-16.0	0.8	-0.92	11
24289	78.18872070	4.32109070	10.57	16.01	232.46	-81.04	2.70	1.68	1.45	0.800	61.9	0.9	-0.77	11
25137	80.69093323	47.91368103	9.23	16.14	-178.48	-153.88	1.28	1.04	0.62	0.590	39.3	0.7	-0.18	11
25860	82.80740356	15.77345181	8.64	18.66	-43.81	-372.89	1.33	0.97	0.58	0.669	50.0	0.8	-0.53	11
26452	84.41486359	68.73518372	9.60	13.14	245.55	-143.16	1.54	0.94	1.04	0.513	-35.6	0.7	-0.89	11
26486	84.50482941	78.35855865	7.73	14.51	69.06	-260.13	0.76	0.51	0.57	0.480	17.0	0.5	-0.37	11
26617	84.86431122	3.95074177	10.35	8.32	254.95	-243.80	2.33	1.40	1.21	0.640	128.3	0.7	-0.43	11
26664	85.00720978	6.06057930	8.67	23.32	54.46	-245.84	1.30	1.10	0.83	0.827	-21.7	0.7	0.13	11

Star (HIP/Gic) (1)	α_{2000} (deg) (2)	δ_{2000} (deg) (3)	V (mag) (4)	π (mas) (5)	$\mu_{\alpha*}$ $(mas\,yr^{-1})$ (6)	μ_{δ} $(mas\,yr^{-1})$ (7)	σ_{π} (mas) (8)	$\sigma_{\mu_{\alpha*}}$ $(mas\,yr^{-1})$ (9)	$\sigma_{\mu_{\delta}}$ $(mas\,yr^{-1})$ (10)	B-V (mag) (11)	V_{rad} $(km\,s^{-1})$ (12)	$\sigma_{V_{rad}}$ $(km\,s^{-1})$ (13)	[Fe/H] (dex) (14)	*remarks* - (15)
26676	85.04057312	12.17809868	10.20	14.30	277.41	-72.17	1.95	1.37	1.00	0.650	23.2	0.9	-1.17	11
28884	91.47965240	26.55483818	9.42	23.97	-179.56	-374.95	1.44	1.06	0.79	0.888	-95.3	0.5	-0.18	11
28905	91.53125000	67.63999176	8.34	27.00	39.62	-314.53	1.11	0.68	0.68	0.771	47.6	0.3	0.05	11
28935	91.60280609	63.83513260	8.40	32.95	-7.47	-319.73	1.06	0.77	0.65	0.846	17.3	0.6	-0.27	11
29111	92.08332062	11.45883846	9.78	17.08	10.99	-287.00	2.15	1.25	1.11	0.881	26.5	0.3	0.10	11
29248	92.50446320	17.93421555	8.48	22.18	210.22	-227.70	1.40	0.80	0.61	0.670	5.3	0.6	-0.50	11
29761	94.01116180	70.78157806	7.43	38.89	-13.09	-443.11	0.74	0.36	0.52	0.776	19.7	0.5	-0.03	11
29777	94.05135345	56.93436050	7.48	18.90	-207.96	-187.04	0.96	0.83	0.69	0.599	22.4	0.6	0.11	11
29814	94.17899323	47.06034470	9.18	20.39	57.31	-493.15	1.30	0.96	0.69	0.769	22.6	0.4	-0.55	11
29824	94.20970154	44.70572281	9.05	24.87	-255.67	-333.47	1.14	0.71	0.60	0.790	-34.4	0.5	-0.26	11
30018	94.75565338	38.53089905	10.22	16.96	147.55	-309.35	1.84	1.97	1.27	0.737	141.4	0.7	-0.45	11
30130	95.10269165	65.49791718	8.62	19.93	12.89	-262.46	1.13	0.65	0.70	0.700	-12.4	0.5	-0.20	11
30833	97.14922333	68.18815613	9.58	13.65	46.64	-229.83	1.47	0.73	0.95	0.679	34.6	0.5	-0.33	11
30890	97.26540375	17.74522781	7.61	20.93	-123.75	-165.42	1.22	0.84	0.70	0.621	-14.4	0.3	-0.30	11
30893	97.27303314	27.00887871	8.59	33.96	-246.64	-417.43	1.42	0.78	0.64	0.906	-47.4	0.3	-0.05	11
30990	97.56528473	60.78411865	8.45	13.88	136.73	-247.27	1.13	1.12	0.79	0.591	60.5	0.5	-0.87	11
31085	97.84629822	-1.57069778	10.06	18.12	-249.17	-343.69	1.86	1.12	1.05	0.849	90.4	0.5	-0.31	11
31597	99.19331360	37.85181046	9.45	13.69	-62.24	-228.20	1.56	1.17	0.92	0.750	77.8	0.6	-0.05	11
31740	99.60284424	48.79860687	10.11	11.92	131.60	-258.21	1.66	1.41	1.21	0.730	85.9	0.4	-0.61	11
32806	102.58161926	60.92894363	8.61	26.01	-240.74	-184.11	1.17	0.78	0.84	0.790	-15.1	3.5	-0.19	11
33582	104.66057587	-0.48047039	9.02	14.63	336.31	-605.95	1.33	0.88	0.73	0.579	-94.3	0.5	-0.61	11
33851	105.40364838	6.40800476	11.88	12.15	4.22	-673.40	3.72	3.23	2.38	0.748	-87.5	0.7	-1.26	11
33940	105.65186310	31.56522560	10.17	17.19	-62.70	-360.54	2.05	1.50	1.27	0.870	143.4	0.7	-0.51	11
33982	105.77023315	38.14225388	9.46	16.48	-21.04	-252.27	1.76	2.13	1.34	0.636	63.9	0.8	-0.96	11
34511	107.27065277	15.42158699	8.00	22.78	-158.37	-287.48	1.09	0.85	0.66	0.631	43.0	0.8	-0.08	11
34642	107.62411499	53.25177765	8.80	10.77	-73.41	-241.43	1.21	1.02	0.83	0.600	-28.6	0.6	-0.73	11
34653	107.65581512	20.44103622	9.09	13.35	147.38	-280.87	1.15	0.88	0.70	0.690	-26.3	0.7	-0.33	11
34902	108.32263947	17.43383408	10.27	11.23	-53.98	-216.66	1.77	1.04	0.90	0.800	-3.7	0.8	-0.44	11
35140	108.96479797	45.04333878	8.67	13.42	185.22	-3.41	1.20	0.91	0.74	0.600	-24.3	0.4	-0.61	11
36491	112.62090302	18.96128273	8.48	20.00	27.80	-436.75	1.45	0.95	0.62	0.538	90.9	0.8	-0.81	11
36710	113.26815033	76.92041016	10.32	12.93	242.95	-201.59	1.42	0.96	1.28	0.722	-71.3	0.6	-0.60	11

Star	α_{2000}	δ_{2000}	V	π	$\mu_{\alpha*}$	μ_{δ}	σ_{π}	$\sigma_{\mu_{\alpha*}}$	$\sigma_{\mu_{\delta}}$	B-V	V_{rad}	$\sigma_{V_{rad}}$	[Fe/H]	*remarks*
(HIP/Gic)	(deg)	(deg)	(mag)	(mas)	$(mas\ yr^{-1})$	$(mas\ yr^{-1})$	(mas)	$(mas\ yr^{-1})$	$(mas\ yr^{-1})$	(mag)	$(km\ s^{-1})$	$(km\ s^{-1})$	(dex)	-
(1)	(2)	(3)	(4)	(5)	(6)	(7)	(8)	(9)	(10)	(11)	(12)	(13)	(14)	(15)
36874	113.71003723	24.95447159	7.37	25.42	128.83	-352.88	0.96	0.95	0.55	0.642	-135.6	0.4	-0.14	11
36954	113.96138000	73.27594757	8.51	25.63	119.63	333.92	0.91	0.57	0.64	0.808	-28.2	0.5	-0.16	11
37510	115.47350311	60.56653976	9.69	12.62	-262.03	-159.79	1.44	1.24	1.20	0.696	3.6	0.7	-0.35	11
38541	118.38800049	30.60507011	8.27	35.29	705.89	-1834.98	1.04	0.84	0.72	0.621	-235.0	0.6	-1.75	11
38822	119.18415070	56.20563507	8.77	17.09	-133.55	-349.77	1.07	0.88	0.78	0.568	30.4	0.6	-0.84	11
39064	119.89139557	20.84388542	7.68	43.21	181.53	-545.03	0.96	0.73	0.43	0.833	-28.8	0.9	-0.24	11
39143	120.09448242	32.12276840	10.26	16.97	-25.05	-203.74	1.66	1.30	1.23	0.860	25.1	0.6	0.07	11
39515	121.14447784	15.36425495	8.48	28.03	-171.40	-246.27	1.18	0.97	0.82	0.850	34.6	0.5	-0.07	11
40497	124.02632904	57.09413910	7.49	31.95	-315.98	-222.43	1.06	0.69	0.62	0.750	18.0	0.5	-0.32	11
40613	124.37228394	-3.98961496	7.74	20.46	-145.25	-438.59	1.12	0.88	0.91	0.584	113.0	0.4	-0.51	11
40674	124.55894470	44.61250305	9.36	14.29	35.01	-265.78	1.27	1.09	0.90	0.673	-1.3	0.7	-0.46	11
40778	124.84403992	54.08600616	9.73	10.36	-35.28	-627.59	1.44	1.01	0.99	0.484	65.9	1.0	-1.64	11
42084	128.66630554	9.37145138	8.93	19.37	345.46	-224.82	1.35	1.18	0.95	0.801	-12.9	0.4	0.09	11
42499	129.96163940	11.52267170	7.61	53.98	-108.88	-500.06	0.98	0.76	0.62	0.832	-11.8	0.5	-0.27	11
42563	130.13960266	13.55639839	10.18	18.88	-425.87	-148.92	1.67	1.29	1.02	0.800	-5.3	0.6	-0.39	11
42592	130.21168518	-16.34514236	9.67	7.26	351.17	-483.87	1.31	0.89	0.83	0.431	206.3	0.9	-2.02	11
42887	131.10287476	24.79659462	9.32	6.59	-112.69	-348.20	1.36	1.14	0.91	0.316	57.7	0.7	-1.26	11
43099	131.66490173	-13.35705185	10.24	5.76	-329.53	-161.19	1.49	1.14	0.86	0.311	41.4	3.4	-1.49	11
43393	132.58750916	-5.53602743	9.18	18.78	-182.52	-513.05	1.46	1.11	0.68	0.735	33.3	0.6	-0.52	11
44259	135.19769287	21.45371437	8.78	31.29	270.86	-342.81	1.35	0.88	0.83	0.839	6.4	0.8	-0.16	11
45401	138.78376770	44.04991150	9.00	19.36	33.83	-279.36	1.29	0.76	0.62	0.680	-57.5	0.5	-0.58	11
47174	144.20635986	57.91138077	9.99	11.04	248.08	-312.72	1.68	1.06	0.87	0.639	-2.6	0.5	-0.52	11
47515	145.29788208	11.55709553	8.80	14.37	117.66	-219.32	1.13	0.74	0.58	0.670	9.8	0.6	-0.12	11
48152	147.23374939	13.74425602	8.33	12.44	374.19	-774.73	1.04	1.00	0.44	0.399	-14.8	0.9	-2.18	11
48961	149.81610107	27.52302361	7.78	24.37	-330.57	-78.13	0.89	0.70	0.51	0.582	3.0	0.5	-0.25	11
49344	151.09735107	70.86683655	8.41	15.94	-110.36	-206.99	0.89	0.63	0.69	0.660	-43.7	0.3	0.22	11
49615	151.89086914	-6.43919849	7.72	19.82	-370.58	105.28	1.10	1.07	0.83	0.522	23.2	0.4	-0.38	11
49686	152.13595581	68.43746948	8.79	28.14	-262.40	-136.63	1.06	0.61	0.58	0.770	27.8	0.5	-0.33	11
49942	152.95028687	23.75519562	8.42	16.01	-379.52	74.61	0.99	0.78	0.54	0.637	82.7	0.7	-0.22	11
49988	153.07948303	17.29917908	7.88	14.43	-155.05	-230.16	1.09	0.76	0.60	0.552	61.6	0.3	-0.51	11
50005	153.12446594	-0.63710064	10.25	11.95	184.44	-267.75	1.78	1.29	0.97	0.679	61.1	0.8	-0.53	11

Star	α_{2000}	δ_{2000}	V	π	$\mu_{\alpha*}$	μ_{δ}	σ_{π}	$\sigma_{\mu_{\alpha*}}$	$\sigma_{\mu_{\delta}}$	B-V	V_{rad}	$\sigma_{V_{rad}}$	[Fe/H]	*remarks*
(HIP/Gic)	(deg)	(deg)	(mag)	(mas)	$(mas\ yr^{-1})$	$(mas\ yr^{-1})$	(mas)	$(mas\ yr^{-1})$	$(mas\ yr^{-1})$	(mag)	$(km\ s^{-1})$	$(km\ s^{-1})$	(dex)	-
(1)	(2)	(3)	(4)	(5)	(6)	(7)	(8)	(9)	(10)	(11)	(12)	(13)	(14)	(15)
50139	153.53472900	3.15129805	7.75	27.67	229.35	-401.03	1.00	0.78	0.57	0.609	-22.0	0.4	-0.65	11
50355	154.23603821	25.86071396	7.57	28.11	165.30	-295.83	1.13	0.95	0.59	0.595	-14.0	0.6	-0.12	11
50782	155.53953552	11.31024170	7.78	37.30	21.76	-324.43	1.29	0.76	0.69	0.750	-13.4	0.4	-0.17	11
50965	156.14868164	-5.51967478	9.80	9.70	-242.50	-166.16	1.40	1.05	1.00	0.580	20.6	0.6	-0.63	11
51257	157.05061340	-6.60057783	7.89	31.12	-374.53	-281.04	0.94	0.77	0.58	0.810	30.4	0.6	0.19	11
51769	158.68055725	-10.10957909	10.50	16.19	-183.38	127.56	1.80	1.41	1.10	0.684	51.4	0.7	-0.65	11
51897	159.04521179	15.87193203	9.09	14.59	101.71	-218.36	1.31	0.94	0.65	0.600	-24.6	0.6	-0.53	11
51942	159.17103577	21.60326004	8.71	22.18	-244.63	-104.08	1.24	0.79	0.62	0.790	46.8	0.8	-0.23	11
52470	160.89093018	48.21412277	8.02	39.56	-330.11	181.11	0.98	0.70	0.64	0.749	-32.3	0.7	-0.45	11
52668	161.54457092	56.47119141	10.32	12.35	-282.14	-127.69	1.82	1.29	1.25	0.790	28.1	1.6	-0.55	11
53070	162.86718750	20.27749062	8.21	19.23	-260.72	-456.01	1.11	0.71	0.62	0.498	65.4	0.8	-1.56	11
53127	163.01770020	58.36984634	9.08	12.64	-248.90	-121.58	1.33	0.73	0.67	0.660	1.2	1.0	-0.16	11
53537	164.28984070	21.80485725	7.94	20.22	-150.60	-214.55	0.99	0.70	0.59	0.624	9.9	0.3	0.21	11
53822	165.17674255	15.45299053	9.43	16.83	-300.51	-15.04	1.32	0.83	0.69	0.860	53.8	0.8	-0.05	11
54109	166.07888794	5.79568911	8.25	19.03	-300.90	53.10	1.11	1.05	0.81	0.637	19.2	0.7	-0.02	11
54210	166.38290405	38.27599335	8.70	22.07	-336.93	58.12	1.09	0.91	0.79	0.689	50.5	0.4	-0.46	11
54541	167.41758728	2.45624876	7.69	32.73	-277.41	39.33	0.97	0.75	0.66	0.777	10.3	0.6	0.09	11
54772	168.19999695	35.72886276	9.77	8.11	70.65	-508.99	1.42	1.09	1.02	0.432	-196.7	0.9	-1.75	11
55022	168.97595215	2.08669019	9.21	7.69	207.68	-8.64	1.18	0.90	0.83	0.425	61.5	0.8	-1.31	11
55135	169.31066895	29.57061958	9.26	9.23	-212.46	9.43	1.30	1.05	1.00	0.620	46.4	0.6	-0.61	11
55592	170.81762695	19.89379311	9.97	8.72	-327.41	-315.95	1.51	0.91	0.84	0.494	98.3	1.1	-0.99	11
55717	171.24725342	28.94324112	8.67	24.99	-291.28	-168.94	1.12	0.88	0.76	0.805	15.2	0.3	0.00	11
55820	171.60417175	10.42289734	8.65	18.94	-380.47	-13.07	1.12	0.84	0.75	0.675	26.7	0.6	-0.11	11
56132	172.59323120	35.84172058	9.87	10.91	-250.35	14.68	1.68	1.76	1.43	0.669	-17.6	0.8	-0.64	11
56291	173.09713745	76.65501404	11.53	10.52	114.55	-603.35	1.83	1.46	1.25	0.650	-121.8	0.9	-2.26	11
56832	174.75416565	6.05790091	7.60	29.15	-335.25	-120.78	0.94	0.80	0.66	0.710	24.0	0.6	-0.06	11
57265	176.14877319	25.53657722	10.38	6.14	-518.75	-46.47	1.77	1.38	1.16	0.491	198.0	0.9	-1.04	11
57349	176.37712097	47.66688156	8.06	19.17	-591.55	-290.72	0.87	0.65	0.50	0.622	28.0	0.5	-0.52	11
57450	176.64648438	50.88185501	9.91	13.61	-869.93	-543.81	1.51	0.96	0.86	0.582	64.2	0.9	-1.44	11
57713	177.53268433	4.90738678	9.19	21.01	-251.97	-195.30	1.48	1.36	1.05	0.776	48.2	0.5	-0.47	11
57735	177.58720398	-1.25245309	9.26	18.37	-405.11	38.48	1.32	0.92	0.64	0.787	21.9	0.6	0.00	11

Star (HIP/Gic) (1)	α_{2000} (deg) (2)	δ_{2000} (deg) (3)	V (mag) (4)	π (mas) (5)	$\mu_{\alpha*}$ $(mas\ yr^{-1})$ (6)	μ_{δ} $(mas\ yr^{-1})$ (7)	σ_{π} (mas) (8)	$\sigma_{\mu_{\alpha*}}$ $(mas\ yr^{-1})$ (9)	$\sigma_{\mu_{\delta}}$ $(mas\ yr^{-1})$ (10)	B-V (mag) (11)	V_{rad} $(km\ s^{-1})$ (12)	$\sigma_{V_{rad}}$ $(km\ s^{-1})$ (13)	[Fe/H] (dex) (14)	*remarks* - (15)
57866	178.03474426	18.75518608	8.40	39.48	30.12	-301.35	1.32	0.84	0.76	0.860	1.3	0.5	-0.11	11
57992	178.41590881	86.23036194	8.28	32.39	-222.58	241.06	0.69	0.64	0.52	0.720	9.7	0.4	-0.56	11
58253	179.20997620	13.37740707	9.95	11.98	-320.47	-173.65	1.49	0.90	0.73	0.700	28.9	0.6	-0.51	11
58443	179.76284790	-4.77748013	9.01	12.71	111.21	-177.25	1.22	0.96	0.70	0.581	-22.8	0.7	-0.35	11
58536	180.05995178	5.36352205	8.40	27.81	-299.18	-128.12	1.03	0.84	0.48	0.759	17.2	0.2	-0.15	11
58843	181.02317810	3.34075189	9.21	15.97	59.41	-575.87	1.26	0.83	0.59	0.585	9.5	0.4	-0.79	11
58949	181.30220032	-1.50903952	8.16	30.58	-514.39	56.84	0.99	0.55	0.52	0.754	16.6	0.3	-0.23	11
59014	181.50395203	14.64909172	10.10	17.27	244.22	-291.48	1.47	1.17	0.77	0.824	-31.6	0.3	-0.52	11
59033	181.54998779	27.49979591	9.99	13.35	-234.09	48.85	1.49	1.26	0.84	0.690	-45.0	0.7	-0.42	11
59109	181.81280518	-5.73377991	10.00	5.75	-280.70	-227.75	1.55	1.17	0.81	0.413	57.8	0.7	-2.32	11
59490	183.00570679	13.26128483	10.17	9.16	-216.36	-439.05	1.49	1.02	0.78	0.469	99.3	0.4	-1.45	11
59572	183.23971558	10.03771687	7.92	32.30	210.10	-357.84	1.01	0.95	0.53	0.792	-7.4	0.4	0.22	11
59589	183.30465698	10.82165527	7.57	29.50	8.73	-590.32	0.85	0.75	0.47	0.667	-24.5	0.2	-0.54	11
59655	183.51484680	4.99556684	8.71	21.94	-244.67	-103.59	1.21	1.00	0.73	0.810	20.1	0.8	0.16	11
59670	183.54251099	53.59118652	9.64	9.61	-310.15	-21.90	1.21	0.89	0.97	0.527	-7.5	0.5	-0.65	11
59932	184.39704895	45.16862488	9.64	11.61	-283.48	-46.15	1.39	0.99	0.83	0.680	23.3	0.5	-0.13	11
60268	185.36721802	61.74725342	8.23	24.27	-298.56	-261.06	0.79	0.55	0.59	0.622	-83.7	0.5	-0.85	11
60551	186.19120789	38.31874084	8.03	26.94	-586.93	64.39	0.82	0.76	0.57	0.585	-2.8	0.8	-0.70	11
60632	186.39564514	1.28396392	9.66	10.95	-32.64	-470.63	1.29	0.95	0.64	0.445	155.1	0.9	-1.81	11
60747	186.74942017	1.56622410	10.48	10.95	44.09	-327.41	1.76	1.13	0.86	0.706	153.1	0.7	-1.08	11
61811	190.01441956	68.80244446	7.88	22.25	-438.44	30.57	0.68	0.57	0.61	0.610	-3.1	0.5	0.02	11
61816	190.02932739	20.80911446	8.94	20.81	203.80	-368.82	1.58	0.93	0.82	0.816	-22.0	0.7	-0.23	11
61974	190.50057983	72.96403503	9.25	15.38	-287.50	-67.43	0.94	0.89	0.86	0.615	-43.2	0.7	-0.86	11
62198	191.22023010	13.48935318	9.04	12.40	-269.75	-47.05	1.26	0.72	0.65	0.660	-9.4	0.6	0.00	11
62349	191.63624573	24.14505005	6.83	22.98	-114.26	-216.46	0.84	0.62	0.48	0.540	6.0	0.7	-0.11	11
62366	191.71604919	22.48811150	9.52	12.23	-256.72	1.16	1.46	0.76	0.71	0.600	-17.4	0.6	-0.38	11
62607	192.43678284	1.18803751	8.13	30.12	-79.55	-644.49	0.91	0.61	0.48	0.686	2.4	1.0	-0.81	11
62628	192.49494934	47.13080215	10.11	8.79	-312.40	-27.92	1.42	0.88	0.92	0.537	-21.7	0.5	-0.77	11
63063	193.81652832	7.83270025	9.93	19.28	115.89	-125.37	1.68	1.14	0.83	0.809	113.5	0.6	-0.48	11
63239	194.36718750	18.67645264	9.82	13.68	-231.38	112.82	1.54	0.88	0.78	0.751	-30.9	0.7	-0.53	11
63336	194.67893982	33.24570847	10.22	11.84	-264.18	-3.70	1.80	1.19	1.11	0.743	-10.4	0.6	-0.64	11

Star (HIP/Gic) (1)	α_{2000} (deg) (2)	δ_{2000} (deg) (3)	V (mag) (4)	π (mas) (5)	$\mu_{\alpha*}$ $(mas\,yr^{-1})$ (6)	μ_δ $(mas\,yr^{-1})$ (7)	σ_π (mas) (8)	$\sigma_{\mu_{\alpha*}}$ $(mas\,yr^{-1})$ (9)	σ_{μ_δ} $(mas\,yr^{-1})$ (10)	B-V (mag) (11)	V_{rad} $(km\,s^{-1})$ (12)	$\sigma_{V_{rad}}$ $(km\,s^{-1})$ (13)	[Fe/H] (dex) (14)	*remarks* - (15)
63346	194.70529175	68.78524017	8.07	29.07	-296.74	245.93	0.69	0.54	0.55	0.676	9.1	0.8	-0.67	11
63977	196.64881897	11.04453564	8.48	19.94	-244.69	-66.28	1.12	0.89	0.65	0.600	-20.8	0.5	0.09	11
64103	197.05480957	3.77682924	9.67	14.41	-275.98	-52.93	1.48	1.00	0.90	0.702	-56.4	0.6	-0.36	11
64132	197.16291809	51.06645966	10.21	6.22	-67.13	-223.40	1.45	1.12	1.04	0.341	-58.6	0.7	-1.10	11
64150	197.21258545	5.20724630	6.78	38.07	82.53	-667.75	0.88	0.47	0.46	0.667	23.6	0.4	-0.09	11
64698	198.90403748	9.01602936	8.42	18.80	-362.68	-121.69	1.15	0.97	0.67	0.667	-6.9	0.7	-0.26	11
64747	199.04687500	35.88586807	8.29	22.39	267.28	-173.36	0.98	0.76	0.65	0.640	-46.5	0.6	-0.51	11
65040	199.98065186	6.85745859	9.77	15.43	-235.23	-86.89	1.31	1.07	0.75	0.654	83.4	1.5	-0.82	11
66051	203.12904358	36.03512955	7.96	16.67	83.69	-288.43	0.91	0.68	0.57	0.590	-28.9	0.4	-0.56	11
66127	203.33796692	26.11985779	9.89	18.42	-213.51	96.99	1.38	1.09	0.86	0.820	7.6	0.6	-0.23	11
66354	204.00735474	1.20218372	10.85	12.26	18.20	-279.78	2.15	1.29	1.03	0.670	-40.5	0.9	-1.33	11
66509	204.50196838	19.14808464	8.81	18.98	133.89	-321.88	1.19	0.78	0.66	0.668	-45.3	0.8	-0.62	11
67882	208.54437256	10.24798012	9.01	20.43	188.96	-210.40	1.38	0.87	0.86	0.729	28.8	0.3	-0.20	11
68321	209.78952026	33.86093521	10.05	5.37	89.08	-429.10	1.60	1.37	1.19	0.410	-171.7	0.9	-2.23	11
68714	211.00662231	22.52509880	10.16	12.17	114.14	-312.87	1.69	0.79	0.77	0.681	37.6	0.8	-1.04	11
77210	236.46833801	5.04071236	9.15	20.73	-249.26	69.29	1.35	1.25	1.15	0.834	1.3	1.9	-0.88	11
77466	237.24392700	45.79370499	9.18	14.11	-273.17	111.84	0.89	0.69	0.74	0.650	-53.3	0.3	-0.55	11
78113	239.25161743	20.59430504	10.00	15.13	107.36	-235.70	1.88	0.87	0.87	0.820	15.9	0.8	0.02	11
78620	240.75071716	-6.45310307	10.20	10.83	-230.56	41.43	1.72	1.56	1.35	0.698	-64.2	0.6	-1.54	11
78640	240.80541992	42.24629211	9.86	8.03	-194.99	-365.97	1.12	0.87	0.88	0.481	-152.6	0.6	-1.53	11
79117	242.23081970	1.85203457	10.16	19.99	-203.75	-380.28	1.75	1.09	1.03	0.850	110.7	0.6	-0.66	11
80003	244.96524048	22.63896561	11.52	9.12	-40.27	-451.14	3.01	1.98	2.32	0.723	158.6	1.0	-1.42	11
80262	245.77525330	17.46879768	8.44	24.97	-132.57	304.26	1.06	0.82	0.78	0.724	-36.9	0.6	-0.33	11
80700	247.14978027	3.25295258	8.81	21.50	-12.87	-526.94	1.27	0.93	0.88	0.770	25.2	0.7	-0.17	11
80789	247.43843079	30.69477081	10.24	11.80	-181.72	112.81	1.53	0.92	1.12	0.578	-70.4	0.6	-0.96	11
80837	247.61857605	4.17822409	7.27	24.34	-433.63	-1392.51	0.90	0.81	0.73	0.545	-47.9	0.5	-0.72	11
81170	248.67646790	-4.22906303	9.60	20.71	-133.67	-701.27	1.46	1.41	1.38	0.736	-169.9	0.5	-1.54	11
81223	248.84819031	8.81591511	9.10	15.36	51.36	-248.63	1.39	0.95	0.92	0.605	12.3	0.6	-0.26	11
81312	249.10833740	30.94168282	7.10	25.37	-2.57	-465.28	0.72	0.51	0.64	0.555	-5.0	0.7	-0.22	11
81461	249.57244873	-2.44216514	8.50	14.37	-179.36	-284.90	1.17	0.78	0.77	0.613	-35.9	0.3	-0.58	11
81598	249.95826721	5.50720930	8.62	26.39	102.30	-303.29	1.42	1.29	1.03	0.876	51.3	0.4	-0.28	11

Star (HIP/Gic) (1)	α_{2000} (deg) (2)	δ_{2000} (deg) (3)	V (mag) (4)	π (mas) (5)	$\mu_{\alpha*}$ $(mas\,yr^{-1})$ (6)	μ_{δ} $(mas\,yr^{-1})$ (7)	σ_{π} (mas) (8)	$\sigma_{\mu_{\alpha*}}$ $(mas\,yr^{-1})$ (9)	$\sigma_{\mu_{\delta}}$ $(mas\,yr^{-1})$ (10)	B-V (mag) (11)	V_{rad} $(km\,s^{-1})$ (12)	$\sigma_{V_{rad}}$ $(km\,s^{-1})$ (13)	[Fe/H] (dex) (14)	*remarks* - (15)
81813	250.66073608	68.10216522	7.56	41.15	-282.18	426.88	0.57	0.53	0.59	0.769	9.3	0.2	-0.08	11
82540	253.07405090	15.64843750	9.13	17.46	-102.57	-224.78	1.16	0.81	0.72	0.700	-7.0	0.4	-0.41	11
82588	253.24501038	-0.02642298	6.65	59.04	-711.28	-1484.34	0.87	0.69	0.52	0.749	45.3	0.4	-0.21	11
82896	254.10064697	68.02516174	8.70	19.73	-72.78	264.35	0.70	0.66	0.77	0.659	-14.7	0.6	-0.38	11
82964	254.30558777	71.46322632	8.14	19.75	-190.32	85.63	0.68	0.63	0.74	0.618	-16.5	0.4	0.15	11
82995	254.40174866	26.90564728	9.61	15.70	79.32	243.33	1.33	0.80	0.93	0.800	-14.4	0.6	-0.20	11
83604	256.33050537	26.93636513	10.00	6.28	-244.87	115.69	1.55	0.97	1.13	0.587	-113.6	0.6	-0.73	11
83691	256.57464600	12.60682583	8.53	23.54	-203.92	127.89	1.11	0.84	0.78	0.750	-22.8	0.5	-0.17	11
85137	260.98889160	37.28020096	8.89	25.66	-15.83	-335.25	0.96	0.76	1.03	0.800	3.1	0.4	-0.18	11
85373	261.67254639	31.05944443	9.67	14.04	-358.78	73.88	1.24	0.89	1.15	0.840	-73.4	0.8	-0.64	11
85378	261.67999268	31.07719040	8.48	14.51	-361.71	73.45	0.93	0.67	0.89	0.626	-73.4	0.7	-0.61	11
85436	261.89410400	26.79496002	7.69	33.36	-101.32	275.08	0.92	0.59	0.74	0.820	-24.4	0.5	0.17	11
85437	261.89596558	27.02563286	8.70	19.64	-9.42	370.59	1.14	0.73	0.90	0.725	-72.2	0.5	-0.12	11
86321	264.56503296	18.55707741	9.77	8.93	-187.72	-204.56	1.47	0.88	0.89	0.480	-240.6	0.9	-1.00	11
86431	264.90362549	37.18375397	8.39	18.32	-497.68	-820.42	0.78	0.61	0.76	0.576	33.6	0.7	-0.50	11
86443	264.93997192	2.41655636	9.94	8.35	-366.72	74.59	1.60	1.14	0.77	0.458	-398.0	1.2	-2.55	11
86453	264.97940063	44.06536865	9.02	13.76	-104.35	-185.21	0.86	0.67	0.84	0.630	-12.7	0.5	-0.60	11
86568	265.36233521	70.46440125	9.72	17.00	-211.17	79.77	1.01	0.96	1.07	0.760	-51.1	0.5	-0.40	11
87017	266.71142578	10.11675739	8.51	15.47	-28.24	-228.63	1.01	0.84	0.63	0.525	35.7	0.5	-0.31	11
87055	266.82952881	78.39132690	8.55	18.09	-120.38	177.00	0.64	0.56	0.66	0.660	-50.5	0.5	-0.23	11
87062	266.86654663	-8.77992916	10.60	10.34	244.76	-365.31	2.20	1.58	1.22	0.605	84.2	0.4	-1.99	11
87467	268.07522583	36.40184021	10.35	5.91	-154.71	-244.43	1.17	1.13	1.09	0.520	-60.8	0.7	-2.53	11
88227	270.25738525	11.06874752	8.89	21.73	-36.89	-230.77	1.26	0.82	0.82	0.739	-3.2	0.7	-0.26	11
89144	272.90850830	32.17737198	11.10	9.40	-96.72	-207.54	1.82	1.68	1.73	0.780	-38.0	0.8	-0.49	11
89215	273.09115601	5.40122652	10.37	17.00	-499.64	-645.95	1.88	1.53	1.41	0.755	-1.5	0.8	-1.36	11
90365	276.59140015	8.61576462	8.32	26.30	-195.91	-468.58	1.05	0.88	0.75	0.764	-18.1	0.4	-0.15	11
91360	279.49508667	-6.80547714	8.34	26.97	-129.82	-397.67	1.12	0.76	0.72	0.833	-49.2	0.6	-0.10	11
92277	282.09146118	-5.09140110	10.34	14.09	198.71	-229.78	1.93	1.50	1.21	0.704	15.2	0.4	0.01	11
92388	282.40975952	13.21860886	8.59	27.53	-197.56	-222.03	1.22	0.91	0.75	0.730	-54.5	0.6	-0.23	11
92532	282.85491943	38.62657166	7.15	33.31	323.60	44.24	0.61	0.64	0.56	0.594	-13.2	0.4	-0.43	11
92781	283.59667969	-4.60516977	9.05	11.85	-133.49	-430.27	1.50	1.11	1.05	0.586	21.4	0.7	-0.82	11

Star (HIP/Gic) (1)	α_{2000} (deg) (2)	δ_{2000} (deg) (3)	V (mag) (4)	π (mas) (5)	$\mu_{\alpha*}$ $(mas\ yr^{-1})$ (6)	μ_{δ} $(mas\ yr^{-1})$ (7)	σ_{π} (mas) (8)	$\sigma_{\mu_{\alpha*}}$ $(mas\ yr^{-1})$ (9)	$\sigma_{\mu_{\delta}}$ $(mas\ yr^{-1})$ (10)	B-V (mag) (11)	V_{rad} $(km\ s^{-1})$ (12)	$\sigma_{V_{rad}}$ $(km\ s^{-1})$ (13)	[Fe/H] (dex) (14)	*remarks* - (15)
92918	283.97070312	-5.74521637	7.46	29.77	-200.21	-388.80	1.04	0.89	0.73	0.747	-73.4	0.3	-0.03	11
93080	284.40975952	72.84113312	11.29	9.19	-104.14	353.00	1.45	1.25	1.40	0.780	-29.3	0.9	-0.57	11
93269	284.98995972	64.05381012	9.17	14.45	-175.92	-107.90	0.82	0.92	0.82	0.690	-142.3	0.5	-0.46	11
93445	285.46258545	16.06344032	10.38	9.72	-147.50	-303.45	1.62	1.02	0.93	0.655	40.3	1.0	-0.80	11
94396	288.18768311	18.81275368	10.16	17.22	113.53	166.37	1.82	0.91	1.02	0.873	-63.8	0.6	-0.28	11
94449	288.33633423	-0.59509206	9.18	7.52	-315.27	-447.88	1.34	0.80	0.71	0.538	-65.6	0.6	-0.94	11
94582	288.73181152	71.52918243	9.55	18.21	113.70	170.93	0.79	0.79	0.70	0.770	7.6	0.6	-0.35	11
94931	289.75228882	41.63460541	8.87	28.28	98.78	-631.15	0.85	0.72	0.70	0.806	-121.1	0.6	-0.87	11
96077	293.01052856	50.18154526	8.05	19.16	-90.41	292.02	0.63	0.61	0.51	0.659	-22.1	0.6	-0.61	11
96115	293.13296509	26.39059258	9.37	6.93	1.36	-172.83	1.46	0.61	1.00	0.390	-129.1	0.7	-2.54	11
96185	293.36282349	33.20186615	6.62	31.29	-464.12	224.34	0.62	0.51	0.48	0.595	-166.8	0.7	-0.66	11
96308	293.73175049	11.42410088	7.91	23.69	278.96	7.57	1.10	0.75	0.61	0.670	-59.8	0.9	-0.27	11
96344	293.81158447	69.92833710	9.79	12.43	-105.90	-220.93	0.89	0.91	0.96	0.600	-1.3	0.6	-0.60	11
96427	294.06497192	4.76532269	9.18	13.51	11.07	-215.44	1.34	1.10	0.74	0.660	64.0	0.8	-0.20	11
96512	294.30880737	70.74145508	9.98	19.20	-64.35	-150.58	1.02	1.11	0.97	0.810	-19.5	0.8	-0.35	11
96673	294.81130981	-2.61242032	10.29	8.20	217.14	-147.42	1.70	1.21	0.73	0.665	-111.4	0.8	-0.81	11
96780	295.07519531	79.71932220	10.34	10.55	192.18	188.66	1.09	0.99	1.16	0.700	-29.8	0.6	-0.86	11
96943	295.61386108	8.15505219	8.99	21.05	154.03	141.52	1.24	0.97	0.48	0.733	-22.1	0.5	-0.45	11
97514	297.29861450	65.95504761	8.52	9.84	40.55	212.40	0.66	0.46	0.68	0.525	9.9	0.5	-0.33	11
97781	298.04293823	67.42598724	11.22	9.54	49.22	187.52	1.39	1.21	1.29	0.900	-30.3	0.6	0.34	11
97940	298.56231689	1.94342387	8.78	21.12	-2.75	-272.20	1.59	0.93	0.83	0.878	10.0	0.8	0.01	11
97950	298.60726929	1.94138086	8.93	23.29	-1.00	-269.94	2.03	1.04	0.93	0.900	9.8	0.4	-0.12	11
98020	298.79031372	10.74094200	8.83	25.32	-37.73	289.98	1.15	0.89	0.92	0.599	-192.8	0.8	-1.75	11
98288	299.55664062	69.14039612	9.27	14.20	144.82	136.01	0.74	0.73	0.75	0.630	-5.8	0.7	-0.20	11
99267	302.25588989	42.86526108	10.11	12.04	118.85	340.50	1.12	0.83	0.79	0.510	-196.4	1.0	-2.13	11
99542	303.02362061	46.30050278	9.06	24.28	223.48	291.91	0.88	0.70	0.62	0.810	-40.5	0.4	-0.32	11
99963	304.22369385	33.10865784	9.26	13.41	-127.95	-257.34	1.13	0.75	0.70	0.585	20.9	0.6	-0.32	11
100279	305.10232544	6.03133965	10.14	10.19	33.27	-364.11	1.72	1.64	1.52	0.621	99.2	0.8	-0.97	11
100568	305.89935303	-21.37061691	8.65	22.88	541.98	-1055.78	1.23	1.15	0.96	0.554	-171.8	0.7	-1.24	11
100682	306.18923950	25.05196953	10.83	7.49	91.52	-245.18	1.73	0.99	1.02	0.427	-321.4	1.5	-2.85	11
100792	306.54965210	9.45011711	8.33	17.94	118.10	-549.35	1.24	0.96	0.97	0.503	-247.7	0.6	-1.28	11

Star (HIP/Gic) (1)	α_{2000} (deg) (2)	δ_{2000} (deg) (3)	V (mag) (4)	π (mas) (5)	$\mu_{\alpha*}$ $(mas\,yr^{-1})$ (6)	μ_{δ} $(mas\,yr^{-1})$ (7)	σ_{π} (mas) (8)	$\sigma_{\mu_{\alpha*}}$ $(mas\,yr^{-1})$ (9)	$\sigma_{\mu_{\delta}}$ $(mas\,yr^{-1})$ (10)	B-V (mag) (11)	V_{rad} $(km\,s^{-1})$ (12)	$\sigma_{V_{rad}}$ $(km\,s^{-1})$ (13)	[Fe/H] (dex) (14)	*remarks* - (15)
101146	307.53536987	4.57156801	11.47	10.71	-201.83	-421.04	3.19	1.83	1.76	0.874	-119.4	1.0	-1.07	11
101369	308.17926025	19.52651215	11.63	10.11	-74.14	-366.26	2.83	1.19	1.16	0.880	-24.8	0.9	-0.70	11
102346	311.05426025	21.90742302	10.09	12.14	177.29	123.40	1.84	0.91	0.79	0.760	-28.9	0.7	-0.54	11
102923	312.77783203	7.02700377	9.82	20.71	237.77	-361.96	1.62	1.41	0.84	0.900	-61.8	0.6	-0.07	11
103269	313.81982422	42.30018616	10.28	14.24	55.90	-390.99	1.42	1.05	1.04	0.590	-131.4	0.9	-1.78	11
103754	315.37118530	79.29594421	8.65	20.24	117.85	186.76	0.66	0.64	0.62	0.717	-2.5	0.4	0.07	11
103812	315.55072021	19.90088844	9.06	17.10	4.94	222.96	1.30	0.93	0.67	0.666	-61.3	0.7	-0.67	11
103895	315.77398682	44.80445862	9.15	18.85	287.29	-60.03	0.98	0.86	0.73	0.680	-9.2	0.4	-0.23	11
103897	315.77554321	29.48228264	10.20	7.90	-261.34	-167.64	1.68	1.07	1.05	0.637	-123.1	0.5	-0.93	11
104076	316.28665161	73.20310211	8.73	15.04	132.91	136.39	0.71	0.64	0.70	0.510	-33.6	0.4	-0.32	11
104375	317.16940308	73.69680786	8.69	32.59	-322.34	-399.50	0.73	0.55	0.59	0.832	6.4	0.4	-0.38	11
104587	317.79522705	45.45591354	7.83	32.68	-241.49	-298.83	0.79	0.61	0.62	0.780	-49.9	0.6	-0.03	11
104601	317.84561157	71.66744232	9.74	8.65	219.15	234.11	1.06	1.08	0.90	0.540	-22.9	0.5	0.15	11
104659	317.99597168	17.72774696	7.37	28.26	-121.62	-899.24	1.00	0.69	0.54	0.525	-44.5	0.5	-1.42	11
104913	318.77395630	62.84111404	9.56	14.51	122.87	260.66	0.89	0.87	0.89	0.751	-64.6	0.6	-0.27	11
105488	320.49060059	27.45288467	10.51	10.90	204.44	153.08	1.68	1.09	1.07	0.530	-273.4	1.0	-1.55	11
105888	321.67877197	5.44163942	8.49	13.02	167.04	-246.55	1.09	0.95	0.65	0.572	-84.6	0.6	-0.80	11
106047	322.19717407	65.61939240	10.43	10.58	149.96	205.88	1.42	1.27	1.23	0.850	-26.2	0.6	0.02	11
106356	323.11889648	1.01229441	8.31	16.43	-282.39	-333.06	1.16	0.98	0.63	0.610	12.9	0.7	-0.52	11
106403	323.26181030	30.35974312	8.11	7.50	155.57	7.32	0.93	0.64	0.64	0.413	-19.2	0.7	-0.98	11
106825	324.53509521	-2.30315042	8.62	27.21	-462.99	-280.43	1.21	1.00	0.62	0.844	7.5	0.3	-0.05	11
106924	324.81729126	60.28383255	10.36	15.20	-381.63	232.70	1.20	1.08	0.99	0.551	-245.4	1.0	-1.91	11
107020	325.11566162	-2.01757932	8.54	24.66	221.73	-111.58	1.16	1.01	0.60	0.672	-38.4	0.5	-0.35	11
107038	325.18658447	84.33348846	8.37	34.61	344.49	61.16	0.63	0.66	0.54	0.868	-6.4	0.7	0.01	11
107294	325.98800659	27.38999939	10.05	9.19	-239.18	-159.50	1.57	1.02	0.98	0.480	-95.1	0.7	-1.45	11
107895	327.91430664	0.84940821	8.60	28.47	335.23	-72.51	1.17	0.95	0.64	0.848	-29.1	0.5	0.00	11
108056	328.39495850	35.84844208	9.15	9.55	-112.59	139.46	1.19	0.71	0.79	0.580	-98.1	0.6	0.12	11
108103	328.54727173	4.97911930	9.25	15.44	274.42	-11.32	1.38	1.31	0.83	0.630	-46.9	0.9	-0.52	11
108170	328.73028564	61.98785019	9.81	14.88	-74.92	-171.86	0.99	1.05	0.88	0.840	-53.8	0.3	-0.12	11
108200	328.81729126	32.64477539	11.07	10.60	761.65	128.51	2.06	1.30	2.01	0.686	-186.1	1.0	-1.86	11
108434	329.48489380	50.84568024	8.88	19.63	271.40	77.84	0.86	0.69	0.70	0.730	-16.0	0.6	-0.08	11

Star (HIP/Gic) (1)	α_{2000} (deg) (2)	δ_{2000} (deg) (3)	V (mag) (4)	π (mas) (5)	$\mu_{\alpha*}$ $(mas\, yr^{-1})$ (6)	μ_{δ} $(mas\, yr^{-1})$ (7)	σ_{π} (mas) (8)	$\sigma_{\mu_{\alpha*}}$ $(mas\, yr^{-1})$ (9)	$\sigma_{\mu_{\delta}}$ $(mas\, yr^{-1})$ (10)	B-V (mag) (11)	V_{rad} $(km\, s^{-1})$ (12)	$\sigma_{V_{rad}}$ $(km\, s^{-1})$ (13)	[Fe/H] (dex) (14)	*remarks* - (15)
108496	329.68798828	0.80972624	10.26	13.31	-70.65	-244.01	2.00	1.28	1.15	0.794	-10.8	0.6	-0.29	11
108525	329.78717041	3.19776654	8.45	28.15	220.63	68.40	1.37	0.94	0.88	0.755	-15.8	0.7	-0.10	11
109049	331.36706543	5.75434923	10.57	9.92	-137.31	-123.44	2.27	2.02	1.62	0.889	-0.3	0.6	-0.23	11
109067	331.41958618	12.37669182	9.55	21.52	202.28	-418.16	1.58	1.23	0.98	0.672	-200.8	0.6	-0.95	11
109144	331.63821411	1.85713542	7.24	19.77	340.90	190.71	1.00	1.05	0.68	0.537	-40.9	0.5	-0.21	11
109384	332.40582275	71.31433105	9.61	18.12	232.79	-87.32	0.87	0.86	0.74	0.780	-64.1	0.8	-0.23	11
109563	332.91400146	6.19344473	8.45	13.78	231.43	67.51	1.15	1.13	0.86	0.594	-12.5	0.6	-0.52	11
109931	333.97772217	24.92799568	8.94	13.29	-182.88	-76.03	1.07	0.74	0.70	0.660	3.7	0.5	-0.14	11
110187	334.78234863	-7.31359863	8.90	11.78	229.95	-143.16	1.33	1.08	1.10	0.599	-77.2	0.5	-0.06	11
110229	334.93444824	83.53366852	8.63	14.17	299.03	40.37	0.80	0.74	0.61	0.580	-14.2	0.5	-0.10	11
110560	335.95452881	24.39253616	10.64	5.62	-79.51	-166.48	1.69	1.18	1.06	0.573	-46.2	0.9	-0.65	11
110916	337.06768799	28.11199570	11.00	10.77	223.35	26.98	1.91	1.30	1.23	0.740	-7.3	0.5	-0.56	11
111195	337.90090942	2.16217875	10.71	8.99	51.80	-327.98	2.00	1.34	1.20	0.520	-212.7	1.0	-1.75	11
111300	338.20248413	10.40489197	9.34	16.86	-248.01	-217.74	1.37	1.15	1.04	0.823	22.5	0.5	-0.68	11
111332	338.33969116	-9.06355572	8.73	15.05	297.40	-61.32	1.15	0.96	0.71	0.576	-33.3	0.6	-0.47	11
111473	338.77362061	11.88140678	8.66	23.10	-335.35	-326.23	1.12	0.74	0.76	0.866	-18.3	0.6	0.10	11
111764	339.59387207	9.85863304	10.61	16.02	-183.57	-176.88	1.94	1.86	1.51	0.850	7.3	0.4	-0.07	11
111783	339.62878418	10.53934193	9.50	16.15	-273.82	-536.32	1.47	1.23	0.94	0.764	-58.0	0.6	-0.39	11
111803	339.68951416	25.57036972	10.03	10.94	226.32	18.60	1.64	1.04	1.01	0.820	-22.2	0.3	0.02	11
111977	340.22796631	66.52342987	7.46	34.05	216.88	388.65	0.60	0.55	0.51	0.635	-47.5	0.4	-0.61	11
112229	340.96133423	3.88684034	7.41	23.66	150.64	331.81	0.95	0.85	0.69	0.515	-33.6	0.4	-0.88	11
112245	341.02426147	64.57067108	7.50	39.82	50.31	-297.90	0.71	0.75	0.55	0.719	-45.4	0.7	-0.27	11
112666	342.25228882	77.95301056	10.16	11.27	239.94	-13.17	1.12	1.05	0.97	0.760	-97.8	0.6	-0.54	11
112811	342.69140625	1.86516070	9.33	16.66	100.35	-384.38	1.33	0.97	0.84	0.683	-4.1	0.8	-0.81	11
113033	343.37292480	27.75495720	11.46	12.98	500.48	-186.19	2.64	1.45	1.50	0.800	-279.2	0.8	-1.38	11
113514	344.83105469	12.19233322	8.35	20.59	332.17	-156.65	1.14	0.90	0.83	0.580	-122.8	0.5	-0.67	11
113896	345.98864746	-4.79486084	6.68	32.50	319.14	38.14	0.93	0.70	0.58	0.581	-12.9	0.3	-0.17	11
113989	346.27539062	68.41706085	7.49	33.65	592.73	162.01	0.59	0.52	0.60	0.646	-16.0	0.5	-0.64	11
114069	346.53771973	4.68673468	9.26	16.91	250.25	14.05	1.45	1.24	1.07	0.665	7.6	0.8	-0.42	11
114098	346.63522339	-0.19614220	9.33	27.80	-237.08	-29.97	1.29	0.84	0.80	0.879	-32.2	0.8	-0.23	11
114450	347.68121338	18.90904999	8.56	12.78	-205.78	-185.56	1.28	0.79	0.77	0.590	-26.2	0.4	-0.10	11

Star (HIP/Gic) (1)	α_{2000} (deg) (2)	δ_{2000} (deg) (3)	V (mag) (4)	π (mas) (5)	$\mu_{\alpha*}$ $(mas\,yr^{-1})$ (6)	μ_{δ} $(mas\,yr^{-1})$ (7)	σ_{π} (mas) (8)	$\sigma_{\mu_{\alpha*}}$ $(mas\,yr^{-1})$ (9)	$\sigma_{\mu_{\delta}}$ $(mas\,yr^{-1})$ (10)	B-V (mag) (11)	V_{rad} $(km\,s^{-1})$ (12)	$\sigma_{V_{rad}}$ $(km\,s^{-1})$ (13)	[Fe/H] (dex) (14)	*remarks* - (15)
114458	347.71096802	0.40973017	9.01	22.57	-23.60	-271.45	1.31	0.94	0.81	0.854	23.5	0.7	-0.09	11
114661	348.41174316	39.41738892	11.02	14.09	173.67	-313.88	2.18	1.63	1.28	0.689	-56.3	1.2	-2.68	11
115222	350.07458496	54.48757935	11.46	11.39	170.55	81.18	2.20	1.83	1.60	0.780	36.0	0.6	-0.40	11
115331	350.40213013	44.09788132	7.36	45.63	636.25	219.18	0.82	0.49	0.54	0.801	3.6	0.3	-0.09	11
115359	350.49285889	16.63253784	8.92	14.97	406.56	-49.04	1.22	0.93	0.86	0.610	-40.4	0.5	-0.63	11
115373	350.57565308	12.15933037	10.83	8.92	244.39	-1.04	1.91	1.34	1.30	0.660	-87.7	1.0	-1.11	11
115381	350.59909058	-0.41486961	8.56	26.95	212.21	-250.97	1.37	0.76	0.80	0.853	-3.7	0.4	-0.06	11
115684	351.57662964	33.18867493	9.58	11.29	-120.00	-181.55	1.39	0.89	0.72	0.735	-33.5	1.9	-0.27	11
115704	351.63684082	60.62853622	10.49	8.85	457.54	40.28	1.43	1.23	1.32	0.469	-105.4	1.1	-2.24	11
116085	352.84252930	59.16551590	6.76	59.31	1106.08	113.05	0.67	0.57	0.62	0.839	-25.4	0.4	0.05	11
116386	353.75848389	25.39853668	10.88	10.47	271.75	-196.01	1.89	1.28	1.05	0.810	-124.8	0.6	-0.54	11
116410	353.84640503	2.22532988	8.42	25.82	110.91	316.39	1.28	0.98	0.80	0.720	-12.9	0.6	-0.69	11
116441	353.92724609	20.58065033	9.10	13.28	-130.97	-117.18	1.15	0.69	0.66	0.560	-38.2	0.5	-0.94	11
116454	353.95535278	0.44551590	10.19	18.10	-234.99	-186.09	1.71	1.18	1.10	0.891	-3.0	0.4	-0.45	11
116498	354.11163330	33.03755188	10.13	16.58	304.19	17.51	1.45	1.29	0.90	0.980	-23.0	0.7	-0.49	11
116613	354.49371338	46.19943619	6.58	43.26	357.25	-11.01	0.80	0.42	0.49	0.665	-0.1	0.4	0.02	11
117041	355.89547729	-7.92333174	10.11	8.46	609.63	-163.86	1.68	1.53	1.26	0.671	-86.4	0.7	-0.99	11
117364	356.96212769	-5.24419737	8.39	17.08	-177.42	-165.23	1.07	1.02	0.77	0.622	-35.7	0.6	-0.11	11
117367	356.96835327	4.17547560	7.69	21.43	351.04	-31.87	1.03	0.91	0.51	0.627	-15.5	0.4	-0.20	11
117577	357.66842651	17.34466553	10.49	18.47	208.36	167.16	1.85	1.11	0.90	0.880	29.4	0.5	-0.45	11
117719	358.12268066	-9.40695477	10.10	12.49	201.09	9.89	1.77	1.33	1.05	0.766	15.8	0.7	-0.60	11
117918	358.76739502	20.38483047	8.94	22.08	267.65	11.91	1.12	0.76	0.61	0.805	-28.2	0.8	-0.55	11
117953	358.88507080	3.50144601	7.72	34.09	-208.34	-293.98	0.94	0.74	0.59	0.751	15.1	0.6	-0.47	11
118010	359.04763794	59.76760483	7.67	20.01	194.99	282.12	0.74	0.66	0.60	0.638	3.3	0.4	-0.17	11
118115	359.38964844	-9.64751911	7.89	20.98	454.84	-146.12	1.20	0.97	0.58	0.643	-31.2	0.5	-0.02	11
8572	27.63602829	-9.35078621	10.34	7.32	255.90	94.70	1.01	1.17	1.14	0.432	36.2	0.8	-2.62	11
12710	40.84187317	13.43249416	11.47	4.85	340.90	-147.40	0.67	1.59	1.52	0.526	221.0	0.6	-2.12	22
18973	60.98022461	39.73866653	10.71	4.14	275.30	-205.80	0.57	1.63	1.39	0.560	87.5	0.6	-0.08	22
27182	86.41825867	14.68891907	9.05	17.56	64.90	-189.90	2.43	0.96	0.75	0.650	38.5	0.7	-1.05	22
30098	95.01602173	38.34558868	10.74	12.59	99.60	-182.70	1.74	2.29	1.49	0.746	220.2	0.7	-1.98	22
32567	101.93723297	58.64292145	10.32	6.93	-6.90	-477.10	0.96	1.37	1.24	0.444	191.1	1.2	-1.49	22

Star (HIP/Gic) (1)	α_{2000} (deg) (2)	δ_{2000} (deg) (3)	V (mag) (4)	π (mas) (5)	$\mu_{\alpha*}$ $(mas\ yr^{-1})$ (6)	μ_{δ} $(mas\ yr^{-1})$ (7)	σ_{π} (mas) (8)	$\sigma_{\mu_{\alpha*}}$ $(mas\ yr^{-1})$ (9)	$\sigma_{\mu_{\delta}}$ $(mas\ yr^{-1})$ (10)	B-V (mag) (11)	V_{rad} $(km\ s^{-1})$ (12)	$\sigma_{V_{rad}}$ $(km\ s^{-1})$ (13)	[Fe/H] (dex) (14)	*remarks* - (15)
36430	112.46185303	32.86619186	10.41	8.54	18.10	-199.80	1.18	1.66	1.31	0.540	29.1	0.6	-2.47	22
36513	112.67194366	24.08617973	10.80	5.20	163.40	-233.30	0.72	1.17	1.00	0.350	-238.4	1.0	-2.71	22
45554	139.26667786	3.02490592	10.87	5.59	49.40	-287.10	0.77	1.28	1.15	0.523	222.3	0.7	-1.01	22
46516	142.31484985	8.63346481	11.15	4.51	198.90	-307.80	0.62	1.60	1.31	0.390	266.1	1.5	-2.80	22
51191	156.85102844	1.40004909	11.03	5.43	-186.20	-296.10	0.75	1.41	1.26	0.498	88.6	0.9	-1.34	22
53025	162.73593140	53.24755478	10.35	8.97	-222.30	-188.60	1.24	1.02	0.92	0.455	133.5	0.8	-1.88	22
53971	165.61355591	79.23381805	11.76	4.13	-346.90	-88.00	0.57	1.50	1.34	0.472	3.4	0.8	-1.44	22
57244	176.07322693	40.53832626	12.02	4.40	-110.80	-252.90	0.61	2.18	1.57	0.535	-3.1	1.5	-2.52	22
59376	182.73237610	0.39842474	11.09	5.20	-56.50	-435.90	0.72	1.14	0.93	0.449	99.3	0.6	-2.22	22
61361	188.60472107	15.28027725	12.01	3.26	-290.90	-35.80	0.45	2.34	1.82	0.448	-73.2	1.1	-2.58	22
63100	193.92045593	12.55853748	11.32	5.16	-280.50	-258.50	0.71	1.43	1.22	0.521	2.9	0.7	-1.77	22
65206	200.44841003	74.20912170	11.66	4.91	-445.60	39.10	0.68	1.41	1.31	0.480	-45.3	2.1	-2.56	22
65418	201.12750244	20.45613861	12.18	3.11	-92.20	-202.90	0.43	1.39	1.25	0.468	57.5	1.2	-1.71	22
66673	205.01039124	-0.03854727	11.47	3.92	-227.50	-82.40	0.54	1.29	1.16	0.405	441.9	1.7	-3.52	22
68592	210.62536621	-5.65144348	11.13	4.37	-56.60	-397.50	0.60	1.92	1.48	0.397	81.2	1.4	-2.80	22
72920	223.54463196	25.56359291	11.00	5.16	-165.10	-288.00	0.71	1.34	1.22	0.400	-62.9	1.2	-2.88	22
77637	237.74555969	8.42326450	9.95	10.07	-234.80	-159.80	1.39	1.47	1.51	0.591	-51.6	1.0	-1.15	22
81276	248.99409485	45.86646271	11.24	3.31	-156.00	154.90	0.46	1.13	1.17	0.360	-246.3	1.0	-1.50	22
81578	249.90673828	34.28016663	11.00	6.46	-139.20	180.60	0.89	1.29	1.66	0.600	-39.6	1.1	-1.09	22
82398	252.54779053	22.31389236	11.26	6.46	-149.00	-368.00	0.89	1.07	1.22	0.570	-78.0	0.9	-1.60	22
83320	255.43325806	16.15093231	11.46	4.69	-286.60	-244.20	0.65	1.42	1.39	0.460	-113.7	1.2	-2.63	22
91129	278.82986450	28.69872856	11.39	4.43	-16.40	-278.40	0.61	1.26	1.35	0.448	-86.0	1.3	-2.88	22
100984	307.11642456	62.01453781	11.47	8.39	-205.50	-145.90	1.16	1.81	1.76	0.775	-67.8	0.7	-1.05	22
106447	323.40237427	0.39552456	12.14	3.17	243.90	-32.30	0.44	6.40	2.88	0.462	-239.3	1.6	-2.69	22
110140	334.65209961	8.44581985	10.38	7.48	283.80	-103.20	1.03	1.55	1.23	0.489	-235.1	0.8	-1.55	22
117522	357.50567627	8.72315025	11.34	5.83	372.00	-49.00	0.81	1.80	1.22	0.532	-167.8	0.9	-2.42	22
G130-32	0.01702500	34.18856430	8.50	20.86	-228.80	-58.10	3.08	1.10	1.20	0.650	-30.5	0.5	-0.58	33
G30-46	2.05598330	15.00853062	11.01	8.91	220.70	-51.20	1.32	1.70	1.60	0.890	-22.6	0.6	0.20	33
G31-36	3.56396246	-5.58169460	10.92	8.47	181.40	-48.00	1.25	2.10	2.20	0.810	36.1	0.7	-0.30	33
G243-21	5.55999565	62.02637100	9.66	8.73	245.60	24.60	1.29	2.50	2.50	0.660	5.7	0.8	0.16	33
G130-65	5.66082478	23.90870094	11.62	4.92	57.00	-249.10	0.57	1.60	1.60	0.430	-271.3	1.1	-2.33	33

Star (HIP/Gic) (1)	α_{2000} (deg) (2)	δ_{2000} (deg) (3)	V (mag) (4)	π (mas) (5)	$\mu_{\alpha*}$ $(mas\ yr^{-1})$ (6)	μ_{δ} $(mas\ yr^{-1})$ (7)	σ_{π} (mas) (8)	$\sigma_{\mu_{\alpha*}}$ $(mas\ yr^{-1})$ (9)	$\sigma_{\mu_{\delta}}$ $(mas\ yr^{-1})$ (10)	B-V (mag) (11)	V_{rad} $(km\ s^{-1})$ (12)	$\sigma_{V_{rad}}$ $(km\ s^{-1})$ (13)	[Fe/H] (dex) (14)	*remarks* - (15)
G1-4	6.92210007	4.84068060	10.69	12.40	365.40	21.70	1.83	1.70	1.70	0.890	-31.0	0.5	-0.49	33
G31-55	7.36107492	-2.34918880	10.70	7.85	220.80	-266.80	0.96	1.50	1.50	0.560	-28.4	0.6	-1.11	33
G217-54	7.80125427	55.58206177	10.57	9.30	257.60	36.10	1.37	2.40	2.20	0.860	5.0	0.3	0.21	33
G158-102	8.92188740	-6.71017218	10.82	8.82	-145.70	-154.60	1.30	1.90	2.10	0.700	-0.5	0.8	-0.82	33
G172-16	9.64449978	47.63056946	10.97	8.64	294.10	20.20	1.00	2.30	2.20	0.580	-85.0	0.6	-1.64	33
G69-21	11.66600418	33.82573700	10.34	9.20	250.20	-23.20	1.36	1.50	1.60	0.680	-15.7	0.8	-0.57	33
G32-49	11.90062046	14.64067745	10.94	11.11	94.50	-189.90	1.64	1.90	1.90	0.890	-7.8	0.4	-0.49	33
G1-35	14.38990021	10.58813858	11.67	5.63	267.00	-92.30	0.83	2.40	2.40	0.720	-19.2	0.6	-0.61	33
G242-75	14.87849617	69.48100281	10.05	10.69	241.90	-97.50	1.58	1.80	1.90	0.790	-14.6	0.3	-0.11	33
G70-31	15.88099957	5.07848597	11.82	5.52	9.90	-181.00	0.82	2.00	2.00	0.740	-99.5	0.3	-0.61	33
G172-38	16.40271187	49.45146561	11.08	8.07	147.50	-378.20	1.19	1.90	1.80	0.760	-196.2	0.9	-0.63	33
G270-159	17.43275070	-3.65865278	11.12	9.10	207.50	9.20	1.34	2.50	2.60	0.860	71.4	0.6	-0.33	33
G271-11	18.03247070	-0.61593890	11.45	4.50	163.60	46.90	0.67	1.50	1.50	0.590	56.9	0.5	-0.57	33
G172-46	19.16161156	51.85642624	11.15	11.72	149.60	-306.10	1.73	3.20	2.90	0.910	-270.0	1.3	-0.70	33
G33-48	19.13096237	9.62285519	8.75	14.50	276.10	-120.30	2.14	1.60	1.60	0.580	1.6	0.7	-0.38	33
G271-57	20.99714088	-7.71055555	11.17	8.15	-171.40	-60.50	1.20	2.60	2.80	0.770	6.3	0.5	-0.62	33
G2-38	21.72986603	12.00720787	11.38	6.02	-13.90	-359.40	0.73	1.80	1.80	0.510	-171.9	0.9	-1.55	33
G271-70	22.10132027	-7.60629702	9.28	9.10	-61.00	-168.50	1.34	1.30	1.60	0.550	3.8	0.7	-0.18	33
G271-75	22.44468307	-7.51000547	10.74	9.83	-47.90	-178.00	1.45	1.90	2.00	0.830	-55.6	0.6	-0.29	33
G173-2	22.72993279	52.74521255	10.05	13.37	-184.90	-33.50	1.98	1.80	1.70	0.860	-38.1	0.7	-0.07	33
G172-58	22.81628799	48.00484467	10.17	9.61	309.00	-36.70	1.11	1.60	1.60	0.430	-25.9	0.9	-1.94	33
G72-12	23.03840446	34.55577087	10.82	9.30	161.10	-223.20	1.37	1.80	1.80	0.830	-33.8	0.8	-0.25	33
G172-60	23.54173279	52.66543198	9.55	12.40	251.00	-130.50	1.83	1.40	1.40	0.730	52.5	0.7	-0.18	33
G172-61	23.59453392	48.74098587	11.00	9.30	363.10	-59.70	1.13	2.10	2.00	0.700	-202.6	0.8	-1.18	33
G2-47	23.81129646	5.64018345	10.78	11.26	284.70	-35.10	1.37	2.40	2.30	0.760	18.1	1.8	-1.00	33
G2-50	24.20779228	4.45748901	11.37	5.12	163.90	-195.30	0.62	1.70	1.80	0.500	-123.2	0.9	-1.19	33
G72-25	25.42072868	27.67760849	8.68	19.89	277.60	-131.80	2.94	1.20	1.10	0.730	11.4	0.3	-0.27	33
G219-20	26.43549919	57.84775925	9.51	9.30	225.30	-39.60	1.37	3.30	2.80	0.600	-39.7	0.7	-0.34	33
G71-33	26.30754089	3.51369452	10.63	8.91	224.10	-12.10	1.03	1.20	1.20	0.480	-9.6	1.5	-2.33	33
G133-45	27.38977432	43.77005386	11.78	5.06	76.30	-226.10	0.62	1.90	1.80	0.540	-93.8	1.0	-1.50	33
G271-161	27.61633301	-5.78240538	9.60	10.06	114.80	121.20	1.49	1.40	1.40	0.640	13.2	0.5	-0.24	33

Star (HIP/Gic) (1)	α_{2000} (deg) (2)	δ_{2000} (deg) (3)	V (mag) (4)	π (mas) (5)	$\mu_{\alpha*}$ $(mas\,yr^{-1})$ (6)	μ_{δ} $(mas\,yr^{-1})$ (7)	σ_{π} (mas) (8)	$\sigma_{\mu_{\alpha*}}$ $(mas\,yr^{-1})$ (9)	$\sigma_{\mu_{\delta}}$ $(mas\,yr^{-1})$ (10)	B-V (mag) (11)	V_{rad} $(km\,s^{-1})$ (12)	$\sigma_{V_{rad}}$ $(km\,s^{-1})$ (13)	[Fe/H] (dex) (14)	*remarks* - (15)
G71-55	30.96243286	-0.53917497	10.78	7.99	-35.10	-255.40	0.93	1.10	1.10	0.470	-30.9	0.7	-1.82	33
G245-44	32.00876617	74.00494385	9.88	8.64	209.30	-43.20	1.28	1.80	1.80	0.690	44.5	0.7	0.28	33
G134-3	32.18346405	45.09605789	10.32	8.39	263.70	-122.00	1.24	1.50	1.50	0.630	73.1	0.6	-0.60	33
G4-2	32.83348846	9.62153053	10.68	9.95	142.40	-267.70	1.47	2.50	2.30	0.740	38.3	0.3	-0.80	33
G74-10	33.78947449	32.39492798	12.59	7.07	448.50	-154.50	0.82	6.30	6.10	0.810	-44.5	0.8	-1.78	33
G94-49	34.23563004	27.41345215	10.40	9.83	-113.00	-248.70	1.45	1.40	1.40	0.660	-164.2	0.6	-0.82	33
G94-70	37.05536652	25.84680557	9.37	10.97	215.70	-120.30	1.62	1.20	1.20	0.530	50.5	0.9	-0.65	33
G74-30	38.53173828	40.29902649	11.63	5.48	202.30	-61.60	0.67	2.30	2.20	0.600	-68.7	0.6	-1.12	33
G134-40	39.42262650	43.99293518	10.18	7.78	233.00	-249.30	1.15	1.50	1.50	0.520	-53.6	0.8	-0.74	33
G246-11	42.10624313	62.89711761	10.71	5.09	168.30	97.00	0.75	2.70	2.70	0.600	-22.7	0.8	-0.31	33
G36-47	44.33265305	26.28154945	11.46	5.70	259.70	-220.90	0.66	1.90	2.00	0.520	88.7	0.6	-1.77	33
G221-3	45.05932617	70.80566406	12.26	4.34	182.20	-126.40	0.64	3.40	3.50	0.890	47.9	0.8	-0.07	33
G76-57	46.58712006	5.88631105	11.52	4.53	23.10	-299.60	0.67	2.50	2.40	0.690	-28.5	0.7	-0.28	33
G95-11	47.51863861	34.84755325	11.95	5.98	249.50	-4.60	0.69	5.20	6.20	0.580	205.7	0.8	-2.09	33
G5-19	47.86060333	12.61932182	11.17	8.23	-23.90	-468.30	0.95	2.10	2.10	0.600	-216.6	0.6	-1.69	33
G37-37	50.90980148	33.97508621	12.28	3.61	-71.50	-357.00	0.42	2.00	1.90	0.490	-137.1	1.3	-2.43	33
G5-40	51.91435242	21.04307175	10.79	6.63	48.70	-331.40	0.98	1.50	1.60	0.570	-117.8	0.9	-0.82	33
G6-13	52.38449478	12.80281639	11.47	6.11	72.70	-106.70	0.90	2.00	2.00	0.810	-31.1	0.7	-0.31	33
G79-42	52.40681839	10.56559181	10.78	6.34	210.40	-296.10	0.77	1.70	1.60	0.500	20.3	0.7	-1.22	33
G79-43	52.50001907	9.43691158	11.60	5.03	118.20	-178.80	0.58	2.50	2.40	0.480	-1.7	1.3	-2.32	33
G5-44	53.57446671	22.98726463	9.18	10.83	150.70	-169.00	1.60	0.90	0.90	0.610	25.4	0.5	-0.06	33
G78-41	53.73811722	38.30670166	10.21	9.83	144.10	-144.20	1.45	2.50	2.50	0.670	-10.7	0.6	-0.65	33
G6-22	54.45927811	19.82347298	11.07	7.37	-49.70	-254.30	1.09	1.30	1.30	0.780	-77.0	0.8	-0.38	33
G79-56	55.42676163	9.39259720	11.82	7.50	264.00	-251.00	0.92	2.20	2.50	0.730	-61.4	0.7	-1.50	33
G79-63	56.01959610	9.93871975	11.58	5.38	394.00	-223.00	0.79	2.60	2.50	0.820	105.0	0.9	-0.22	33
G81-8	63.11938095	41.99058533	10.53	6.79	-2.10	-302.70	1.00	1.40	1.30	0.640	1.9	0.8	-0.46	33
G7-31	63.99036789	7.89573050	11.50	5.03	143.20	-271.90	0.74	2.70	2.70	0.760	29.5	0.8	-0.20	33
G82-18	66.44487762	5.26753902	11.74	9.61	157.90	-447.90	1.17	1.80	1.80	0.830	-89.5	0.8	-1.41	33
G39-18	67.93505096	38.30371475	10.98	3.89	111.50	-189.00	0.57	3.00	2.90	0.650	-142.2	0.6	0.16	33
G8-40	68.14108276	26.46093941	10.70	11.26	191.50	-206.80	1.66	1.80	1.80	0.850	6.5	0.9	-0.30	33
G39-23	68.33630371	34.05301285	10.96	8.73	130.10	-158.00	1.29	1.90	2.00	0.890	-24.3	0.3	0.21	33

Star (HIP/Gic) (1)	α_{2000} (deg) (2)	δ_{2000} (deg) (3)	V (mag) (4)	π (mas) (5)	$\mu_{\alpha*}$ $(mas\,yr^{-1})$ (6)	μ_{δ} $(mas\,yr^{-1})$ (7)	σ_{π} (mas) (8)	$\sigma_{\mu_{\alpha*}}$ $(mas\,yr^{-1})$ (9)	$\sigma_{\mu_{\delta}}$ $(mas\,yr^{-1})$ (10)	B-V (mag) (11)	V_{rad} $(km\,s^{-1})$ (12)	$\sigma_{V_{rad}}$ $(km\,s^{-1})$ (13)	[Fe/H] (dex) (14)	*remarks* - (15)
G175-40	69.28878021	55.27243805	10.80	9.10	310.60	-80.10	1.34	3.00	3.00	0.850	76.0	0.8	0.02	33
G8-46	69.45775604	20.06802177	11.03	9.40	73.80	-221.60	1.39	1.40	1.50	0.880	83.6	0.6	-0.28	33
G82-42	70.50002289	-4.27956963	12.50	4.02	2.50	-347.60	0.49	4.20	4.60	0.610	-8.5	0.6	-1.29	33
G81-33	71.20476532	43.20515442	8.74	23.76	249.80	159.00	3.51	0.90	1.00	0.870	49.1	0.6	0.00	33
G84-9	71.33836365	3.97051382	11.47	4.75	86.00	-215.40	0.70	1.40	1.40	0.550	-104.5	0.9	-0.94	33
G85-21	72.86737823	19.36123276	10.85	5.35	154.80	-188.10	0.79	1.50	1.60	0.590	-65.6	1.1	-0.59	33
G84-22	73.95526123	-1.63158059	11.18	6.58	24.10	-280.60	0.97	1.50	1.50	0.660	-93.8	0.6	-0.78	33
G96-16	75.54701996	45.03817368	9.86	15.28	-46.70	-319.40	2.26	1.30	1.20	0.860	-9.9	0.7	-0.19	33
G96-17	75.53101349	42.44158173	10.19	14.02	-206.70	-203.80	2.07	1.40	1.30	0.850	-31.1	0.5	-0.43	33
G97-43	82.19673157	4.79588604	9.10	19.44	44.50	299.40	2.87	1.40	1.40	0.740	57.3	0.5	-0.59	33
G97-46	82.96208954	16.22028923	12.24	4.46	94.50	-312.60	0.66	3.10	3.20	0.760	-70.5	0.8	-0.61	33
G99-40	88.23098755	-3.49025011	9.19	10.97	268.80	-49.80	1.62	1.20	1.10	0.560	49.6	0.6	-0.45	33
G191-55	89.36911011	58.68017578	10.47	9.20	191.10	-110.00	1.07	2.90	2.90	0.500	-258.4	1.2	-1.94	33
G101-14	90.30200958	46.45011139	11.33	4.46	-65.40	-176.30	0.66	1.60	1.60	0.680	25.6	0.9	-0.20	33
G100-52	90.64237976	27.40293694	9.18	13.37	84.80	-191.20	1.98	1.40	1.30	0.680	17.0	0.9	-0.14	33
G102-44	90.68071747	13.07698059	10.84	7.78	232.20	-148.30	1.15	1.50	1.50	0.710	-28.8	0.5	-0.62	33
G192-18	91.65840149	56.44895172	10.90	13.58	19.30	-325.70	2.01	3.90	4.00	0.880	52.9	0.5	-0.73	33
G99-54	91.29025269	6.44833326	10.51	10.43	131.30	-152.10	1.54	1.90	1.80	0.760	56.3	0.8	-0.57	33
G100-60	92.11853790	22.43707848	11.54	5.52	197.40	-132.40	0.82	1.70	1.90	0.740	-45.8	0.9	-0.43	33
G192-21	92.50205231	50.15151215	8.52	17.11	205.80	-265.70	2.53	1.20	1.30	0.560	-18.6	0.6	-0.64	33
G101-25	93.26070404	38.91038132	10.79	9.00	132.20	-199.60	1.33	3.60	3.40	0.820	-47.6	0.4	-0.14	33
G98-53	93.45762634	33.41725922	11.14	3.69	22.40	-329.50	0.54	1.70	1.80	0.510	144.8	0.8	-0.38	33
G192-28	96.51712036	51.29272461	11.35	6.79	184.90	-247.50	0.83	2.40	2.30	0.610	-68.5	0.4	-1.32	33
G106-46	96.28343201	0.64911944	9.09	14.02	-51.40	-245.60	2.07	0.90	1.00	0.570	-9.6	0.6	-0.62	33
G103-53	100.94363403	25.52507973	10.19	10.31	-7.60	-314.30	1.52	2.00	2.10	0.680	9.2	0.8	-0.70	33
G103-58	101.62562561	35.87373734	10.00	9.40	-59.90	-200.60	1.39	2.30	2.30	0.610	-1.2	0.8	-0.62	33
G87-13	103.73456573	35.51627350	11.07	5.48	53.50	-241.70	0.67	3.80	3.90	0.480	206.4	0.7	-1.23	33
G108-46	104.91210938	9.09096909	11.04	5.82	132.60	-205.60	0.86	2.60	2.40	0.590	35.3	0.3	-0.77	33
G107-43	105.52983856	36.94966507	10.27	10.43	-64.90	-211.10	1.54	2.50	2.50	0.640	80.7	0.5	-0.90	33
G88-5	106.53142548	18.63553047	10.21	11.26	214.10	-88.80	1.66	1.20	1.20	0.720	-70.1	0.7	-0.57	33
G110-38	106.72556305	18.13643265	11.34	9.40	9.10	-167.70	1.39	1.70	1.70	0.790	65.5	0.5	-0.67	33

Star (HIP/Gic) (1)	α_{2000} (deg) (2)	δ_{2000} (deg) (3)	V (mag) (4)	π (mas) (5)	$\mu_{\alpha*}$ $(mas\ yr^{-1})$ (6)	μ_δ $(mas\ yr^{-1})$ (7)	σ_π (mas) (8)	$\sigma_{\mu_{\alpha*}}$ $(mas\ yr^{-1})$ (9)	σ_{μ_δ} $(mas\ yr^{-1})$ (10)	B-V (mag) (11)	V_{rad} $(km\ s^{-1})$ (12)	$\sigma_{V_{rad}}$ $(km\ s^{-1})$ (13)	[Fe/H] (dex) (14)	*remarks* - (15)
G107-50	107.47035217	42.65370941	11.81	5.25	15.00	-256.00	0.61	1.90	1.90	0.490	148.2	1.1	-2.25	33
G108-58	107.51078796	-1.29958057	11.84	4.73	8.40	-195.10	0.55	1.60	1.70	0.490	142.5	1.0	-2.24	33
G112-6	109.67667389	3.69551110	11.11	8.07	78.10	-334.00	0.99	1.70	1.70	0.690	135.1	0.6	-1.00	33
G87-35	110.18698883	29.34507179	11.10	7.31	112.20	-203.60	1.08	2.30	2.40	0.760	69.4	0.5	-0.48	33
G265-26	111.70265198	89.58106232	11.40	3.66	-48.60	-258.90	0.54	1.10	1.20	0.550	-36.2	0.4	-0.43	33
G87-45	113.24451447	31.11652756	11.44	6.95	76.10	-286.90	0.85	3.20	3.20	0.640	8.4	1.5	-1.49	33
G88-38	113.27664948	17.08782005	11.09	6.68	208.80	-133.00	0.99	1.70	1.80	0.770	-16.8	0.8	-0.17	33
G89-33	114.46957397	5.72173882	10.36	7.99	232.10	-172.70	1.18	2.00	1.90	0.620	83.4	0.4	-0.62	33
G89-34	114.50767517	5.58660269	8.21	19.01	-198.30	-140.70	2.81	1.70	1.70	0.610	152.6	0.4	-0.29	33
G90-37	120.27460480	32.76589584	12.17	3.72	160.10	-208.90	0.45	2.60	2.70	0.520	23.5	0.9	-1.21	33
G90-38	120.71669769	36.03265381	11.25	8.23	42.10	-282.10	1.00	3.40	3.20	0.730	51.1	0.6	-1.00	33
G234-24	122.57016754	69.78121948	10.96	6.90	283.50	-78.20	0.84	2.50	2.60	0.470	-176.8	0.8	-1.60	33
G50-23	123.28235626	9.11175251	12.58	5.18	132.30	-314.50	0.77	5.10	5.10	0.860	32.7	0.5	-0.63	33
G40-14	124.03065491	19.69767189	11.20	5.22	135.30	-313.30	0.60	1.40	1.40	0.380	-67.2	0.9	-2.71	33
G113-22	124.24073792	0.01770000	9.68	14.50	224.40	-150.40	1.77	0.90	0.90	0.590	54.0	0.7	-1.30	33
G194-32	129.14344788	58.65836716	11.39	4.13	-66.80	-229.30	0.61	2.60	2.60	0.620	44.1	0.5	-0.18	33
G51-20	129.39038086	31.55118561	11.84	6.20	-109.80	-315.70	0.92	2.20	2.20	0.760	7.2	0.3	-0.75	33
G115-34	133.99719238	38.66248703	11.22	5.45	88.70	-285.20	0.63	1.90	1.80	0.400	-79.8	0.4	-2.38	33
G114-48	138.42901611	-3.89803600	10.65	7.57	55.20	-224.80	1.12	2.20	2.30	0.650	-56.1	0.7	-0.51	33
G116-15	138.97915649	40.24324036	10.39	8.91	-85.40	-221.50	1.32	1.20	1.20	0.640	-18.2	0.2	-0.67	33
G161-14	140.05436707	-5.36633062	12.36	3.87	81.70	-184.70	0.47	3.80	4.00	0.570	66.0	0.7	-1.22	33
G116-26	140.96406555	40.15530777	10.22	10.31	-386.90	-55.00	1.52	1.50	1.50	0.690	58.9	0.3	-0.59	33
G49-19	144.71090698	28.40242004	10.59	6.24	51.30	-344.20	0.92	2.20	2.20	0.550	76.1	2.8	-0.53	33
G48-29	145.18000793	1.00822222	10.48	6.95	148.20	-508.60	0.81	1.50	1.50	0.370	-57.4	1.6	-2.66	33
G116-45	146.15785217	38.61071014	11.30	4.89	212.70	-250.20	0.60	2.10	2.00	0.490	-33.7	0.7	-1.05	33
G161-73	146.40762329	-4.67461681	10.84	7.19	151.10	-256.60	0.88	2.20	2.40	0.500	121.2	0.9	-1.40	33
G116-56	147.46524048	41.18517685	9.91	9.95	-123.20	-224.60	1.47	1.30	1.30	0.630	10.4	0.5	-0.49	33
G43-5	147.46493530	6.60990000	12.51	5.25	68.10	-329.50	0.61	4.10	4.00	0.630	99.5	1.5	-2.28	33
G43-7	147.55787659	5.15065813	11.75	6.84	210.20	-220.00	1.01	4.00	3.90	0.800	-25.8	0.8	-0.68	33
G116-64	148.77635193	32.93080139	12.10	4.15	-133.70	-266.70	0.48	3.00	3.00	0.470	78.3	0.6	-1.78	33
G42-34	150.80117798	19.84084129	10.70	13.16	-82.50	-343.60	1.95	1.50	1.60	0.850	37.5	0.8	-0.81	33

Star	α_{2000}	δ_{2000}	V	π	$\mu_{\alpha*}$	μ_{δ}	σ_{π}	$\sigma_{\mu_{\alpha*}}$	$\sigma_{\mu_{\delta}}$	B-V	V_{rad}	$\sigma_{V_{rad}}$	[Fe/H]	*remarks*
(HIP/Gic)	(deg)	(deg)	(mag)	(mas)	$(mas\ yr^{-1})$	$(mas\ yr^{-1})$	(mas)	$(mas\ yr^{-1})$	$(mas\ yr^{-1})$	(mag)	$(km\ s^{-1})$	$(km\ s^{-1})$	(dex)	-
(1)	(2)	(3)	(4)	(5)	(6)	(7)	(8)	(9)	(10)	(11)	(12)	(13)	(14)	(15)
G162-16	151.01251221	0.59161669	9.83	10.31	-195.90	68.00	1.52	1.00	1.00	0.590	42.7	0.8	-0.64	33
G49-38	152.63069153	21.69181442	11.54	7.13	-177.80	-182.60	1.05	1.50	1.50	0.810	129.2	0.7	-0.47	33
G162-53	156.34027100	-2.59884715	11.71	6.48	-194.90	79.80	0.96	1.60	1.60	0.870	59.0	0.2	-0.11	33
G58-12	160.78027344	20.34866142	10.58	8.31	105.60	-278.60	1.23	1.30	1.40	0.610	-1.9	0.6	-0.82	33
G45-9	162.90231323	9.09197521	10.13	9.61	29.20	-218.60	1.42	3.10	3.50	0.740	-17.1	0.4	-0.06	33
G146-71	163.51484680	39.51695633	10.32	7.57	-212.00	-37.00	1.12	1.30	1.20	0.530	10.1	0.8	-0.78	33
G146-76	164.98948669	44.77882004	10.49	15.28	-101.80	-219.80	1.77	1.30	1.30	0.670	-115.2	0.7	-2.31	33
G163-39	165.74284363	-3.38136935	8.88	22.51	134.50	-163.10	3.33	1.10	1.20	0.880	18.1	0.6	0.31	33
G197-8	169.47685242	57.02268219	12.11	4.26	-237.50	-10.80	0.63	3.20	3.30	0.630	26.2	0.9	-0.78	33
G10-12	169.80845642	5.67945290	9.29	25.16	-307.60	-74.20	3.72	1.40	1.40	0.810	133.0	0.7	-0.92	33
G45-48	170.12135315	5.50481939	10.19	10.18	-161.40	196.30	1.50	2.00	1.90	0.750	24.2	0.4	-0.26	33
G176-27	170.46916199	50.62575912	11.30	6.34	253.40	-239.70	0.94	2.80	2.50	0.830	-28.9	1.7	-0.61	33
G56-39	171.55844116	20.85104752	12.20	4.89	-180.70	-139.50	0.60	1.60	1.70	0.680	66.9	0.9	-1.00	33
G120-50	171.84983826	20.70161438	11.51	6.02	-235.60	56.10	0.89	1.50	1.50	0.640	45.6	0.7	-0.85	33
G197-17	172.64358521	61.88177490	10.67	8.23	-231.70	80.30	1.22	3.20	3.20	0.710	-41.7	0.4	-0.47	33
G57-7	173.14218140	10.90313625	10.13	8.55	-268.10	-217.40	1.26	1.50	1.40	0.600	28.1	0.8	-0.54	33
G147-62	173.67625427	36.21334076	11.35	5.35	61.70	-194.90	0.62	3.00	2.80	0.450	-3.5	0.8	-1.63	33
G236-82	177.00294495	70.85980988	10.80	7.92	-225.30	50.80	1.17	1.90	2.00	0.630	-70.7	0.8	-0.91	33
G197-45	182.37043762	51.93362045	10.73	10.97	-235.30	-114.30	1.62	2.30	2.20	0.720	23.4	0.6	-0.92	33
G123-9	182.73066711	44.00328827	10.50	10.83	-398.10	-174.20	1.32	1.40	1.30	0.620	-22.4	1.1	-1.32	33
G12-20	182.75689697	12.14330578	12.10	6.90	-291.10	70.50	1.02	2.30	2.40	0.810	45.3	0.4	-0.86	33
G199-20	187.54280090	52.82161331	11.29	5.28	-259.10	-80.60	0.61	2.30	2.20	0.440	15.4	0.7	-1.61	33
G59-25	188.74246216	23.14831352	8.75	12.77	72.50	-220.10	1.89	0.90	0.90	0.590	-41.9	0.8	-0.07	33
G164-5	189.39932251	37.92812347	12.10	4.62	-227.30	-95.10	0.56	4.10	3.80	0.580	-59.9	0.9	-1.28	33
G60-46	193.76828003	7.79856396	11.68	6.63	-77.60	-227.50	0.81	2.70	2.70	0.660	-33.0	0.4	-1.32	33
G14-23	195.37304688	-9.45279694	9.64	8.82	-98.40	91.50	1.30	1.10	1.20	0.550	24.1	0.5	-0.37	33
G14-26	195.79806519	-6.12199450	9.73	9.00	-126.30	30.80	1.33	1.30	1.40	0.590	-11.8	0.6	-0.30	33
G62-9	195.82606506	4.12428331	11.31	8.91	-180.40	99.90	1.32	2.10	2.10	0.780	13.5	0.3	-0.67	33
G14-33	197.20214844	-3.97356105	11.18	8.31	-228.80	-99.40	1.01	2.70	2.90	0.670	-91.0	0.6	-1.15	33
G14-38	197.82829285	-4.82584190	10.87	8.55	-163.80	-51.40	1.26	2.50	2.70	0.740	3.7	0.6	-0.52	33
G14-41	199.02348328	-3.35667777	10.19	9.95	-150.80	96.30	1.47	1.50	1.50	0.710	-13.8	0.6	-0.44	33

Star	α_{2000}	δ_{2000}	V	π	$\mu_{\alpha*}$	μ_{δ}	σ_{π}	$\sigma_{\mu_{\alpha*}}$	$\sigma_{\mu_{\delta}}$	B-V	V_{rad}	$\sigma_{V_{rad}}$	[Fe/H]	*remarks*
(HIP/Gic)	(deg)	(deg)	(mag)	(mas)	$(mas\ yr^{-1})$	$(mas\ yr^{-1})$	(mas)	$(mas\ yr^{-1})$	$(mas\ yr^{-1})$	(mag)	$(km\ s^{-1})$	$(km\ s^{-1})$	(dex)	-
(1)	(2)	(3)	(4)	(5)	(6)	(7)	(8)	(9)	(10)	(11)	(12)	(13)	(14)	(15)
G165-21	204.48841858	39.17504120	9.18	20.86	-227.60	-145.80	3.08	0.90	1.10	0.900	-24.4	0.5	0.14	33
G165-24	205.52835083	36.83250427	12.01	7.50	10.80	-259.20	0.92	4.40	4.00	0.770	-42.4	0.8	-1.05	33
G150-40	207.21726990	27.66931915	10.73	6.58	-243.80	-196.70	0.80	2.20	2.10	0.500	-50.9	0.5	-1.08	33
G65-16	208.95143127	12.43881989	8.56	19.44	-95.80	-321.80	2.87	1.10	1.00	0.620	29.6	0.4	-0.65	33
G165-63	215.07612610	37.95622253	10.37	10.06	-205.90	167.30	1.49	3.10	2.90	0.820	-7.2	0.6	0.12	33
G239-12	214.71905518	73.23741150	11.62	4.78	-160.30	-148.40	0.55	2.10	2.30	0.410	-172.0	0.7	-2.56	33
G135-42	215.54437256	20.25115204	10.45	8.07	155.80	-189.30	1.19	1.50	1.50	0.620	102.4	0.6	-0.59	33
G124-45	217.00488281	-1.14115834	11.19	7.78	-327.40	130.90	1.15	1.50	1.60	0.720	12.3	0.6	-0.63	33
G178-27	217.11819458	37.98900986	11.23	5.67	-183.40	-247.20	0.66	3.50	3.20	0.430	-180.5	0.8	-2.11	33
G201-1	217.30026245	54.53823853	11.78	4.26	-116.80	-165.50	0.63	2.90	2.80	0.560	-104.4	0.8	-0.83	33
G66-9	218.80310059	12.22204399	12.02	5.09	-202.70	-249.80	0.59	2.10	2.20	0.510	-48.0	0.8	-2.68	33
G201-5	219.03483582	55.55130386	11.49	4.86	122.90	-291.80	0.56	3.10	3.10	0.410	-35.6	1.1	-2.60	33
G178-50	222.05131531	41.52047729	10.56	10.56	-45.30	-296.20	1.56	1.30	1.30	0.750	-17.1	0.6	-0.65	33
G223-82	221.98574829	62.93506622	11.26	10.06	-212.80	93.40	1.49	3.90	3.90	0.850	-95.9	0.7	-0.76	33
G166-47	222.51060486	32.64896774	12.04	3.96	-187.00	-38.20	0.46	2.60	2.40	0.410	-66.4	0.8	-2.52	33
G66-51	225.20860291	2.12708616	10.63	11.11	-177.50	-109.30	1.36	1.40	1.40	0.710	-118.8	0.4	-1.09	33
G66-60	226.20381165	10.23811913	10.78	8.47	-481.50	-30.80	1.25	2.00	2.00	0.820	10.5	1.0	0.00	33
G167-21	227.20477295	28.65242577	11.59	9.20	-79.60	-195.30	1.36	1.90	1.90	0.840	-28.0	0.5	-0.80	33
G201-44	228.48899841	53.86436462	10.51	8.31	-28.70	-254.90	0.96	1.60	1.60	0.450	-144.6	0.7	-1.83	33
G16-20	239.57759094	2.05169725	10.80	10.69	-85.30	-240.30	1.24	1.70	1.60	0.620	170.5	0.5	-2.04	33
G202-25	239.98608398	45.73796844	11.04	9.72	37.00	-259.90	1.44	2.10	2.00	0.870	-0.3	0.6	-0.38	33
G168-22	240.31652832	23.07936096	10.66	8.55	-239.70	140.90	1.26	1.40	1.40	0.710	-79.8	0.6	-0.49	33
G16-28	240.90434265	2.61833882	12.09	6.24	-144.10	-168.40	0.76	1.80	1.80	0.720	2.9	0.4	-1.27	33
G168-26	240.83270264	21.96991348	11.19	7.57	-297.30	-93.50	0.88	1.60	1.60	0.550	-302.4	0.8	-1.80	33
G202-35	243.73919678	49.76841736	11.02	6.15	-161.90	-207.70	0.75	1.50	1.40	0.500	-108.2	0.5	-1.24	33
G202-43	245.08639526	51.17391205	12.18	4.70	-260.10	135.10	0.57	3.60	3.20	0.590	-186.6	0.7	-1.39	33
G17-16	246.95089722	-1.06908894	9.63	16.77	-347.50	-102.00	2.48	1.20	1.20	0.720	-162.6	0.5	-0.95	33
G153-60	247.70648193	-4.06632757	10.57	9.40	-198.10	-231.40	1.39	2.40	2.40	0.730	52.5	0.5	-0.48	33
G153-64	248.12510681	-8.56060028	11.44	8.91	-150.10	-207.50	1.09	2.50	2.80	0.700	115.2	0.7	-1.54	33
G169-21	249.27185059	31.32330894	12.11	4.50	-156.10	170.90	0.67	3.40	3.20	0.670	-124.4	0.7	-0.71	33
G139-6	255.34364319	13.82574177	10.07	12.40	-200.90	28.50	1.83	1.20	1.10	0.710	-48.3	0.4	-0.58	33

Star (HIP/Gic) (1)	α_{2000} (deg) (2)	δ_{2000} (deg) (3)	V (mag) (4)	π (mas) (5)	$\mu_{\alpha*}$ $(mas\ yr^{-1})$ (6)	μ_{δ} $(mas\ yr^{-1})$ (7)	σ_{π} (mas) (8)	$\sigma_{\mu_{\alpha*}}$ $(mas\ yr^{-1})$ (9)	$\sigma_{\mu_{\delta}}$ $(mas\ yr^{-1})$ (10)	B-V (mag) (11)	V_{rad} $(km\ s^{-1})$ (12)	$\sigma_{V_{rad}}$ $(km\ s^{-1})$ (13)	[Fe/H] (dex) (14)	*remarks* - (15)
G169-44	256.26950073	28.03717995	11.75	7.25	-259.40	-81.20	1.07	2.20	2.00	0.750	-86.9	0.8	-0.93	33
G181-28	256.77621460	34.35960770	12.02	4.36	-225.00	-111.00	0.51	5.20	5.90	0.440	-169.8	1.1	-2.68	33
G170-21	257.31478882	22.73602867	12.58	4.50	-175.80	-187.00	0.52	2.70	2.70	0.600	-221.7	1.1	-1.81	33
G139-49	264.20046997	2.83879447	10.70	10.43	-137.80	-190.30	1.27	1.30	1.30	0.670	-95.7	0.7	-1.23	33
G204-30	267.49429321	37.52183914	10.27	9.72	-215.20	-165.50	1.44	3.20	3.00	0.600	-70.7	0.6	-0.98	33
G227-16	267.36529541	64.39154053	11.10	10.31	225.90	-131.60	1.52	2.90	3.10	0.860	-16.7	0.6	-0.40	33
G183-9	268.24884033	15.35081100	11.87	4.19	-93.30	-225.10	0.51	2.00	2.00	0.530	110.9	1.1	-1.58	33
G182-32	268.77621460	37.74655533	11.99	4.73	-187.30	-362.30	0.55	4.40	4.10	0.560	-184.7	0.9	-1.63	33
G183-16	270.38092041	20.74371910	11.88	7.50	-163.00	-197.70	0.92	1.80	1.80	0.790	-109.5	0.8	-1.15	33
G140-34	270.76705933	10.17744446	12.07	4.62	-69.10	-233.50	0.68	2.20	2.20	0.700	-29.9	0.5	-0.73	33
G206-8	271.77743530	29.36441040	12.26	5.70	-104.60	-217.20	0.84	3.00	3.00	0.790	65.5	0.8	-0.65	33
G204-49	273.14920044	40.55669022	10.85	9.83	6.30	-390.30	1.45	1.40	1.30	0.730	-42.5	0.5	-0.97	33
G140-53	274.46737671	5.45205545	10.93	8.55	-197.00	-73.80	1.26	2.70	2.50	0.770	-42.1	0.8	-0.54	33
G21-19	279.29916382	-0.88984168	11.89	4.97	-84.00	-289.20	0.61	1.40	1.50	0.630	-126.7	0.8	-1.09	33
G21-22	279.79046631	0.12065278	10.74	6.11	-168.90	-446.20	0.90	1.50	1.50	0.540	59.3	0.7	-0.97	33
G184-32	282.47982788	28.09730530	12.56	3.16	-101.80	-260.80	0.39	4.00	3.80	0.500	-161.6	1.0	-1.44	33
G141-47	283.31887817	10.62391376	10.54	7.85	-50.90	-197.70	0.96	1.80	1.70	0.540	-23.4	1.3	-1.34	33
G92-16	294.45025635	4.30997801	10.18	7.25	-64.30	-244.60	1.07	1.90	1.80	0.700	26.9	0.9	-0.03	33
G208-32	294.47720337	44.98462296	9.64	10.31	-241.90	-180.70	1.52	1.10	1.10	0.510	-116.0	0.7	-0.94	33
G142-44	294.72152710	16.42614937	11.15	7.71	-194.80	-186.80	0.94	1.90	1.80	0.660	-280.9	0.6	-1.17	33
G125-25	294.82174683	38.04461288	11.30	5.94	104.30	189.70	0.88	1.90	1.90	0.700	-97.9	0.5	-0.56	33
G260-29	294.68997192	62.63092041	10.44	11.56	-30.80	266.40	1.71	3.70	3.70	0.820	-29.3	0.9	-0.37	33
G23-23	300.71719360	14.26318073	11.07	9.61	-95.10	-157.30	1.42	1.60	1.50	0.850	37.6	0.8	-0.45	33
G143-33	302.09173584	15.04279995	11.59	4.86	-159.10	-180.70	0.59	1.70	1.70	0.500	-89.6	0.4	-1.38	33
G186-18	304.16104126	29.53073311	11.39	7.71	226.70	129.10	1.14	2.50	2.40	0.820	-105.3	0.8	-0.51	33
G143-43	304.25558472	17.26276588	10.75	11.41	-163.40	-210.60	1.69	1.10	1.10	0.750	33.0	0.8	-0.89	33
G230-44	309.46633911	51.73551559	11.08	7.57	-34.90	205.40	1.12	2.50	2.40	0.750	-9.5	0.6	-0.32	33
G24-25	310.06707764	0.55549723	10.57	10.56	141.60	-144.30	1.22	1.40	1.40	0.610	-308.6	0.9	-2.12	33
G230-45	310.06958008	54.21994019	11.43	9.72	83.40	224.70	1.44	3.00	2.70	0.800	-79.8	0.7	-0.87	33
G230-47	310.38891602	57.49453354	10.12	10.69	-7.30	-241.90	1.58	3.30	3.20	0.740	-42.5	0.6	-0.39	33
G210-33	311.34753418	40.39088440	11.20	4.97	-202.80	-105.30	0.61	1.50	1.40	0.470	-175.2	0.7	-1.42	33

Star (HIP/Gic) (1)	α_{2000} (deg) (2)	δ_{2000} (deg) (3)	V (mag) (4)	π (mas) (5)	$\mu_{\alpha *}$ $(mas\ yr^{-1})$ (6)	μ_{δ} $(mas\ yr^{-1})$ (7)	σ_{π} (mas) (8)	$\sigma_{\mu_{\alpha *}}$ $(mas\ yr^{-1})$ (9)	$\sigma_{\mu_{\delta}}$ $(mas\ yr^{-1})$ (10)	B-V (mag) (11)	V_{rad} $(km\ s^{-1})$ (12)	$\sigma_{V_{rad}}$ $(km\ s^{-1})$ (13)	[Fe/H] (dex) (14)	*remarks* - (15)
G25-5	312.33590698	1.92505836	10.11	10.31	-43.60	-189.20	1.52	1.30	1.30	0.670	-37.9	0.6	-0.66	33
G265-39	311.08328247	85.56439209	9.10	15.55	275.10	-53.50	2.30	1.10	1.10	0.630	-22.5	0.6	-0.71	33
G262-32	314.75091553	65.04447937	10.73	14.02	-367.90	-38.00	2.07	2.40	2.50	0.820	-90.2	0.8	-0.97	33
G26-1	321.69931030	-8.39890003	11.27	6.34	56.70	-221.60	0.73	2.30	2.50	0.490	14.5	0.9	-1.87	33
G25-31	321.85812378	7.66276646	10.65	7.99	-141.50	-195.30	1.18	2.60	2.50	0.580	70.7	1.2	-0.98	33
G232-18	322.65539551	48.86656952	10.53	6.68	-198.10	52.50	0.99	2.30	2.20	0.600	-261.4	0.7	-0.57	33
G26-8	322.93942261	-1.92733061	10.47	11.41	203.00	-68.60	1.69	1.70	1.70	0.850	-83.1	0.7	-0.32	33
G126-10	323.75091553	10.92063904	11.83	4.07	-101.20	-151.10	0.50	2.10	2.10	0.470	-101.7	0.8	-1.38	33
G26-22	325.29495239	-7.48076963	11.90	5.18	-85.10	-252.50	0.77	4.10	4.40	0.680	88.9	0.7	-0.88	33
G214-1	326.98181152	33.10755157	12.08	5.48	197.90	-13.50	0.64	2.10	2.00	0.570	-119.6	0.8	-2.03	33
G126-36	327.08038330	19.97517014	9.95	11.56	-103.50	-241.00	1.41	1.10	1.10	0.610	-87.0	0.9	-1.03	33
G265-43W	325.39273071	85.91363525	10.52	13.80	239.80	108.50	2.04	2.80	3.00	0.800	-131.7	0.4	-0.76	33
G93-47	328.03710938	7.64446115	10.77	6.90	200.60	40.50	1.02	1.80	1.90	0.630	-34.7	0.5	-0.58	33
G214-5	329.79324341	41.04139709	11.52	5.90	-291.90	-192.60	0.68	1.80	1.70	0.530	-235.7	1.4	-2.12	33
G27-8	330.80630493	-1.22029448	11.39	5.82	199.50	-127.80	0.71	1.70	1.60	0.510	-53.0	0.8	-1.53	33
G126-52	331.05575562	19.54845810	11.02	6.02	-3.40	-298.20	0.70	1.10	1.10	0.380	-242.1	1.2	-2.57	33
G18-29	331.61508179	5.92587757	10.61	9.50	35.70	-190.80	1.41	2.00	1.90	0.750	-4.9	0.5	-0.52	33
G126-56	332.32955933	11.69862747	11.73	5.25	191.70	61.10	0.78	1.70	1.80	0.690	-53.2	0.8	-0.76	33
G156-4	336.32681274	-5.54553604	10.97	9.20	-17.90	-221.20	1.36	1.80	1.90	0.770	-44.7	0.4	-0.55	33
G156-7	336.38900757	-4.02529430	11.82	4.89	-13.30	-247.20	0.60	3.70	4.00	0.610	-56.6	0.6	-1.06	33
G241-7	336.42810059	69.52659607	10.50	9.10	172.80	91.50	1.34	1.80	1.90	0.620	-114.2	0.7	-0.97	33
G27-33	338.19650269	-5.95460558	11.51	8.23	-215.70	-148.30	1.00	2.70	3.00	0.760	-15.0	0.6	-1.08	33
G233-26	339.98480225	61.71876526	11.88	5.41	-160.40	-102.10	0.66	3.80	4.00	0.670	-314.5	0.8	-1.16	33
G28-16	341.91043091	6.42221117	11.59	7.99	250.60	-77.40	1.18	2.70	2.70	0.810	-25.0	0.5	-0.86	33
G67-40	345.44311523	11.82143307	10.66	9.50	286.70	-79.40	1.41	1.70	1.60	0.750	-29.3	0.4	-0.64	33
G190-10	346.99896240	41.85565567	11.22	9.40	344.60	-95.90	1.09	1.80	1.70	0.610	-111.6	0.9	-1.92	33
G28-48	348.25216675	1.80319166	11.11	11.72	-68.50	-148.80	1.73	1.50	1.50	0.870	25.1	0.6	-0.90	33
G68-3	348.32144165	20.94276428	9.74	20.37	101.40	-226.30	2.48	1.00	1.00	0.800	-94.4	0.5	-1.07	33
G128-43	349.27697754	31.72630310	11.30	7.50	-137.80	-128.40	1.11	2.20	2.10	0.830	-73.1	0.7	-0.27	33
G217-2	349.89379883	58.61155319	12.02	4.36	273.50	67.70	0.65	3.10	3.20	0.640	-302.5	0.9	-0.97	33
G216-45	351.85070801	50.26315308	11.07	6.48	191.60	71.20	0.96	2.50	2.40	0.680	36.3	0.8	-0.52	33

Star (HIP/Gic) (1)	α_{2000} (deg) (2)	δ_{2000} (deg) (3)	V (mag) (4)	π (mas) (5)	$\mu_{\alpha*}$ $(mas\,yr^{-1})$ (6)	μ_{δ} $(mas\,yr^{-1})$ (7)	σ_{π} (mas) (8)	$\sigma_{\mu_{\alpha*}}$ $(mas\,yr^{-1})$ (9)	$\sigma_{\mu_{\delta}}$ $(mas\,yr^{-1})$ (10)	B-V (mag) (11)	V_{rad} $(km\,s^{-1})$ (12)	$\sigma_{V_{rad}}$ $(km\,s^{-1})$ (13)	[Fe/H] (dex) (14)	*remarks* - (15)
G128-80	353.74972534	33.02474594	11.99	5.15	241.20	14.00	0.76	4.60	4.50	0.820	-22.0	0.6	-0.25	33
G217-15	355.08245850	59.26098251	10.47	10.06	239.10	-59.40	1.49	2.70	2.70	0.830	-68.1	0.5	-0.03	33
G171-15	356.26129150	44.66766739	11.55	8.07	51.30	-228.20	0.94	1.90	1.80	0.640	-333.6	0.9	-2.12	33
G129-44	358.91058350	21.81556892	10.34	7.57	-181.60	-145.90	1.12	1.40	1.50	0.630	-96.3	0.6	-0.41	33
G158-11	359.19015503	-6.84970570	10.69	7.44	218.60	-138.00	1.10	2.10	2.20	0.620	65.6	0.7	-0.66	33
G30-34	359.69992065	9.24085045	9.20	15.55	352.50	-140.20	2.30	1.30	1.30	0.670	30.5	0.5	-0.58	33